Tunable Plasmonic Metamaterial

A Dissertation by

Mehdi Keshavarz Hedayati

Submitted to the Faculty of Engineering of
Christian-Albrechts-Universität zu Kiel
in Partial Fulfillment
of the Requirements
for the Degree of
DOCTOR OF PHILOSOPHY

February 2014

1. Gutachter:	Prof. Dr. Mady Elbahri
2. Gutachter:	Prof. Dr. Franz Faupel
3. Gutachter:	Prof. Dr. Andreas Heilmann
Datum der mündlichen Prüfung:	27.06.2014

General Declaration

I hereby declare that this thesis contains no material which has been accepted for the award of any other degree or diploma at any university or equivalent institution and that, to the best of my knowledge and belief, this thesis contains no material previously published or written by another person, except where due reference is made in the text of the thesis. I declare that the current thesis has been prepared subject to the Rules of Good Scientific Practice of the German Research Foundation.

Six chapters of this thesis are six original research papers wherein I was the first author and hence contributed to writing and performing the experiments. All theses articles are published in peer reviewed journals. For using of each copyrighted materials (articles), a written permission from the publisher was obtained. However, the contents of the abstract, introduction, summary and outlook of the current dissertation were the principal responsibility of myself, the candidate, working at the Christian-Albrechts-Universität zu Kiel under the supervision of Prof. Mady Elbahri. I have renumbered sections and figures of submitted or published papers in order to generate a consistent presentation within the thesis. Moreover, most of the figures and graphs are resized or regenerated and the references are renumbered in order to provide an uniform and consistent style of presentation within the current dissertation. Since the funding agencies related to each part of the work are acknowledged at the end of each chapter (Chapters 4-9), in the acknowledgment section of the dissertation, the name of agencies are omitted.

Mehdi Keshavarz Hedayati
Christian-Albrechts-Universität zu Kiel

Date:

Signature:

To My Beloved Wife & Parents

Acknowledgements

I would like to express my deep gratitude to Professor Mady Elbahri my research advisor and supervisor, for his incredible support, kind and patient guidance, enthusiastic encouragement and useful critiques of this research work. His willingness to give his time so generously has been very much appreciated. I am very grateful for all of the things he has taught me (in research and personal life). In particular, I should thank his self control and ability to tolerate my moody and quick temper within the last few years!

I would like also to acknowledge Professor Franz Faupel, my second advisor who allowed me to work in his lab and use his resources. I appreciate his continuous encouraging comments and discussions. I am also grateful to Professor Carsten Rockstuhl, the external collaborator who did the simulation of the experimental data. His efforts, comments and scientific discussions, in particular his contribution to one of our paper (Chapter 8) is appreciable.

Six chapters of current dissertation (chapters 4-9) are my peer-reviewed articles wherein I was the first author. Hence, I should acknowledge all the co-authors (Mady Elbahri, Franz Faupel, Carsten Rockstuhl, Thomas Stunskus, Vladimir Zaporojtchenko, Mojtaba Javaherirahim, Babak Mozooni, Ramzy Abdelaziz, Ali Tavassolizadeh, Venkata Sai Kiran Chakravadhanula, Mohammad Jamali, Ahnaf Usman Zillohu, Christoph Etrich, Stephan Fahr, Hala Jarallah El-Khozondar, Muhammad Bawa'aneh, Andrei Lavrinenko) whose contribution and support undoubtedly helped me to finish my PhD research work successfully. I would also like to extend my thanks to the technician of the laboratory, Stefan Rehders who helped me concerning technical problems with sputtering chamber.

I would like to acknowledge the helps from my colleagues and friends in Kiel within the last few years who supported me in different ways. I should acknowledge M.Sc. Mojtaba Javaherirahim, who worked almost 2 years with me as a graduate assistant. His help in performing the experiments, accelerated significantly my progress. I would like to thank M. Sc. Babak Mozooni and M. Sc. Ali Tavassolizadeh who partly involved in the experiments and helped me in software issues, graphical drawings, photography, proof-reading and provided me a great time out of work. I am grateful to M. Sc. Usman Zillohu, my group mates who has done some of the spin-coatings of my samples (Some of them are presented in Chapter 9). I am thankful to Dr. VS. Chakravandhanula, Dr. Ulrich Schurmann and Dr. Viktor Hrkac who did all the TEM measurements of my samples. The helps of Dr. Shahin Homaeigohar

in proof-reading of this dissertation is very appreciable. I never forget the supports and family like friendship of Dr. Mostafa Enayat, for all his support and help before start of my PhD (during master studies). I am also very thankful to my group fellows, M.Sc. Ramzy Abdelaziz and M. Sc. Duygu Disci-Zayed, who provided a friendly environment in the office. Our non-stop discussion in the office helped me to change my mind while I was upset or disappointed!

A special thanks to all my family members. Words can not express how grateful I am to them. In particular, I wish to express my gratitude and appreciation to my parents who supported me in all aspects of my life. They raised me with a love of science and supported me to reach my goals. Their love and presence keep my life the one that I want. Moreover, I would not be where I am today without their financial support during my undergraduate studies. My two brothers have been my best friends all my life and I love them and thank them for all the great times. I am also very grateful to my parents in-law who have been supportive and welcoming to the family. They have been generous with their love and encouragement despite the long distance between us. I am also thankful to my brother-in-law for the great and golden time that we had in Paris.

And last not the least, my deepest and most heartfelt appreciation goes out to my wife, Zahra, who has always encouraged me towards excellence. She has been a true and great supporter and has unconditionally loved me during my good and bad times. Without her love, encouragement, patience and support this dissertation would not have materialized. She has been with me all these years and has made them certainly the best years of my life.

Mehdi Keshavarz Hedayati
Christian-Albrechts-Universität zu Kiel

Kiel, 2014

Publications, Awards and Presentations

Patents

- M. Elbahri, M. K. Hedayati, V. Zaporotchenko, T. Strunkus, F. Faupel, Absorberschicht für den VIS- und/ oder NIR-Spektralbereich, German Patent DE102011113571.

- M. Elbahri, M. K. Hedayati, C.V. Chakravanhanula, V. Zaporotchenko, T. Strunkus, F. Faupel, Metall-Komposit-Beschichtung mit hoher optischer Transmissivität im visuellen Spektrum, German Patent DE102010050110.

- M. Elbahri, M. K. Hedayati, C.V. Chakravanhanula, V. Zaporotchenko, T. Strunkus, F. Faupel, Metal composite coating having high optical transmissivity in the visible spectrum, WO Patent 2,012,055,397

Peer-reviewed Articles

- M. K. Hedayati,M. Javaherirahim, H. J. El-Khozondar,Mohamed ,A. U. Zillohu, H. J. El-Khozondar, M. Bawa'aneh, A. Lavrinenko, F. Faupel, M. Elbahri, Photo-driven super absorber as an active metamaterial with a tunable molecular-plasmonic coupling, Advanced Optical Materials 2014, doi: 10.1002/adom.201400105.

- M. K. Hedayati, S. Fahr, C. Etrich, F. Faupel, C. Rockstuhl, M. Elbahri, The hybrid concept for realization of an ultra-thin plasmonic metamaterial antireflection coating and plasmonic rainbow, Nanoscale 2014, 6, 6037-6045.

- M. K. Hedayati, F. Faupel, M. Elbahri, Review of plasmonic nanocomposite metamaterial absorber, Materials 2014, 7, 1221-1248.

- M. K. Hedayati, A. U. Zillohu, T. Strunskus, F. Faupel, M. Elbahri, Plasmonic tunable metamaterial absorber as ultraviolet protection film, Applied Physics Letters 2014, 104, 041103.

- C. Etrich, S. Fahr, M. K. Hedayati, F. Faupel, M. Elbahri, C. Rockstuhl, Effective optical properties of plasmonic Nanocomposites, Materials 2014, 7, 727-741.

- R. Abdelaziz, D. Disci-Zayed, M. K. Hedayati, J. Pöhls, A. U. Zillohu, B. Erkartal, V. S. K. Chakravadhanula, V. Duppel, L. Kienle, M. Elbahri, Green chemistry and nanofabrication in a levitated Leidenfrost drop, Nature Communications 2013, 4, doi: 10.1038/ncomms3400.

- M. K. Hedayati, F. Faupel, M. Elbahri, Tunable broadband plasmonic perfect absorber at visible frequency, Applied Physics A 2012, 109, 769-773.

- A. U. Zillohu, R. Abdelaziz, M. K. Hedayati, T. Emmler, S. Homaeigohar, M. Elbahri, Plasmon-mediated embedding of nanoparticles in a polymer matrix: Nanocomposites patterning, writing, and defect healing, The Journal of Physical Chemistry C 2012, 116, 1720417209.

- M. K. Hedayati, M. Javaherirahim, B. Mozooni, R. Abdelaziz, A. Tavassolizadeh, V. S. K. Chakravadhanula, V. Zaporojtchenko, T. Strunkus, F. Faupel, M. Elbahri, Design of a perfect black absorber at visible frequencies using plasmonic metamaterials, Advanced Materials 2011, 23, 5410-5414.

- M. K. Hedayati, M. Javaherirahim, B. Mozooni, R. Abdelaziz, A. Tavassolizadeh, V. S. K. Chakravadhanula, V. Zaporojtchenko, T. Strunkus, F. Faupel, M. Elbahri, Perdect plasmonic absorber: Design of a perfect black absorber at visible frequencies using plasmonic metamaterials, Advanced Materials 2011 (Frontispiece), 23, 5409.

- M. Jamali, M. K. Hedayati, B. Mozooni, M. Javaherirahim, R. Abdelaziz, A. U. Zillohu, M. Elbahri, Photoresponsive Transparent Conductive Metal with a Photobleaching Nose, Advanced Materials 2011, 23, 4243-4247.

- M. Elbahri, M. K. Hedayati, C.V. Chakravanhanula, M. Jamali, T. Strunkus, V. Zaporotchenko, F. Faupel, An Omnidirectional Transparent Conducting-Metal-Based Plasmonic Nanocomposite, Advanced Materials 2011, 23, 1993-1997.

Awards

- Khwarizimi Youth Award (2nd rank in Innovation) in 15th Khwarizmi Youth Festival, The Iranian Research Organization for Science and Technology, Tehran, Iran (December 2013).

- Best Student Poster Award (First Rank), The 7th International Congress on Advanced Electromagnetic Materials in Microwaves and Optics, Bordeaux, France (September 2013).

- SPP5 Student Travel Grant, The Fifth International Conference on Surface Plasmon Photonics, BEXCO, Busan, South Korea (May 2011).

Conferences: Presentations and Posters

- M. K. Hedayati, M. Elbahri, Perfect Plasmonic Absorber for Visible Frequency, The 7th International Congress on Advanced Electromagnetic Materials in Microwaves and Optics, 16-19 September 2013, Bordeaux, France.

- M. K. Hedayati, B. Mozooni, F. Faupel, M. Elbahri, Tunable broadband plasmonic perfect absorber at visible frequencies, 3rd International conference on metamaterials, photonic crzstals and plasmonics (META12), 19-22 April 2012, Paris, France.

- M. K. Hedayati, M. Javaherirahim, M. Elbahri, A smart transparent conductor with a gas sensing ability, 3rd International conference on metamaterials, photonic crzstals and plasmonics (META12), 19-22 April 2012, Paris, France.

- M. K. Hedayati, T. Strunkus, V. Zaporotchenko, F. Faupel, M. Elbahri, Perfect plasmonic absorber at visible frequencies, The 5th International conference on surface plasmon photonics, 15-20 May 2011, BEXCO, Busan, Korea.

- M. K. Hedayati, M. Jamali, T. Strunkus, V. Zaporotchenko, F. Faupel, M. Elbahri, New transparent conductive metal based on polymer composite, 75th annual meeting of the DPG and DPG spring meeting, , 13-18 March 2011, Dresden, Germany.

- M. K. Hedayati, V. S. K. Chakravadhanula, V. Zaporotchenko, M. Elbahri, F. Faupel, Transparent conductors based on metal-polymer composites, Materials Science and Engineering (MSE) 2010, 24-26 August 2010, Darmstadt, Germany.

Contents

Chapter 1

Abstract

Plasmonic metamaterials are artificial materials typically composed of noble metals in which the features of photonics and electronics are linked by coupling photons to conduction electrons of metal (known as surface plasmon). These rationally designed structures have spurred interest noticeably since they demonstrate some fascinating properties which are unattainable with naturally occurring materials. Complete absorption of light is one of the recent exotic properties of plasmonic metamaterials which has broadened its application area considerably. However, up to date all of the applied methods (perforated metallic films, grating structured systems, and conventional metamaterials) are costly and suffer from a lack of flexibility. Furthermore, their absorbance is mainly limited to a narrow spectral range or their fabrication is costly. So, such drawbacks make their vast application almost impossible. Here, in this dissertation, we design, fabricate and characterize a novel perfect absorbers based on nanocomposites whose total thickness is only a few tens of nanometers and its absorption band is broad, tunable and insensitive to the angle of incidence. The nanocomposites consist of metal nanoparticles embedded in a dielectric matrix with a high filling factor close to the percolation threshold. The filling factor can be tailored by vapor phase co-deposition of the metallic and dielectric components. Accordingly, three types of metals (gold, silver and copper) as the inclusions of the nanocomposite and four different mirrors (gold, silver, copper and aluminum) are used as the base layer. The high absorption of these metamaterials are originated from the huge absorption capability of the metallic nanoparticles (smaller than 5 nanometer in diameter) via localized plasmon resonance, confinement of the light within the tiny gap between nanoparticles as well as interference of the light by reflection through the layers. To functionalize the system, polymer-photoswitchable molecules were added as the top or spacer layer which enable us to demonstrate a photodriven perfect absorber in which the absorption band can be broadened or narrowed by ultraviolet or visible light illumination, respectively. In this approach, the absorption tuning is originated from the bond-breakage of the molecules which can be activated by irradiation. Due to the strong interaction of the molecules and metal mirror, plasmon-exciton coupling happens which not only enhances the absorption but also shifts or splits the absorption band. Also as the specific highlight of the idea, we show that a thin plasmonic nanocomposite film on a silicon wafer covered by a silicon dioxide film would diminish the reflection in a broad range of frequency and make a new class of plasmonic anti-reflection coating. Our novel concept (called

hybrid ARC) combines two possible arrangements for the layers in an anti-reflection coating into a single structure; albeit at two different wavelengths. Its performance originates from the strong dispersive nature of the nanocomposite. Furthermore, we show that the current metamaterial on a metal reflector can be used for visualization of different colorations as a plasmonic rainbow despite its sub-wavelength thickness.

Chapter 2

Introduction

2.1 Materials for energy

Air pollution and global warming are two of the furthermost anxieties of human health and political stability. Energy insecurity and rising prices of conventional energy sources such as fossil fuel and atomic energy are the other challenges of the growing society of the current century [1]. One solution to the imminent energy shortage is to adopt renewable energy sources and technologies [2]. Principally, every form of energy in the earth is solar in origin. Oil, coal, natural gas and woods were initially formed by photosynthetic processes and further turned to their known form by long and complex chemical reactions. Even the wind energy has a solar source as it is routed from the temperature differences in dissimilar areas of the earth. Solar energy is more favorable than other resources since it is clean and can be supplied with no ecological contamination [3]. According to International Energy Agency (IEA): "The development of affordable, inexhaustible and clean solar energy technologies will have huge longer-term benefits. It will increase countries' energy security through reliance on an indigenous, inexhaustible and mostly import-independent resource, enhance sustainability, reduce pollution, lower the costs of mitigating climate change, and keep fossil fuel prices lower than otherwise. These advantages are global. Hence the additional costs of the incentives for early deployment should be considered learning investments; they must be wisely spent and need to be widely shared [4]." However, the energy cost of solar industry is still high, and massive efforts is needed to reduce the price. In fact, most of the price of solar panels is owing to the expenses of silicon materials and processing [5]. Consequently, any method which reduces the material quantity of the cells whereas increasing the output would be desired. Among the various strategies which are applied for expenses reduction, deployment of plasmonic metamaterial in solar panels is rather new but it is nowadays considered as a potential approach for realization of more cost effective solar materials. Thanks to the localized nature of the plasmonic system, the thickness of the absorbing layer of solar materials can be considerably reduced [5] which could ultimately lessens the solar energy cost.

2.2 Plasmonic and Metamaterial

Plasmons are resonant modes that entail the interaction amid free charges and electromagnetic waves. Their oscillation originates from the restoring force that the distorted charge distribution applies on the mobile charges as soon as they are dislocated from the equilibrium state [6]. In other words, surface plasmon polaritons are the waves that propagate along the interface of a conductor and insulator [7], evanescently confined in the perpendicular direction [8]. Surface plasmon modes can be localized in space in some nanostructured surfaces or around nanoparticles, with fields confined to a sub-wavelength dimension. On the contrary, flat surfaces allow surface plasmon to spread over a distance determined by absorption in the metal or by geometry [6]. The light-matter interaction is considerably enhanced via light coupling to the material surface (i.e. surface plasmon excitation). Consequently, the incident electromagnetic wave can be confined and localized in an area smaller than that predicted by the diffraction limit resulting in a huge electromagnetic field intensification [9].

Although the concept of plasmonic has drawn the attention of scientists and physicists in 20^{th} century, it has been in use since the first millennium BC when ancient civilizations made use of them for decoration and artistic purposes [10]. A glimpse at the old colored (stained) glasses (e.g. the Roman Lycurgus cup and stained glasses in churches), colorful statues (e.g. the mask of the Tutankhamen's mummy), painted tiles (the Immortal Soldiers at the Darius' palace in Susa and the Ishtar Gate in Babylon) one can observe the range of different colors (blue to red) mainly arose from different metal/metal oxides particles embedded in a dielectric (ceramic) matrix. The colorful facades of the mentioned ancient sculptures might not be only plasmon originated but also the existence of metal/metal oxide particles in their top surface is one of the major reasons of their charming color. [11, 12]. Jaber-ibn-Hayyan, prominent Iranian chemist, was one of the first researchers who wrote a unique treatise of technical recipes dealing with the manufacture of colored glasses, making lustre-painted glass (stained glass) and coloring gemstones in the late 8^{th} century (details can be found in [13]). Recent chemical and microscopic [14] analyses of a selection of lustre ceramics dating from the last quarter of the 10^{th} century AD to the second half of the 13^{th} century AD from Iran, Egypt and Syria as well as those of the 13^{th} century Spanish lusters [15] proved the existence of copper, gold and silver nanoparticles (NPs) as the main coloring components (Figure 2.1). In Figure 2.2, a lustre analyzed by Padovani et al. [16] is shown wherein they found the traces of silver and copper nanoparticles by a X-ray absorption fine structure (XAFS) study on lustred glazes of shards belonging to 10^{th} and the 13^{th} century potteries from the National Museum of Iran [16].

Nevertheless, physical explanation of the plasmonic phenomena was not clear before the first report of Maxwell Garnett in 1904 when he reviewed the work of his contemporary researchers on coloration of silver and gold particles and analyzed stained glasses (as a well known nanocomposite) theoretically [17]. Afterwards, Gustav Mie [18] proposed an exact solution of the Maxwell's equations and provided an easy way to interpret the optical properties of nanoparticles which has been used till nowadays. The plasmonic research has redrawn great attention in the last 3 decades because of considerable advances in production techniques of nanostructure materials (i.e. Nanotechnology). Nowadays the application of

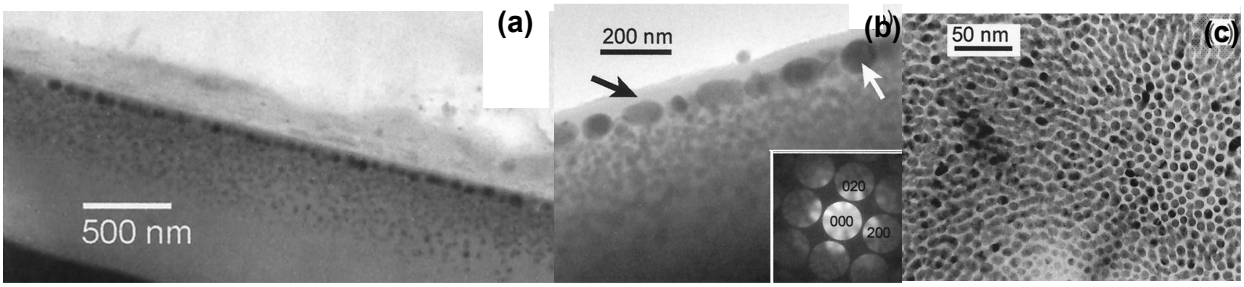

Figure 2.1: *TEM images of a copper-like luster from Paterna, circa the fourteenth century ((a) complete structure of the luster layer and (b) magnification of the outer surface of the luster layer; the inset corresponds to the CBED pattern of a copper particle). (c) TEM image of the inner part of a gold-like luster from Deruta, circa the fifteenth century. (Figure adapted with permission. Copyright 2001, John Wiley and Sons [15].)*

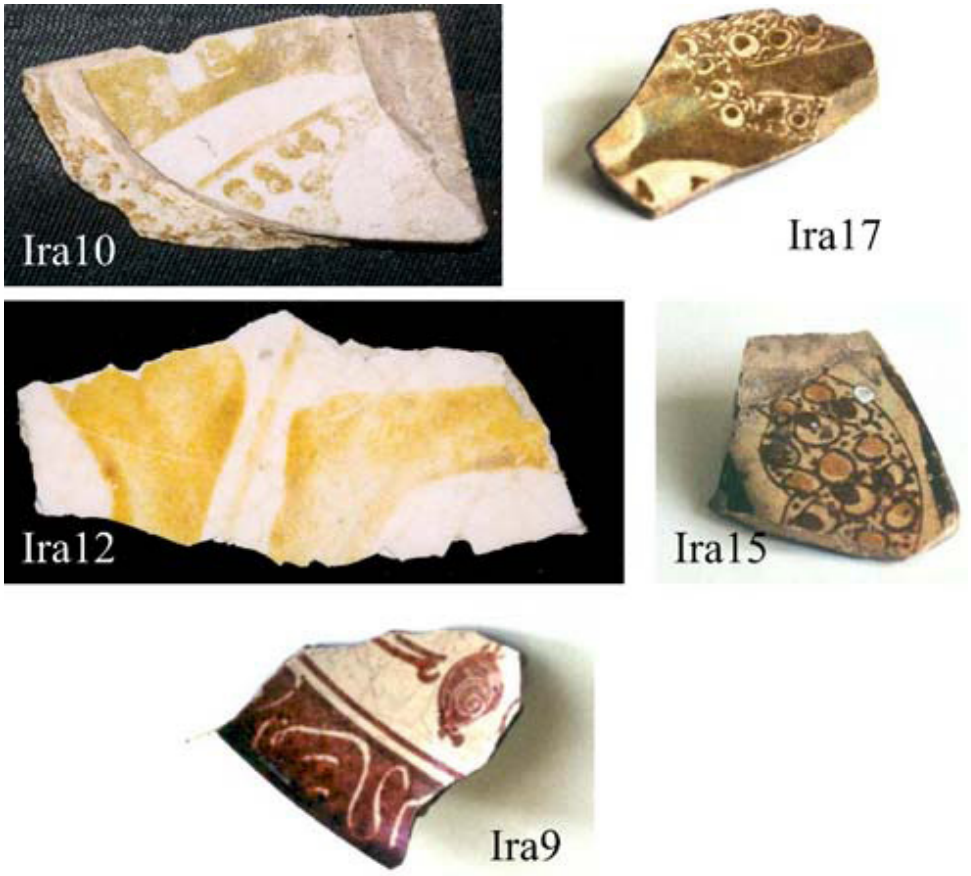

Figure 2.2: *Five shards of a Middle East Medieval lustre pottery, dated on the basis of stylistic criteria by archaeologists of the National Museum of Iran. They belong to excavations in Neishabur, Ray and Kashan and show white glazes enriched with gold or reddish metallic decorations (Figure adapted with permission. Copyright 2006, Springer [16].)*

plasmonics is not limited only to decorative purposes but also a vast number of new potential utilities of this class of nanostructures has been proposed and demonstrated so far such as sensor [19] and catalytic activity [20] to cancer therapy [21], genetics [22] and energy [23]. In particular, now plasmonics researchers are turning their interest on solar cells, where plasmonics could potentially improve absorption, providing a substantial reduction in the physical thickness of absorber layers, and enabling a new alternative for solar-cell design [5]. In that sense, by proper design of plasmonic sustaining nanostructures, the electromagnetic wave can be concentrated and 'folded' into the absorbing layer, thus increasing the absorption [5]. Within the last decade, with the birth of metamaterial, the capability of plasmonics for energy harvesting has become more noticeable than before. In other words, manipulating light at the nanoscale by means of plasmonics is complemented by metamaterials [9].

Metamaterials as artificial materials consist of designed inclusions which can show striking and unique electromagnetic properties not inherent in the individual constituent components. These artificially structured composites could potentially fill the gap in the electromagnetic spectrum where the material response is limited and thereby facilitate building of new devices [24]. Negative refraction [25], artificial magnetism [26], perfect lens (i.e. imaging below the diffraction limit) [27], cloak of invisibility [28], nano-lasing [29] amongst others are the prime applications of metamaterials. Indeed, metamaterials and plasmonics develop a new innovative field in photonics, by which the features of photonics and electronics are merged by coupling a photon to a free electron gas of the metal as surface plasmons (SPs) [30]. Despite early consideration of loss as a major limiting factor against the performance of plasmonic metamaterials, the absorptivity is regarded as a standalone function of them following the first experimental demonstration of metamaterial perfect absorber [31](For details see the review by Padilla and co-workers [32]). Although the initially proposed absorbers were simply designed for a specific frequency (narrowband), the requirement of broadband absorption of light for energy collection initiated the ever growing research which is known today as metamaterial absorbers.

2.3 Metamaterial absorbers

A metamaterial perfect (or super) absorber (MPA) is a device wherein all incident waves are absorbed at the working frequency whereas transmissivity, reflectivity and scattering are hindered [32]. They can be classified into two main categories: resonant (narrowband) absorbers and broadband (multi-band) absorbers. In the resonant absorbers, as the name suggests, resonance at the designed frequency is the origin of high absorption. However, the broadband absorbers usually rely on composite materials (metamaterial) with multiple frequency resonances which are coupled with each other to realize a wide-band light absorption. In both types of the absorbers, the main challenge is the vanishing of reflection. In other words, the reflectivity should be reduced to a negligible value by reducing the impedance mismatch at the interface of two medium. In the following subsections (2.3.1 and 2.3.2), both types of metamaterial absorbers are overviewed.

2.3.1 Resonant (narrowband) perfect absorbers

Perfect absorption of light can be achieved in different frequencies by conventional techniques of optics such as gradient layers [33] and macroporous black metals [34,35]. However either the thickness of the film is high or the absorption completely dissipates through the metals thereby further control of energy flow is unattainable. In metamaterial absorbers, the structure thickness is sub-wavelength and the energy flow can be controlled to some extent via an innovative design. Therefore, in this part, we only overview the trends in narrowband metamaterial absorbers.

The research on metamaterial perfect absorbers started in 2008 when Padilla et *al.* demonstrated the first super absorber [31]. The system consists of two metallic films and one dielectric layer. The top layer is an electric ring resonator (ERR) while the bottom layer is a metallic cut wire. The electric response are provided through the two layers by coupling strongly to impingent electric field at the design frequency. The magnetic response however is realized using anti-parallel currents in the cut wire and the center wire of the ERR. Consequently, any varying magnetic field may couple to these antiparallel currents, thereby resulting in a Lorentz like magnetic response [32]. In other words, by tuning the magnetic and electric response of the structure (via changing the geometry of the cut wire and the separation between the cut wire and electric resonator) independently, they could equalize permittivity and permeability which provide the impedance matching condition. At the resonance (GHz frequency), the reflection and transmission vanish resulting in complete absorption. Authors attributed the loss (absorption) mainly to the dielectric loss which occurs between the two metamaterial elements where the electric field is large. Following

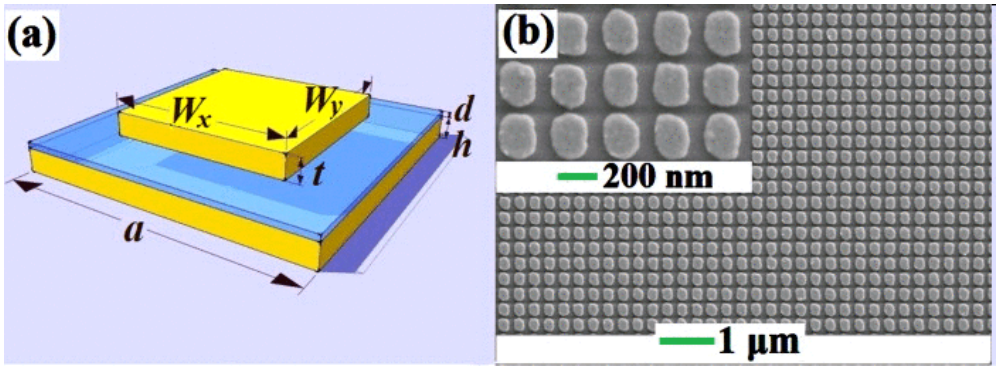

Figure 2.3: *(a) Geometry of the sample studied by Hao et al. [36]. Wx and Wy represent, respectively, the side lengths of the rectangular metallic particle along the x and y axises and t represents its thickness. d and h, respectively, denote the thicknesses of the Al_2O_3 dielectric layer and the gold film. a is the lattice constant. (b) Top view SEM image of the fabricated optical metamaterial absorber. (Figure adapted with permission. Copyright 2010, AIP [36].)*

this report, the trends in metamaterial absorber community started and it initially focused on shifting the resonance to a shorter wavelength (higher frequency). Hence, with slight changes in the pioneering design, highly absorber metamaterials are demonstrated. For

instance in the report by Tao et *al.* [37], the ERR is replaced by a split ring resonator for electrical coupling and the ground cut wire by a flat continuous film. By shrinking the dimension, the authors were able to show the near unity absorption at 1 THz. However, their designed structure was polarization and angle sensitive (similar to the earlier work). This was because of the fact that the light-surface coupling strongly depends on the orientation of the unit cell relative to the incident field. Landy et *al.* [38] significantly solved the problem of polarization sensitivity of the former design by changing the geometry of the top structure. In the new design, an ERR with a fourfold rotational symmetry about the propagation axis was designed and it was therefore polarization insensitive [38]. In a similar work, a terahertz MPA is fabricated based on a simple fishnet metallic film separated from a ground plane by a dielectric spacer, in which a near unity absorption in both polarizations is realized [39]. Liu et *al.* simplified the initial design by replacing the top layer by a a cross-shaped resonator and could achieve near unity absorption in the mid-infrared regime ($6\mu m$) [40].

Complexity of fabrication of the traditional resonators for a higher frequency turned the attention of MPA researchers to a simpler and easily scalable design. The new geometry consisted of metal clusters or cubes above the optically thick metal film while the two layers were separated by a dielectric film. This approach facilitated down-scaling of the operating frequency of MPA to visible and UV. The work of Diem et *al.* [41] is one of the earliest reports based on this novel design in which numerically perfect absorption in THz frequency was demonstrated. This metamaterial consisted of tungsten wire separated from tungsten continuous film by a layer of silicon nitride. In this arrangement a strong resonance with a big field augmentation in the dielectric interlayer and in between the stripes can be obtained. Tuning the size of the top stripes provides the facility to adjust the reflection, and ultimately vanishing it. However, the authors´ calculation shows that the light is partially absorbed by the dielectric and the major absorption occurs at the surface of metallic back plate and the rear side of the top metal structure [41]. Sun et *al.* replaced tungsten with silver in a similar geometry and numerically showed that absorption in different wavelengths can be realized [42].

The experimental realization of perfect absorption in a metamaterial with metallic clusters and film was reported in 2010 by two different research groups. In Qiu´s group [36], they used a rectangular gold cluster atop of aluminum oxide (Figure 2.3) while Giessen and co-workers [43] fabricated gold cylinder atop of a magnesium fluoride film. In both the reports, an optically thick gold film was used in order to suppress transmission. The mechanism of the high absorption is attributed to the excitation of localized electric and magnetic dipoles where the latter originates from circulating antiparallel currents between the top and bottom layer (Figure 2.4). Since the dielectrics used in both the designs were almost loss-less in the operating frequency, the trapped energy is mainly dissipated through the metals [36, 43]. The efforts to shift the realm of high absorption to visible initially faced some technical challenges since the nanostructures with few tens of nanometer in size are needed. Nevertheless, the first narrowband perfect absorber in visible was demonstrated in 2008 [44] in a nanoporous metallic surface. The nanoporous metal surfaces was fabricated by electrochemical deposition of gold above a dense monolayer of latex spheres supported on a gold plate. By removing the latex, unfilled spherical voids will remain which are buried in the gold. The designed structure can simultaneously sustain delocalized SPPs and localized

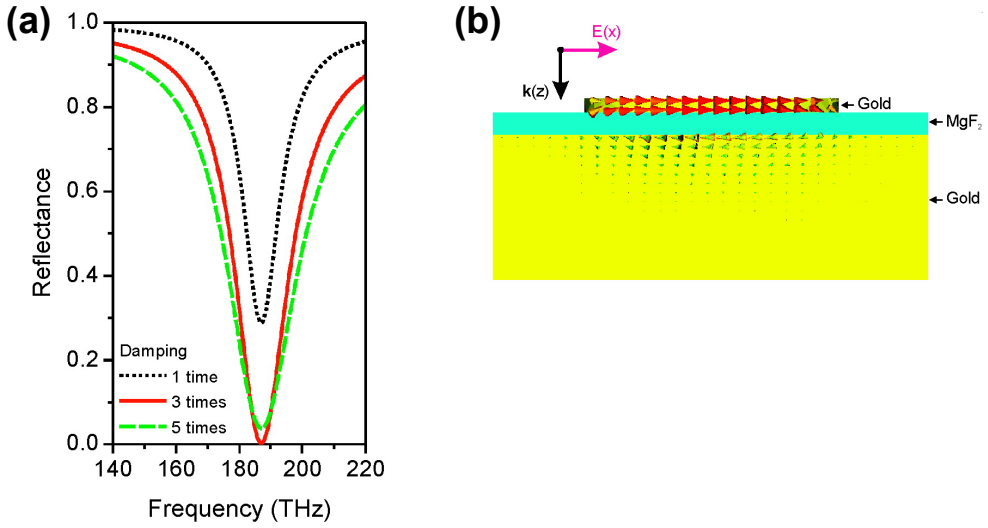

Figure 2.4: *(a) Simulated reflectance spectra in dependence on the damping constant of the gold film. Reflectance with zero intensity is achieved using a damping constant that is equal to three times that of bulk gold. (b) Calculated current distribution at resonance where perfect absorbance occurs. Antiparallel currents are excited in the gold disk and the gold film. (Figure adapted with permission. Copyright 2010, ACS [43].)*

void plasmons. The unique feature of the nanoporous absorber is omnidirectionality and invariance to the incident angle (and polarization) [44]. A narrowband perfect absorber for visible was demonstrated numerically later in a stack of sub-wavelength hole array and thick metal film [45]. In that geometry, the absorption is attributed to the coupling of the light into the top hole array which further couples to the bottom layer. Consequently, no light reflects back and high absorption is achieved. Note that the thickness of the base layer (thicker than the skin depth) already hinders the light transmission completely. Moreover, the successful realization of a narrowband MPA for visible was also demonstrated by the cluster-film geometry which mentioned above [46]. More interestingly, Qiu and co-workers [47] show in a study that the heat generated by the metallic component of the perfect absorber can even lead to reshaping the cluster upon exposure to an intense light. According to their report, by irradiation of the MPA consisted of blocks as the top clusters, the shape of top structure changed to spherical domes by photothermal fusion caused by plasmonic absorption. This approach shows the potential of MPA for photothermal demanded applications such as biotechnology [47].

The common feature of all the narrowband MPAs mentioned above is their physical mechanism in which the magnetic resonance (originated from the antiparallel current within the structure) and electric resonance provide the impedance matching condition and consequently high absorption. However, a numerical study by Chen [48] showed that the assumed significant contribution of magnetic resonance in the impedance matching of MPA to free space is negligible. On the contrary, it is the destructive interference between the direct reflection and the following multiple reflections that in fact confines light in the MPA and ultimately results in the high absorption. He showed that by consideration of the inter-

ference model, surface currents (which are antiparallel in the top and bottom structures) through multiple excitations and superposition can be derived [48]. Accordingly, the very recent numerical study by Shu et *al.* [49] approved the Chen's postulation to some extent where they showed that the high absorption can be achieved even if the top layer is a continuous film (unpatented). They showed that the Fabry-Perot (FP) resonance of the middle dielectric layer plays the major role in this configuration and can provide the narrowband perfect absorption in visible and near-infrared. The simulation of the electric field distribution over the cross-section of the absorber showed that the electromagnetic wave is mainly trapped in the interlayer (dielectric). Moreover, the base metal film not only absorbs the transmitted light, but also supplies a strong reflection (i.e. acts as a mirror) and forms a FP cavity for the dielectric layer [49]. Though the later methodology works well to achieve high absorption in the design wavelength, the structure is much thicker than the conventional MPAs and is not very practical. Although the narrowband MPAs are not efficient absorber for photovoltaics and solar cells, their usefulness in other applications is undeniable. For instance, narrowband MPA could find application as selective emitters, detectors and sensors (radar sensors) amongst others [32].

2.3.2 Broadband (multi-band) perfect absorbers

The trends to design and fabricate broadband MPA were initiated in parallel with its counterpart absorber (narrowband MPA). Kravets et *al.* demonstrated one of the earliest experimental results in this subject in which a broadband absorber for visible is realized based on a thin nanostructured metallic layer shaped in the form of a composite deep diffraction grating [50]. The near unity absorption is demonstrated only for one light polarization and is ascribed to excitation of the localized plasmons coupled to impinging electromagnetic waves [50]. Although the absorption intensity in such a design is high, the polarization sensitivity which is stemmed from the grating geometry would potentially exclude its application as an efficient energy harvesting object. In an other approach, to broaden the absorption band of sub-wavelength hole array and thick metal film MPA (see 2.3.1), Hu et *al.* [51] replaced the top layer (holes array) by a mixed-size sub-wavelength square hole array to enable mixed plasmon resonance coupling (overlapping of resonances). However, the absorption band was widened very small (17 nm) and it acted same as a single band absorber.

A non-resonant broadband absorber was demonstrated by Javey and co-workers in a new dual-diameter nanopillar structure with a small diameter tip for a minimum reflectance and a large diameter bottom for a maximal effective absorption coefficient [52]. But the thickness of such a structure is $2\mu m$ which is even far above the traditional optical absorbers. Lehman et *al.* [53] also showed a very black material (super broadband perfect absorber) with vertically aligned multiwall carbon nanotubes. In analogy to the nanopillars, thickness and mechanical stability are the two major challenges of this absorber. The optimized sample, for instance, needs to have around $16\mu m$ thick nano-tubes.

The broadband MPAs are also demonstrated with combination of old and novel designs. Due to the technological importance of the visible spectrum, the considerable efforts

(mainly successful) are made to shift the realm of absorption to this frequency. A relatively broadband MPA in visible was theoretically investigated by Lin et *al.* [54] in a three-layered structure composed of a lossy dielectric grating as top layer and a lossy dielectric film as the bottom layer whereas the spacer layer assumed to be a low-loss dielectric. An average absorption of above 80% over a range of wavelengths (200 nm) is shown but the presented MPA is highly angular as well as relatively polarization sensitive. The high absorption is attributed to cavity-like resonance (for both the polarizations) as well as the weakly bound surface wave (for TM polarization). In fact, the electromagnetic field is confined within the grating structure, resulting in a strong absorption [54].

In a very different approach to that of conventional metamaterials, Kravets et *al.* [55] designed a new absorber where the whole three layers are replaced with one layer of composite in which the silver clusters are incorporated in an alumina matrix. The thickness of the nanostructured films was 150-160 nm and the diameter of silver particles varies from 100 to 120 nm. This MPA shows a broadband absorption in visible. Physically, the cause of the strong absorption is the excitation of localized plasmons in the isolated silver particles. Owing to dipole-dipole interaction among ensemble of particles and coupling between localized plasmon, the resonances broaden and hence realize a wideband MPA [55]. Although this approach seems to be applicable for solar (heat) collectors, the lack of metal back plate in this design is very detrimental. Generally, the metal mirror is used in solar selective coating to provide high reflection (no emission) at longer wavelengths (near-infrared) to keep the efficiency high. Application of such an approach for solar cells is very unlikely, too. If such a black coating is deposited on any solar cells, no light can reach the cell for generation of hole and electron because of the lack of transparency. In addition to the mentioned limitations, the big size of the nanoparticles imposes a restriction on thickness of the film. In other words, the film should be in the range of 150-160 nm to encompass the particles thereby further thinning of the coating is infeasible.

Inspired from structuring of silicon surface for solar cells, Mo et *al.* [56] proposed that coaxially tapered holes could be an alternative for broadband MPA in visible. Their numerically designed and analyzed structure revealed absorption of more than 88% over a very large wavelength range (300 to 750 nm). Given that the central truncated cone in each hole makes a gradual reduction of the effective index of the film from the base to air (i.e. gradient refractive index), the reflectivity of the structure vanishes significantly. On the other hand, the structure of the top surface enhances the diffraction toward the base. Therefore, the absorption of this structure is considerably higher than that of a flat gold film. Bozhevolnyi and co-workers also used the texturing of a metal surface in order to achieve wideband perfect absorber (Figure 2.5) [57] but in a different geometry to that of Mo et *al´*s. [56]. They realized a non-resonant super absorber in a geometry composed of ultra-sharp convex metal grooves in which adiabatic nano-focusing of gap surface plasmon modes excited by scattering off subwavelength-sized wedges provides the high absorption. The absorption band of the designed structure spans the whole visible with high intensity. Although these classes of broadband absorbers are not practical for application in solar cells, they could find utility in thermophotovoltaics. Following the structuring strategy for achieving high absorption, Cui et *al.* [58] demonstrated an ultra-broadband thin film but in infrared absorber made of sawtoothed anisotropic metamaterial. According to their investigation, shorter wavelengths

electromagnetic waves are harvested at upper parts of the sawteeth of smaller widths, while those of longer wavelengths are trapped at lower parts of larger tooth widths. The observation is attributed to the slowlight modes in anisotropic metamaterial waveguide. In fact, reflection of the impinging light vanishes due to the gradual change of effective index from air to the bottom of the sawteeth which further contributes to absorption enhancement [58]. These researchers also demonstrated in other similar works, that a structure consisted of a periodic array of metal-dielectric multilayered quadrangular frustum pyramids results in an ultra-wide spectral band. Since these pyramids possess resonant absorption modes at multi-frequencies, overlapping of the resonances leads to the total absorption of the incident waves in a wide range of frequency [59]. In an other approach presented by Bozhevolnyi and co-workers [60], a three layers structure is used to fabricate a broadband MPA. But instead of a structured film as the top layer, a periodic array of differently sized and circularly-shaped gap plasmon resonators was used. In such a design, the perfect absorption originates from the localized gap surface plasmons whose resonant excitations only weakly depend on the angle of incidence. Because of the huge field localization by the particles, the authors envision that such arrays can have profound applications in single molecule SERS and in the design of ultrathin highly absorbing photovoltaic devices provided that the SiO_2 layer is replaced by an active semiconductor [60]. Atwater and co-workers [61] also demonstrated a highly absorbing system in a three layers MPA (metal-insulator-metal stack) in which the top layer consisted of crossed trapezoidal arrays of silver. In their design a trapezoid arrays were utilized to broaden the spectra while a crossed symmetric arrangement was implemented to enable a polarization-independent resonant response [61]. Though this 260 nm thick structure yields broadband and polarization-independent resonant light absorptions in visible, its average measured absorption (71%) was relatively far below unity (100%). In the work of Xue et *al.* [62], the number of three layers is increased to five in order to broaden the absorption bandwidth. The new designed structure consists of a two-dimensional periodic metal-dielectric-metal sandwiches array on dielectric/metal substrate and its overall thickness measures 230 nm. Their numerical investigation on this structure showed that a MPA with a bandwidth of about 50 nm in visible region can be achieved. The absorption is attributed to overlapping of two plasmon resonances: one originating from the coupling of electric dipoles between neighboring unit cells and another stemming from magnetic dipole plasmon resonances. Field distribution studies revealed that a magnetic hot spot appears in the dielectric, hence one of the two resonances (at the shorter wavelength) was attributed to the multiple magnetic dipole plasmon resonances induced within a single unit cell while the resonance at the longer wavelength was associated with electric resonance. Nevertheless, the bandwidth of the absorber is rather narrow (50 nm) which limits its utility as a solar absorber [62]. Recently, Qiu and co-workers [63] demonstrated a broadband MPA but operating in infrared in a three layers metamaterials in which the top layer was random metallic nanorods. Due to the diversity of the size and randomness of the chemically synthesized gold nanorods, the resulting absorption resonance was broad [63]. There have been some other unique methods for fabrication of broadband perfect absorbers [64,65], but either they are not categorized under MPA or their thickness is too large which exclude them from application in modern energy harvesting devices.

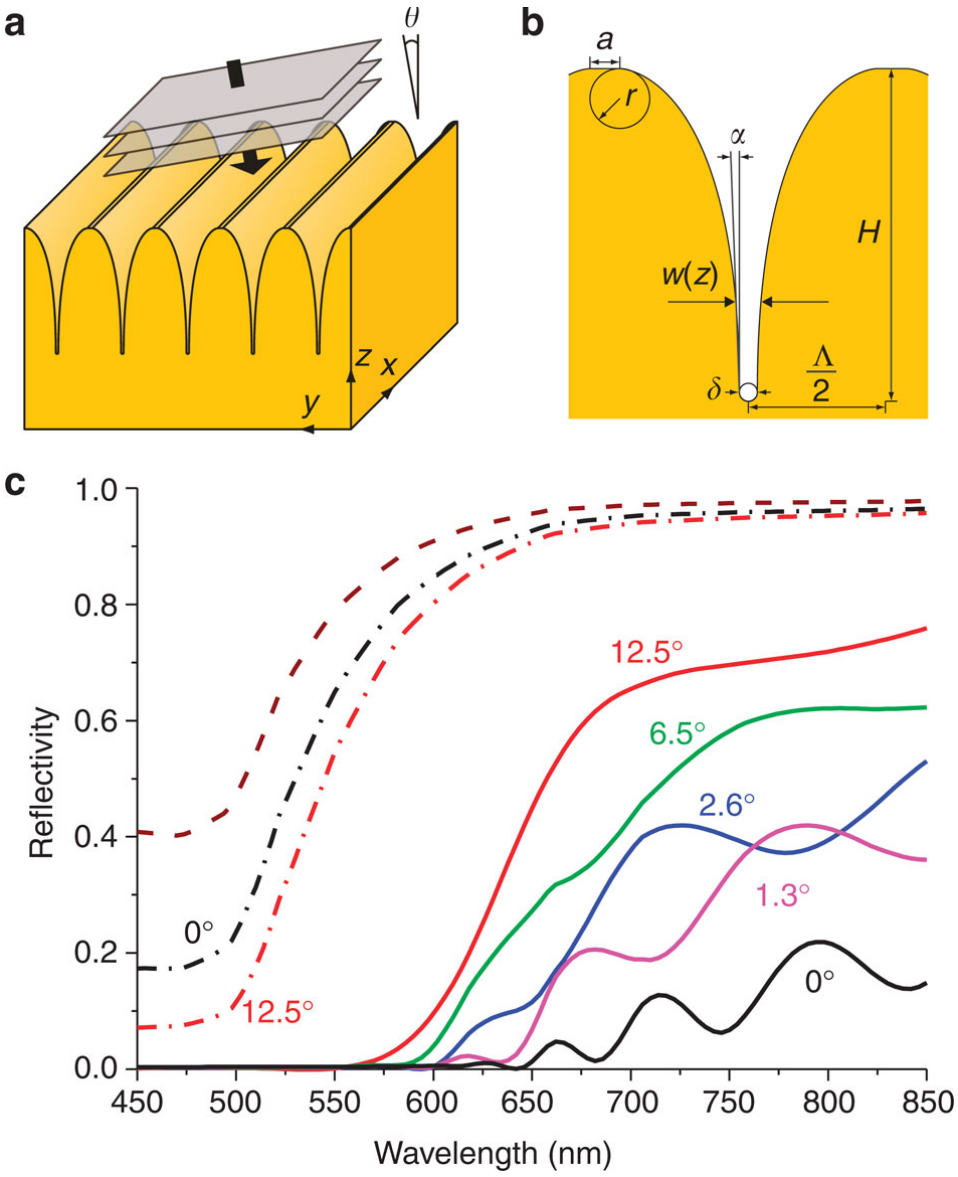

Figure 2.5: *(a) Schematic of the considered configuration, showing orientation of a groove array and incident plane wave, whose phase fronts are represented by grey squares on the arrow indicating the propagation direction of incident light. (b) Geometrical parameters defining the profile of groove arrays. (c) Reflectivity spectra calculated for 250 nm period arrays of 500 nm deep grooves with the following parameters kept constant: $a = r = 10$ nm. Solid lines correspond to the reflection spectra of p-polarized light (which in our case is polarized along the y axis) calculated for normal incidence ($\theta = 0°$) and a minimum gap width ($\delta = 0.3nm$) (which is close to the gold atom diameter), and for different inclination angles: $\alpha = 0, 1.3, 2.6, 6.5, 12.5°$. Reflectivity spectrum for a flat gold surface is shown with a dashed line. Reflectivity spectra for s-polarized (which, in our case, is polarized along the x axis at normal incidence) light are shown with dash-dotted lines for two limiting inclination angles: $\alpha = 0, 12.5°$. (Figure adapted with permission. Copyright 2012, NPG [57].)*

2.3.3 Switchable metamaterial perfect absorbers

Realization of dynamic functionalities such as tunability and switching of electromagnetic waves are current formidable technological challenges in the metamaterials research [66]. The field of MPA is not an exception in that sense, and hence efforts are focused on introducing functionality to the currently available absorbers by an innovative design. One of the initial approaches to enable switching in MPAs was the integration of diodes into the structures. For instance, Zhu et *al.* [67] showed that in the metamaterial consisted of dipole mode electric resonators coupled by microwave diodes on one side of a dielectric substrate and metallic ground plane on the other side, the absorption frequency can be shifted. In other words, through forward or reverse biasing the diodes, the coupling between the resonators can be tuned and result in realization of MPA with a dynamically controlled absorption band in GHz [67]. Jiang and co-workers [68], demonstrated an electrically active MPA in a similar approach to that of Zhu et *al.* but with some design changes. This MPA consisted of arrays of the electric-LC resonators on the top layer of a dielectric substrate and metallic film on the bottom layer. The resonators are connected as a pair by a diode to enable dynamical change of the resonance by an external bias voltage. This MPA could switch between a complete absorber to reflector by applying the appropriate voltage (Figure 2.6) [68].

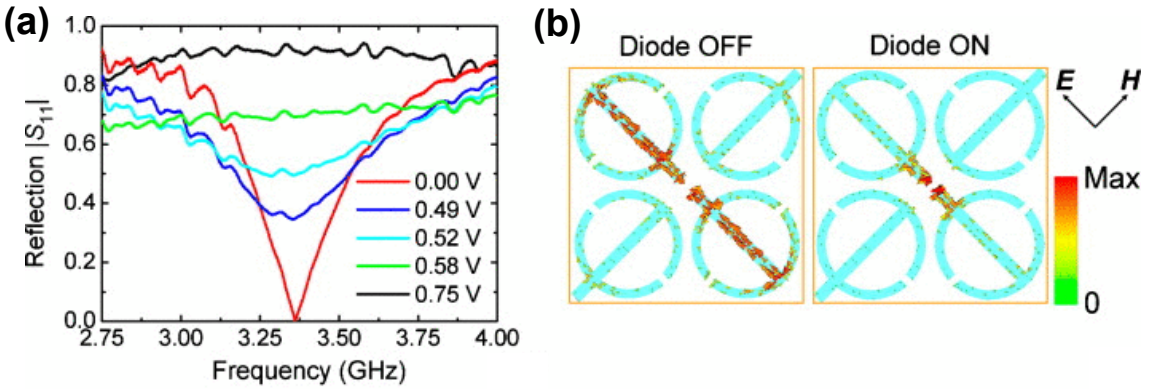

Figure 2.6: *(a) Measured reflection (|S11|) under normal incidence at different forward bias voltages (indicated in the inset). (b) Surface current density distribution on ELCs at peak absorption frequency for one particular polarization. (Figure adapted with permission. Copyright 2010, AIP [68].)*

Real-time control of the optical properties of MPA by light is achieved in a work by Zhao et *al.* [69] in which they realized a dual-band plasmonic absorber by integrating a photosensitive nematic liquid crystal (PNLC) layer onto a traditional design of MPAs. In the designed metamaterial, the top layer particles were asymmetric gold nanodisk array to enable multiple resonance. The dynamic functionality arises from the photosensitivity of PNLC routed from the azo-dye dopants with a photo changeable refractive index. Accordingly, they showed that up to 25 nm resonance tuning can be achieved with this geometry due to the refractive index adjustability of the PNLC [69]. Similar to that, Padilla and co-workers [70] used a liquid crystal (LC) to enable dynamic response of PMA. To do so, they

incorporated LC into the spacer layer of conventional PMA in which the top layer is an electric ring resonator (ERR). They showed that the absorption can be modified by 30% at 2.62 THz, and the resonant absorption can be tuned over 4% in bandwidth, by applying a bias voltage [70]. Despite of growing demand and interest in switchable metamaterial absorbers, the field is still immature and extensive theoretical and experimental studies are needed to realize a robust smart MPA.

2.4 Antireflective coating (ARC)

Reflection of light (light bending power) from interface of two medium is a property which can be appreciable in the case of mirrors however in some optoelectronic devices it is considered as loss. Hence, the later motivated scientists to develop a methodology in order to reduce the reflection loss at the interface. Classically proposed by Rayleigh back to 1879, he showed that the reflectivity at any surface can be reduced provided that the transition of refractive index between the two medium is small [71]. But according to Raut et *al.* [72], a real anti-reflective coating was produced in 1817 by Fraunhofer who observed the reflection reduction after surface etching (texturing). A decade after Rayleigh's work, H. Dennis Taylor a famous English lens designer in 1892 observed that the camera lenses which had become tarnished permitted taking of photographs with a less exposure [73]. In fact, he discovered a decrease in reflection associated with the tarnish on a glass surface [74]. Some years later, F. E. Wright who was working on intentional tarnishing of glass surfaces by chemistry suggested an explanation. He attributed the low reflection of the tarnished glass to creation of a gradual transition of the refractive index from glass to air upon tarnishing [74] which was indeed the Rayleigh proposal and calculation. Generally, the reflection of p- and s-polarized light at the planar interface between two semi-infinite, homogeneous, isotropic media is governed by the well-known Fresnel coefficients [75, 76]. Indeed, physical explanation of majority of the ARCs is similar, nevertheless glare reduction is basically realized either by texturing surfaces or by providing a gradient refractive index layer atop of the substrate.

2.4.1 Structured surface as ARC

In the earlier method, the surface texturing (structuring) with a cross sectional dimension less than that of the incoming light, acts as a medium with spatially varying refractive index [77]. On the other hand, a structure with spatial dimensions comparable or bigger than the impinging electromagnetic wave mainly scatters the light but it does not necessarily enhance the transmission. As it is mentioned above, Fraunhofer seems to be the first user of this concept to realize an ARC. A century later than that work, a biomimetic approach which provides an anti-glare surface is introduced which is known as the "moth's eyes" structures [78]. This idea was initiated upon electron microscope investigation of the corneal lenses of moths. It was observed that the outer surface is covered in a regular array of conical protuberances, typically of about 200 nm height and spacing [79]. However, one of the mostly studied and used methodologies is the pyramidal texturing of silicon for solar

cells. By using the anisotropic etches of the surface, square based pyramids are formed on the surface defined by intersecting (111) crystallographic planes [80]. Although this method has been widely used in solar industry, its large thickness excludes applying it for the state of the art thin film solar panels.

The advances in nanofabrication facilitate the development of new designs of the structuring based ARCs. One of the most efficient ARCs ever realized is reported by Huang et *al.* [81] where they demonstrated that randomly etched nanotips atop of silicon wafer could provide the condition of a super broadband ARC (2200 nm bandwidth). The low reflection is attributed to the changes in the refractive index caused by variations in the height of the silicon nanotips (fine refractive index gradient) [81]. Chhajed et *al.* [82] realized a graded-index antireflection coating using nanostructured low-refractive-index silica deposited by oblique-angle deposition. By this approach, the refractive index of silica (SiO_2) film reduced from 1.47 to around 1.07. By applying such a low index material as the top layer of traditionally known two layers ARC, they could vanish the reflectivity considerably due to the establishment of refractive index gradient [82].

Besides all the mentioned surface structuring methods to enable reflection reduction, plasmonics and metamaterials also contributed to the field of ARCs. In this new approach, metallic particles or structures are placed atop of the reflecting substrate (e.g. silicon wafer). Due to a preferential forward scattering by the plasmonic structures [83–88] or electromagnetic confinement around the top particles [89–92], the reflectivity is strongly reduced, hence allowing nearly perfect impedance matching of light into the substrate [93]. Nevertheless, the light is partially absorbed by the plasmonic structures which makes it different to that of the conventional ARCs. For instance, Polman and co-workers [93] demonstrated that the silicon reflectivity can be considerably reduced by deposition of silver nanostructures atop of Si_3N_4 layers because of the combination effect of plasmon scattering toward the substrate as well as interference through the dielectric film (Figure 2.7) [93]. These types of ARCs are not only limited to metals but also non-metallic scatterers can provide the similar achievement. Spinelli et *al.* [94] demonstrated experimentally that an array of low aspect-ratio Si nanocylinders etched into a Si wafer exhibits an average reflectivity as low as 1.3% in the 450-900 nm spectral range. The resonant Mie modes of the nanostructures strongly interact with the incident light. Their coupling to the substrate results in a strong preferential forward scattering due to the high-mode density in the high-index substrate, thereby vanishing the reflection [94]. Although these novel metamaterials/plasmonic methods are still being studied in research labs, their miniaturized structure and low materials cost associated with their low thickness make them an outstanding candidate for future industrial use.

2.4.2 Gradient film (structure) as ARC

A substitutive choice of vanishing reflectance is to gradually reduce the refractive index of the film from the refractive index of the substrate to the refractive index of the surrounding (mainly air) [72]. This approach has been widely implemented and studied within the last century. Fabrication of the gradient index layers is performed by different techniques. Making the top layer of the substrate porous intentionally by chemical etching, is one of

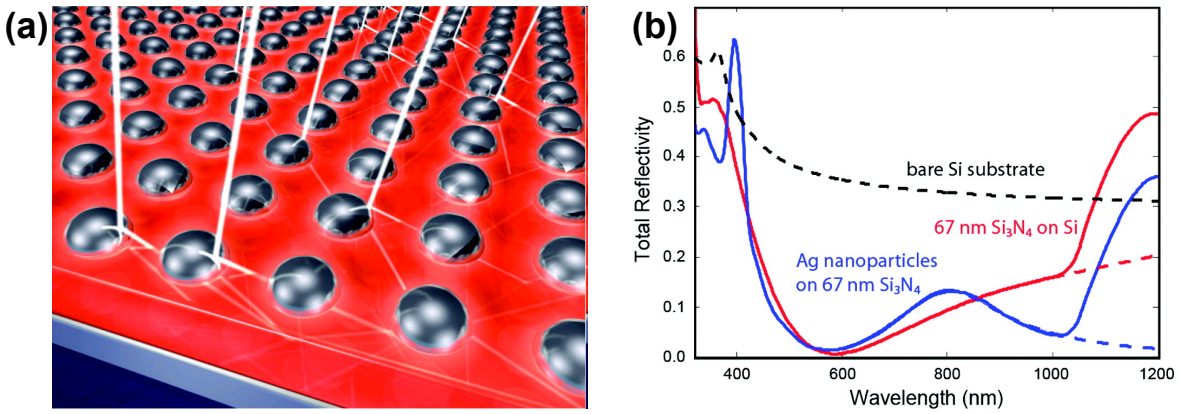

Figure 2.7: *(a) Schematic of the studied configuration by Polman and co-workers [93] (b) Measured total reflection spectrum from a* $300\mu m$ *crystalline Si cell coated with 67 nm* Si_3N_4 *(red) and the same sample with an optimized Ag particle array on top (blue). The particles reduce the reflection for wavelengths above 800 nm, improving the incoupling of light into the Si substrate. The dashed lines are extrapolated data representing the reflection from a semi-infinite substrate. The calculated reflectance of a semi-infinite Si substrate is shown for reference (dashed black line). (Figure adapted with permission. Copyright 2011, ACS [93].)*

the easiest and least expensive methods which has drawn the attention of ARC researchers considerably.

An etchant material removes/dissolves certain leachable components at the surface and leaves or re-deposits other components so as to form a skeletonized, porous surface which possesses a lower refractive index than that of the substrate [95]. These methods were extensively studied in the middle of the 20^{th} century [96, 97]. Instead of using glass, creation of porous polymer is an other alternative to realize a gradient index ARC [98]. For instance, Li et *al.* [99] implemented a similar idea by spin-coating of the solution of a polystyrene (PS)-block-poly(methyl methacrylate) (PS-b-PMMA)/PMMA blend onto an octadecyltrichlorosilane (OTS)-modified glass substrate. Thus, a gradient distribution of PMMA domains in the vertical direction of the entire microphase-separated film is obtained. By following the processes, the PMMA domains are removed leaving a PS porous structure with a gradient refractive index in vertical direction (normal to the surface). Therefore, they could achieve high transparency in visible and infrared due to the strong ARC performance of the porous film [99]. This process later was systematically investigated and improved by Li et *al.* [100]. For more detailed information on polymer based ARCs, the readers are referred to the review by Li et *al.* [101] and the references therein.

Besides the porosity based approach mentioned above, using a double-layers ARC wherein the refractive index gradually descends towards the substrate is an other alternative which is even in use nowadays. One of the prime advantages of the double-layers ARC to that of porous layer, is mechanical robustness. Nevertheless, the limited number of available dielectric materials with low refractive index, restricts the applicability of the double-layer method. Note that the multi-layers ARCs are other alternatives, but because of their large

thickness and materials cost, they are not competitive with the state of the art design of ARC and we do not review them here.

For double-layer ARCs, the top layer facing air normally has the lowest refractive index and the other layer(s) is (are) arranged consecutively according to ascending order of their refractive indices. The other requisite condition of this class of ARC, is the thickness of film which should satisfy the interference condition. In other words, the thickness of each individual layer is generally quarter or half of the incident wavelength. For the case of the double-layer ARC, once the optical thickness is equal, i.e.:

$$n_1 \times \mathrm{d}_1 = n_2 \times \mathrm{d}_2 \tag{2.1}$$

the necessary and sufficient index condition for a double-layer coating to give a zero reflectance is [72]:

$$n_1 \times \mathrm{n}_2 = n_0 \times \mathrm{n}_s \tag{2.2}$$

where n_0,n_1, n_2 and n_s are the refractive indices of the air, top layer, second layer and subtrate, respectively. d_1 and d_2 represnet the thickness of top and second layers, correspondingly. Because of the high refractive index of silicon, two layers of SiO_2/TiO_2 [102] or SiN/SiO_2 [103], MgF_2/ZnS [104] would suffice the above condition and are being used for the silicon based opto-electronic devices. In the last few years, by some innovative designs, new ARCs are fabricated which consolidate both the porous and double layer approaches in order to increase the efficiency of the ARCs. For instance, Xi et *al.* [105] try to combine the both porous and multilayer base ARCs to enable very broad reflection vanishing. To do so, they obliquely deposited SiO_2 to create a film with low density (and low refractive index) atop of a TiO_2 film. By proper control of deposition, they were able to realize a smooth gradient film possessing a refractive index gradient starting from 1.05 up to 2 in very small step. Since the substrate was AlN with a 2.05 index, the performance of their developed gradient-ARC was near to ideal [105]. In analogy to this work, Chhajed et *al.* [106] used a two layers ARC where the first layer possessing a lower density compared with the second layer while the both were SiO_2. For the same reasoning explained above, a braod band ARC is realized [106]. Very recently, Ha et *al.* [107] developed a new design in which the substrate surface is initially textured and then covered with a polymer film. Therefore, they could realize a virtual two layers ARC where the top layer is a low index polymer and the second layer is a polymer-silicon rods composite (Figure 2.8). In such a gradient layer, a broadband ARC is demonstrated. In other words, they have made use of gradient, structuring and quasi-double-layer approach in order to reduce the reflectivity significantly. Nevertheless, the reflection reduction that they achieved was less than previous reports [107].

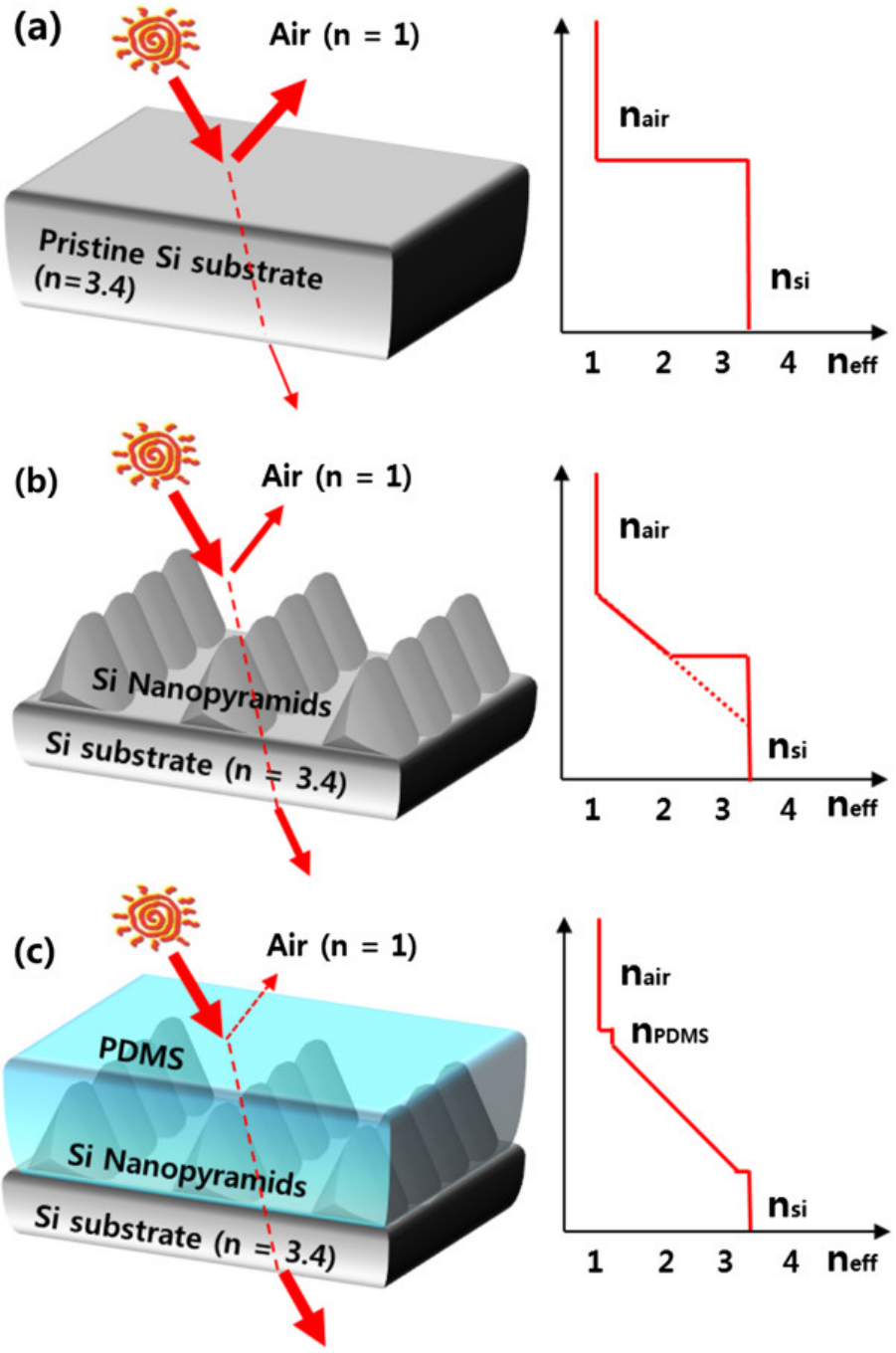

Figure 2.8: *Structure and effective refractive index profiles of various Si models. (a) Pristine Si. (b) Si nanostructure. (c) Si nanostructure deposited via poly(dimethylsiloxane). (Figure adapted with permission. Copyright 2014, Springer [93].)*

2.5 Introduction of thesis

In the present work, a plasmonic metamaterial is designed and fabricated in the frame of nanocomposite consisting of metallic particles embedded into an insulating matrix in order to realize a perfect absorber and a novel antireflective coating. Although the basic geometry of the designed stacks for both the applications (MPA and ARC) are rather similar, there are some dissimilarities which differentiate the highly absorbing system from that of low reflecting structures. For a MPA system, a three layers metamaterial composed of (from base to top) an optically thick metallic film (mirror), a thin dielectric as spacer layer and ultrathin metal-dielectric nanocomposite was designed and fabricated. We found out that for any reflective substrate (R >30%), irrespective of the type and the nature of the spacer layer, the current approach could diminish the reflection thoroughly provided that proper selection of variables is made. Accordingly, we present here that various type of composites ($Ag-SiO_2$, $Au-SiO_2$, $Au-PTFE$, $Au-TiO_2$ and $Cu-PTFE$) on different types of substrates (Au, Ag, Cu, Al) could realize a broadband absorber in visible, though the bandwidth and shape are different. The physical origin of the huge absorption in all combinations of layers is attributed to three main reasons: (i) high absorption of the near percolating spherical particles which is further intensified by creation of hot spot in the small free gap between them, (ii) multiple reflection of light from the base mirror which increases the chance of light trapping among the excited particles, and (iii) destructive interference of the incident light and the reflected one at the interface due to the impedance matching of the system to that of air. Although the mentioned physical phenomena are the major contributors to light absorption in our ultrathin MPA, we do not exclude the possible scattering of the impinging light through agglomerated bigger particles which would considerably reduce the reflectivity.

As mentioned above, all combinations of metals and dielectrics enable us to realize a broadband MPA. However, the intrinsic absorption frequency of the metals utilized in the nanocomposite determines the absorption band maximum and intensity. Considering the bandwidth of different MPAs, the gold based composite outperforms the other alternative composites because of two main reasons. Firstly the plasmonic absorption band as well as its transition band frequency are located in visible, thereby providing the higher absorption in this regime. Secondly, the stability of gold against oxidation, irrespective of the surrounding matrix, is an other unprecedented advantage. Note that the copper based MPA showed a very broad and intense absorption in analogy to gold, but its durability is much less than that of gold. In short, the current approach is enjoying ease of fabrication, has low production cost and possesses high efficiency in the sense of absorption intensity, band-width and angular sensitivity while being ultrathin (20 nm).

For antireflection metamaterials, a silver-silicon dioxide composite is selected as the top layer due to the low absorption loss of silver in visible. In other words, low value of imaginary part of refractive index is one of the prime advantages of silver to other plasmon sustaining metals which turns the attention of researchers to silver for solar absorbers. Herein, we showed that an ultrathin silver-silicon dioxide composite atop of a silicon oxide coated silicon wafer vanishes the reflection in a wide range of frequency enabling realization of a metamaterial based antireflective coating. To reduce the possible loss due to the absorp-

tion of silver, a low filling factor was chosen. Numerical analysis showed that the composite as an effective medium provides a dispersive material where its refractive index is greater (smaller) than that of the spacer layer below (above) the resonance frequency. Below the plasmon resonance wavelength the layer acts as a traditional graded-index coating while it performs as a Fabry-Perot interferometer at longer wavelengths. Therefore, our plasmonic metamaterial based ARC enables us having two different geometries in one design, due to its strong dispersive nature, hence we name it hybrid ARC. Indeed, one could vanish the reflectivity of silicon with other metal based composites, but the extensive loss of other metals excludes them as potential alternatives. The designed ultrathin hybrid antireflector enables us to demonstrate different interference colors by changing the filling factor. On the other hand, we could show that such a plasmonic metamaterial provides a new degree of freedom for creation of interference colors on the metal surface where changing the filling factor of composite (i.e. alteration of refractive index) determines the color while the film thickness of the coating is kept constant. With that potential of our metamaterials, we demonstrated a plasmonic rainbow where the different colors of light are realized in a 45 nm stack of gold composite with a silicon dioxide spacer atop of a gold mirror.

Within the frame of current PhD work, we realized a new optically driven active (dynamic) metamaterial in which the absorption band and intensity can be tuned in real-time via ultraviolet and white light illumination. In order to control the optical response of the absorber, photoswitchable molecules were incorporated to a polymer matrix to design and fabricate a smart perfect absorber. Spirophenanthrooxazine molecules are mixed with a Polystyrene solution and the mixture was spin-coated on an optically thick metallic film. It is found that such a stack has a unique optical property in a sense that its absorption band can be tuned upon ultraviolet (UV) radiation. In other words, the high absorption (almost unity) of such a hybrid system can be dynamically broadened by UV irradiation giving rise to the realization of a photoswitchable perfect absorber. In order to show the potential of this active metamaterial as plasmonic modulator, we integrated the polymer-dye composite as the spacer layer of the perfect absorber stack. Accordingly, by placing of composite within the cavity of a plasmonic perfect absorber, we demonstrate a tunable weak to strong coupling with a 780 meV (270 nm) energy difference between the two peaks after UV illumination. The presented experimental data could open a new pathway for utilization of perfect absorbers as a remote optical sensor or plasmonic switch or modulator.

The current dissertation is based on 6 articles in which the author of the current dissertation was the first author and the main contributor. After the current introduction (overview), experimental procedure of the whole dissertation is presented in details as chapter 3. Then, a review on plasmonic nanocomposites (chapter 4) is shown wherein we focused on our achievements in the field and the future of metamaterial absorbers is discussed. In chapter 5 our paper on perfect absorbers based on gold and silicon dioxide is presented in which the potential of such a metamaterial as a coating for flexible substrates is demonstrated. The next chapter (chapter 6) consists of experimental study of the optical properties of a copper-polymer ($PTFE$) nanocomposite and copper film as a perfect absorber. It follows by a silver-silicon dioxide perfect absorber (Chapter 7) designed for UV-A regime. Accordingly, the absorption is compared with traditional UV protective films and the advantage of our metamaterial to a conventional dye absorber is demonstrated. In chapter 8, the concept of

our novel anti-reflective coating is introduced and experimental verification of the concept (hybrid concept) is shown. Moreover, the potential of tunable plasmonic metamaterials for creation of color in thin film (Rainbow) is discussed and shown. The chapter 9 is experimental demonstration of an active metamaterial in which the absorption band and intensity can be tuned externally. Moreover, the possibility of transition between the weak to strong coupling in the metamaterial is shown. The last chapter (chapter 10) consists of the summary of the dissertation and an outlook.

Chapter 3

Materials and Methods

Within the course of the present PhD work, various instruments and materials were used. In the current chapter, specifications of the materials and instruments as well as conditions of the experiments are briefly presented. General principles of the instruments and the relevant theoretical background are not discussed here and can be found in the cited references.

3.1 Materials

$1,3-Dihydro-1,3,3-trimethylspiro[2H-indole-2,3-[3H]phenanthr[9,10-b](1,4)oxazine]$ powder which will be named as SPO in the rest of this dissertation was obtained from Sigma Aldrich. This molecule is the element that was used as a photochromic dye [108] for production of a photoswitchable film and composite. Polystyrene (PS) powder was purchased from Sigma Aldrich and dissolved in toluene to be used as the matrix of composite.

3.1.1 Targets

A gold target with 99.99% purity was made by *robeco* (Germany) while its diameter and thickness were 51 mm and 2 mm, respectively. A SiO_2 round target with 99.99% purity was provided by Wiliams ADVANCED MATERIALS with diameter and thickness of 50 mm and 2.5 mm, respectively. The silicon dioxide target was bonded to a WAM supplied Cu backing plate with the following dimensions: 50 mm Diameter and 3 mm Thickness. A silver target was provided by Goodfellow GmbH with 99.99% purity and 50 mm diameter and 6 mm thickness. $PTFE$ targets were cut (from the commercial $PTFE$ sheets) in a round shape in order to be fitted into the head of magnetron. Since the $PTFE$ was mainly used for co-sputtering with some metallic targets, it was contaminated with the trace of second metal. Therefore, the target was replaced with a new one very often in order to avoid the side-effects of trace materials.

3.1.2 Substrates

A glass substrate was provided by EYDAM (Thermo SCIENTIFIC (MENZEL-GLÄSER)) with the following dimension: $76 \times 26 \times 1\ mm$. $4''$ Silicon wafers were mainly used as the silicon substrate. They were doped by phosphor (n-doped) and had the resistivity of around 10 $ohm.cm$. The thickness of the wafers were 525 μm and were polished from one side. Because of the size limitation of the analytical tools and also to make sure about the uniformity of the films and composite, the glass and silicon substrates were cut into the size of around $25 \times 25\ mm^2$. All the samples were cleaned by an isopropanol solution and dried by cleanroom's wipes (dastex). For attaching the samples to the substrate a black tape was used. To clean the remnant of the tape from the sample's back-side, cleaning by Isopropanol and wiping by cleanroom's wipe after detaching were performed.

3.2 Metal and nanocomposite film preparation

3.2.1 Cleanroom specifications

Majority of the sputtering deposition of the samples presented in the current dissertation was performed in the cleanroom of Faculty of Engineering, University of Kiel. The white area of the cleanroom was classified as 100 (ISO 5) while the gray area was 1000 (ISO 6). It means that the number of permitted particles of size 5 μm or bigger per cubic meter is 29. The temperature of the environment was controlled continuously and kept at 22°C±2 and the humidity was controlled in the range of $45\% \pm 10$.

3.2.2 Magnetron sputtering chamber specifications

Magnetron sputtering [109] was used for deposition of the films and composites of various types and compositions. The chamber which was used in all experiments (i.e. composite and films) was specially designed and developed in chair for multicomponent materials (Prof. Franz Faupel´s group) [110] for fabrication of the nanocomposite. The machine was a cylindrical custom-build stainless steel vacuum chamber (MDC VACUUM PRODUCTS CORPORATIONS (QD-1200-CH)) located in the cleanroom of Faculty of Engineering (Nanolabor). All the parts of the chamber were located in the gray area while its main door was in the white area to ensure the minimum dust contamination of the substrates and samples after deposition. A rotary pump (VARIAN (8H-110)) was used to pre-evacuate the chamber while a turbo molecular pump (PFEIFFER-VACUUM (TC 100)) was coupled to that to reach the desire minimum pressure (vacuum). Argon was utilized as inert gas for sputtering. It was fed into the chamber through a controller (PFEIFFER- VACUUM (RVC300)). The rotation speed of the pump was reduced to 660 Hz during the sputtering while the evacuation speed was 1000 Hz. During all the deposition processes, the samples were rotating with a constant speed by means of a speed controller motor (ORIENTAL MOTOR CO. LTD. (USM 206-402W)) in order to assure uniformity of the deposited film. After each experiment and

before releasing of the vacuum, the rotation speed of the pump increased to 1000 Hz so as to evacuate the chamber from any particle for two reasons. Firstly to avoid any probable health problem threatening the user. Secondly to minimize the number of probable tiny particles which might enter from the system to the cleanroom. To release the vacuum, nitrogen gas was fed to the chamber to make a flow of gas from the inner chamber to the environment and it helps to keep the system clean. Right after opening the chamber door, a suction tunnel was placed in front of the out-door of the chamber to further minimize the escape of the particles to the environment.

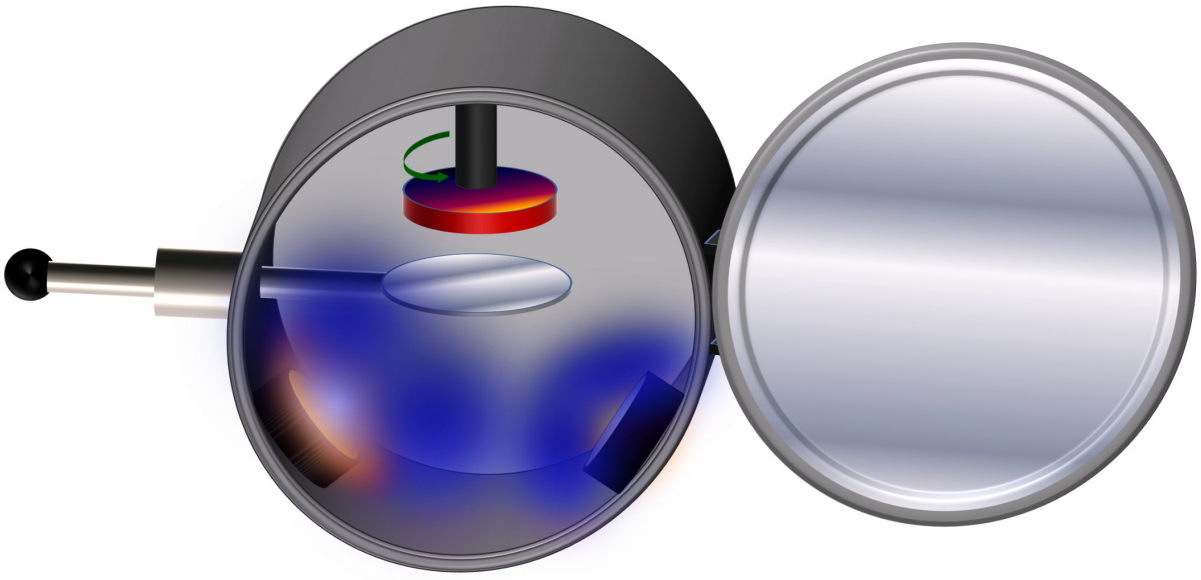

Figure 3.1: *Schematic view of the inner cylinder of the sputtering chamber where two targets are running simultaneously (co-sputtering) while the substrate is rotating.*

3.2.3 Metallic film deposition

For metallic film preparation (gold, silver and copper), a DC magnetron was used where the distance between the center of the sample holder and the head of the magnetron was 14 cm. During the process, the power of the system was adjusted by a controller (ADVANCED ENERGY (MDX 500)). The initial base pressure of the chamber and the sputtering pressure were $10^{-6} mbar$ and $2-5\times10^{-3} mbar$, respectively. The magnetron was switched on prior to film deposition to sputter-clean the target while the samples were shadowed by a shutter. The pre-sputtering time was around 30 s to ensure the deposited film is free of any contamination left from the former experiments.

3.2.4 Dielectric film deposition

For sputtering of the insulating materials (TiO_2, SiO_2 and $PTFE$) RF sputtering was applied to neutralize the charge accumulation at the surface of the substrate during the deposition [111]. The RF generator used in this work was provided by (ADVANCED ENERGY ($CESAR$®(RF Power Generator)). Igniting (initialization) of the plasma at the low pressure of $10^{-3}mbar$ was difficult, therefore at the start, the gas flow was intentionally increased for a second to facilitate the start of plasma by RF-source. It is known that the target temperature increases during RF-sputtering [112], accordingly it is more likely that the rate of sputtering varies by time. Therefore, by selecting a right generator power, it was tried to keep the deposition time as short as possible to minimize the effect of rate instability during deposition.

3.2.5 Nanocomposite deposition

The DC and RF sources were used for deposition of conducting and insulating materials, respectively. They were installed opposite to each other [110] except for the case of co-sputtering of Copper and $PTFE$ where the targets were not opposing. For achieving a reasonable uniformity, the sample holder was rotating continuously during deposition. For preparation of nanocomposites with different filling factors, the deposition rate of each material (metal and dielectric) were determined separately at the same pressure and gas flow rate used for co-deposition. The filling factor was estimated by considering the equivalent film thickness of each component within the time scale of deposition. Then, the ratio of metallic film to overall thickness was considered as the filling factor of the nanocomposite. To confirm the mentioned estimation, EDX analysis (for more details see 3.3.5) of the typical composite with different filling factors was performed which agrees quite well with the value determined by thickness consideration.

3.2.6 Rate determination

In order to tabulate the deposition rate, for metallic and not-metallic films, post measurements were carried out. The films with different powers of generator were deposited and their thicknesses were measured by a profilometer (Dektak 8000). By doing so, one could find the relationship between the power of generator and the deposition rate of the desired materials provided that the other parameters (e.g. gas flow, base pressure etc) were kept constant. However, for the dielectric film, it was intended to use a constant power value, because the rate of deposition did not vary linearly with power. In other words, the rate for each power of generator (RF-source) was measured while for metal deposition, linear interpolation of the tabulated data for rate determination was used.

3.2.7 Spin-coating

For spin coating, *Spincoater*® (P6700 Series) was used. A typical schematic of the spin-coater and the pipette are shown in Figure 3.2. As the solution, the polystyrene (PS) powder purchased from Sigma Aldrich (specification can be found in 3.1) was dissolved in toluene. The solution was subsequently used as the matrix of the composites. SPO molecules were dissolved in acetone and later on mixed with the PS solution. For drop injection, one channel pipette (Eppendorf Research® Variable) was applied. The substrate was held in the vacuum chuck of the spin coater and 70 μl of the desired solution was injected on its surface. The spinning speed of 2000 *rpm* was used for the samples to yield a uniform thin film.

Figure 3.2: *Schematic view of a spin-coater which shows that the drop of solution is dispersed on the spinning substrate and forms a film.*

3.3 Characterizations

3.3.1 Profilometer

For mechanical thickness measurements, the metallic films was deposited on glass. Since the adhesion of metals such as gold is very poor on a bare glass slide, mechanical scratching of the surface (by a tweezers) to wipe off the film from the substrate was gently done without scratching of the glass. In that way, the scracth depth was measured by Dectak 8000 and considered as the film thickness. To assure the accuracy of the measured value, the optical (transmission) spectra of the film were collected by UV-VIS spectrometer and compared with the data of known samples. This confirmaing measurement showed a good agreement between the mechanical estimation and optical one. For measuring the thickness of dielectrics such as SiO_2, the scratching method was not applicable because of great adhesion of the film and substrate. Therefore, the glass or silicon substrate was wrapped with a very thin

band of aluminum foil. In that way, the shadowed area was left uncoated after removal of the aluminum foil and the depth was measured. This method was also applied for thickness evaluation of metallic film and it confirmed the thicknesses values measured by scratching. Since a spectroscopic ellipsometry instrument was purchased by the institute at the last year of the current PhD work, thickness measurements of the dielectric was partly done with Ellipsometer in parallel to the other methods mentioned above (For more details see 3.3.3).

3.3.2 Ultraviolet-visible spectroscopy

All the transmission and reflection spectra measurements of the samples were done by a UV/Vis/NIR spectrometer (Lambda 900, PERKIN ELMER). In addition, angular reflection measurement of the samples with un-polarized light was also performed with the same instrument. The apparatus was connected to a PC and a company made software (UV WinLab) was used for monitoring the instrument. For transmission measurements, the base line was collected by measuring the empty compartment (i.e. air considered as the reference) while for reflection measurements, the mirror provided by the company was used. To extract the absolute value of reflection, the measured reflection spectra of the samples were normalized to the tabulated data of the mirror provided by the manufacturing company. In all types of measurement, the scan step was fixed to 4 nm and the base line was collected twice by full sweep of the desire wavelengths range while the integration and acquisition times were kept constant.

3.3.3 Spectroscopic Ellipsometry

Variable angle spectroscopic Ellipsometry reflection measurements of the films were carried out with J.A. Woollam Co., Inc. M2000 UI (spectroscopic ellipsometer) with a dual lamp system with Deuterium and Quartz Tungsten Halogen (QTH) lamps as the light sources. The instrument photograph is presented in Figure 3.3. The angle sweep step was selected to be 5° or 10° and the angle variation from 45° to 85° was performed. In order to have a comparable study and achieve the best signal-to-noise, 5 seconds acquisition time was applied for all the experiments. Accordingly, the measurement did not take more than few seconds. For analyzing the data, CompleteEASE® software package provided by the company was used. All aforementioned specifications are taken from brochure of LOT-Oriel Group Europe [113]. Note that only a set of experiments for angular polarization measurements of gold-Silicon dioxide were done in the cleanroom of Mads Clausen Institute (University of Southern Denmark) and used in Chapter 5.

3.3.4 Transmission Electron Microscopy

High resolution transmission electron microscopy (HRTEM) images of the nanocomposite samples were taken by Tecnai F30G2 (Philips). The electron micrsocopy analysis was done

Figure 3.3: *Photograph of the Woolam spectroscopic Ellipsometry which was used within the course of the current work for polarization measurements.*

partly by Dr. Venkata Sai Kiran Chakravadhanula, Dr. Ulrich Schürmann and Dr. Viktor Hrkac from the chair of Synthesis and Real Structure. For geometry analysis, nanocomposites with the similar condition as explained above (section 3.2.5) were deposited on commercial Cu lacey carbon TEM grids. Since for high resolution TEM imaging very thin films are preferable, the thickest composite analyzed was only 20 nm thick. However, for imaging the layers, a cross-sectioned samples out of the stacks (overall thickness of the films was 70 nm deposited on silicon) were prepared through Focused Ion Beam (FIB) technique by Ms. Christin Szillus and analyzed by Dr. Schürmann.

3.3.5 Energy Dispersive X-ray spectroscopy

Energy dispersive x-ray spectroscopy (EDX) mounted in a scanning electron microscope (SEM) (Philips X L30) was used to determine the metal amount and distribution in the composite films. To do so, the samples with different filling factors of metal were loaded into the SEM chamber. It was tried to have a pure metal film (as the reference sample) with a thickness similar to the equivalent thickness of the metal in the composite. Firstly, the metal intensity signal on the metallic film was collected and at the same condition (by keeping all the parameters same as those for the reference sample) the signal of the metal incorporated into the dielectric (nanocomposite) was recorded. According to the recorded data, the equivalent thickness of the metal in the composite was calculated and the resulting value was divided to the total thickness of the nanocomposite. The achieved number was considered as the filling factor of the metal in the composite.

Chapter 4

Review of plasmonic nanocomposite metamaterial absorber

M. K. Hedayati, F. Faupel, M. Elbahri, Review of plasmonic nanocomposite metamaterial absorber, *Materials 2014*, 7, 1221-1248.

4.1 Abstract

Plasmonic metamaterials are artificial materials typically composed of noble metals in which the features of photonics and electronics are linked by coupling photons to conduction electrons of metal (known as surface plasmon). These rationally designed structures have spurred interest noticeably since they demonstrate some fascinating properties which are unattainable with naturally occurring materials. Complete absorption of light is one of the recent exotic properties of plasmonic metamaterials which has broadened its application area considerably. This is realized by designing a medium whose impedance matches that of free space while being opaque. If such a medium is filled with some lossy medium, the resulting structure can absorb light totally in a sharp or broad frequency range. Although several types of metamaterials perfect absorber have been demonstrated so far, in the current paper we overview (and focus on) perfect absorbers based on nanocomposites where the total thickness is a few tens of nanometer and the absorption band is broad, tunable and insensitive to the angle of incidence. The nanocomposites consist of metal nanoparticles embedded in a dielectric matrix with a high filling factor close to the percolation threshold. The filling factor can be tailored by the vapor phase co-deposition of the metallic and dielectric components. In addition, novel wet chemical approaches are discussed which are bio-inspired or involve synthesis within levitating Leidenfrost drops, for instance. Moreover, theoretical considerations, optical properties, and potential application of perfect absorbers will be presented.

4.2 Introduction

The present reviews start with a short introduction to the plasmonic absorption while spanning the development of perfect absorbing structures. The general theoretical consideration for metamaterials absorber will be presented in section 2. Section 3 focuses on the design, fabrication and characterization of plasmonic nanocomposite and its implementation as a building block for the design of perfect black absorber (base on gold, copper and silver). Moreover, the similarity and performance of the different metamaterial absorber also will be presented in section 3. Discussion of selective innovative approaches for highly absorber devices is the focus of section 4. The last section (5) presents the prospects and future potential of metamaterial absorbers.

4.2.1 Plasmons and plasmonics

One of the prime applications of nanostructures dates back to more than three millenniums ago [114], when the ancients used metallic particles in ceramic matrix (most probably not aware of the dimension of particles) for decoration purposes. The trace of this old-fashioned nanotechnology nowadays can be seen in many museums and historical sites worldwide in the form of colorful tiles [115], lusters [14], glasses [116] etc. The real origin of the coloration was unknown up to the early 20^{th} century, when theoretical studies shed light into this uncovered optical phenomena [18] which is known today as plasmonics [117] (photonelectron coupling). Surface plasmons are waves that spread over the surface of a conductor. Hence, changing the surface structure alters the light-plasmon interaction, the phenomenon which provides the potential for emerging new photonic devices [7]. In general, materials with a negative real and small positive imaginary dielectric constant are capable of sustaining a surface plasmon resonance (SPR). For materials whose dimensions are far below the sub-wavelength, in particular nanoparticles, plasmon oscillates locally around the particle and hence it is called localized surface plasmon resonance [118]8. In other words, the conduction electrons in the NPs move all in phase upon excitation with incidence light and polarize the particle surface [119]. Since the electrons are displaced from their equilibrium state, the redistribution tendency of surface charge applies a restoring force on the disordered electrons and results in oscillation with a certain frequency, known as plasmon resonance frequency [6]. Therefore, a field builds up inside the particle while establishing a dipolar field on the outer surface of particle. This strongly enhanced near field around the NPs which considerably increase their absorption and scattering cross section, is the primary reason immense attention to plasmonic nanoparticles [119]. In fact, the optics has been revolutionized within the last few decades owning to the plasmonic nanostructures and consequently, design of sub-diffraction opto-electronic devices is nowadays possible.

4.2.2 Energy and metals

The oil crisis in the late 70s [120] redrew attention toward plasmonic materials, although not for luxury purposes but rather as a new alternative absorber for solar collectors where light

trapping is highly desired [121]. As discussed in the last section, the near field enhancement of plasmonics could be also applicable in solar cells to reduce the thickness (accordingly the material cost) of photovoltaic devices significantly [89]. Ceramic-metals alloy (also known as cermet [121]) were in use since then as a method of choice for solar thermal collector. These categories of composites withstand the harsh environment and do not degrade at high temperature. To enhance their absorption, graded coating (out of composite) on a metallic substrate is applied where the refractive index decreases monotonically in passing from the substrate to the surface [121,122]. In other words, traditional Rayleigh configuration for low reflection has been used in order to achieve low reflection loss and high absorption, simultaneously. Even thought cermet coating works well for realization of high absorption in visible range, the film is bulky and thick and hence does not match with the miniscule modern devices. However, fast growth of nanotechnology in the last two decades and the development of metamaterial in the beginning of the 21st century [27] unlocked a new door to design of miniaturized and efficient absorber. In analogy with cermet coating, nanofabricated structures replaced the traditional top composite layer (in a triple layer absorber) in order to achieve a similar goal but on a smaller scale. In this novel approach, the performance was similar in the sense of absorption intensity but the band-width was narrow [31,36,37]. This originated from the fact that the new developed coating material (conventional metamaterial) was designed for a single frequency, and to reach multiple wavelengths, multiple types of structures in a single system are required. The latter is rather costly, time consuming and relatively hard, especially when it is intended to absorb short wavelength light (visible or UV). Hence, development of alternatives or redesign of traditional cermet seems necessary as a way to maintain high while down-scaling the size to few 10ths of nanometers.

4.2.3 Highly absorber structures: metal nanostructure and films

Beside the variety of applications routed from individual nanoparticles (NPs) [123, 124], interacting NPs provide greater localization of the electromagnetic field [125, 126] which broaden the usefulness of nanoscale metallic particles. Due to the localization of surface plasmon, the ensemble of NPs, which are no more distant from each other than the diameter of each individual particle, could strongly trap the incident light in a subwavelength scale (gap between the NPs) which could create huge localized field. The spectrum of such groups of NPs is determined by the interaction between the individual LSP resonances. The magnitude of the confined field and its frequency depend significantly on the shape, size and the space between NPs [127]. Similar to particles' ensemble, but in a simpler situation, strong interaction of electric field can happen when a metallic particle (or collection of particles) is situated atop of a metal surface. This system can be named as coupling of localized and delocalized plasmon resonance [128]. In other words, when a dipole is located in proximity of a conducting layer (mirror), in addition to the dipole-dipole interaction [129–132], dipole interaction with the induced image in the mirror influences the resonance [132–134](optical response). Study of the dipole-conductive film dated back to late 80s when Holland and Hall [135] analyzed the interaction of silver or gold particles (dipoles) and silver film (conducting surface) which were separated by LiF layer (Figure 4.1a). They considered the observation of frequency shift as a universal feature of the dipole-surface interaction caused

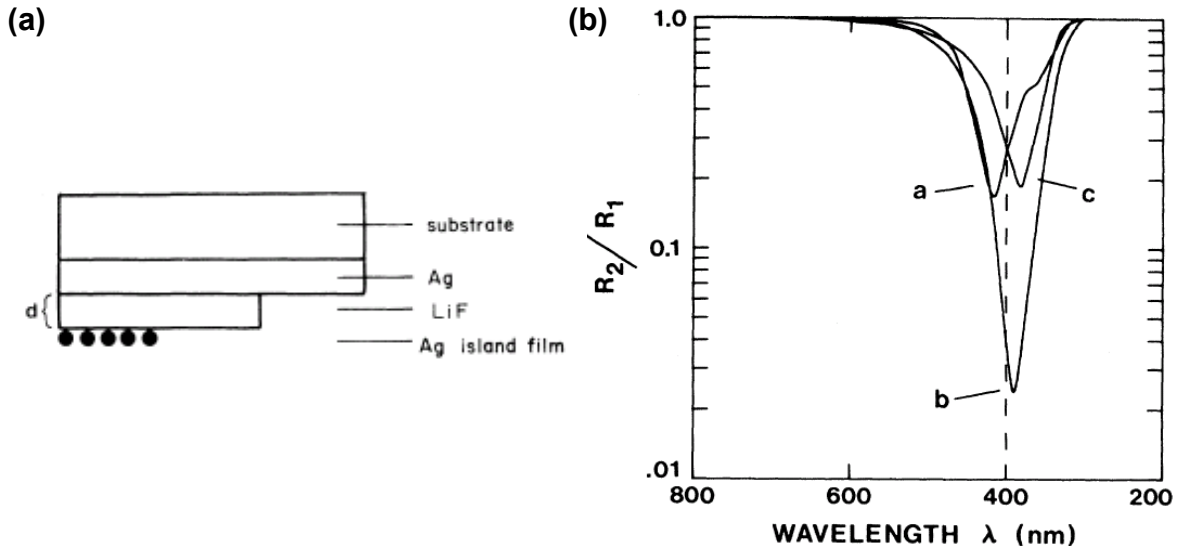

Figure 4.1: *(a) Cross section of the three-layer sample geometry used in [135]. (b) Measured specular reflectance of silver-island samples R2 (normalized by Ag-LiF reflectance R1) as a function of wavelength for three different values of spacer-layer thickness d. The minima near 400 nm correspond to absorption by the silver islands. Curve a, d=8 nm; curve b, d=27 nm; curve c, d= 36 nm. (Figure adapted with permission. Copyright 1982, American Physical Society.)*

by the coupling between the dipole and its own image in the metal surface as it is shown in Figure 4.1b [135]. Following this work, Borensztein et al. improved the calculation method of earlier work by taking into account the interactions of a silver sphere with both its own image field reflected from the conducting surface and with the image field of all the other spheres [136]. Cesario et *al.* [137] studied a very similar system except that the top layer was lithographically fabricated gold particles and the spacer was a 10 *nm* ITO layer. They observed appearance of two separate peaks. They attributed one of the peaks to the localized surface plasmon of the nanostructures and their own interaction. While the second peak referred to the surface plasmon polariton trapped at the goldglass interface which was excited by the energy transfer of LSP of the structure to the SPP of the film (grating coupling) [137]. There have been so many similar works in the mentioned combination where the frequency shift and coupling of plasmon resonance were studied [133, 133, 138–140]. However, one of the first reports of highly absorbing film-particle absorber was theoretically shown by Papanikolaou in which silver spheres (90 *nm* in diameter) are sited on top of silver film (40 *nm* thick) [141]. Although the aim of the work was not realization of a highly absorbing system, but rather to study the effect of particle arrangement on optical properties, the author achieved this outcome.

Although the currently recognized field of metamaterials absorber looks novel, it has basically the old geometry of metallic particle-film (dipole-conductive metal) which has been extensively studied in the last few decades. In other words, patterned micro (nano-) structures replace the older particles and molecules due to the advances in nanofabrication tech-

niques. Nevertheless, considering the high absorption in metamaterials as a new objective (despite early consideration of absorption as a limiting factor), broadened the application of this field. The work of Padilla and colleagues is the start of metamaterials perfect absorber [31] or more precisely, renaissance of electric dipole (resonator)-film interacting structures. In that early work, the authors showed that metamaterials consisting of two standard split ring resonators connected by an inductive ring parallel to the split-wire, placed in a distance from a cut-wire, could absorb light completely in certain wavelength ranges. The geometry of their designed metamaterial absorber is illustrated in Figure 4.2 [31].

This work inspired the researchers working with metamaterials to reexamine the optical structures that had been developed up until that time. Accordingly, a tremendous number of perfect absorber structures were designed and developed (theoretically and experimentally) which realize almost unity absorption at different frequencies. However, the principle behind all the methods was the same and the structures were mainly composed of three layers; top metallic structure and substrate with a dielectric interlayer. Moreover, fabrication of the top structured layers was carried out mainly by lithography. The latter fact makes large area coverage difficult and limits the down-scaling (of nanostructure) below 50 nm because lithographically production of smaller features is rather complicated (For details of the development of metamaterials electromagnetic absorber, see the recent review by Padilla and coworkers [32]).

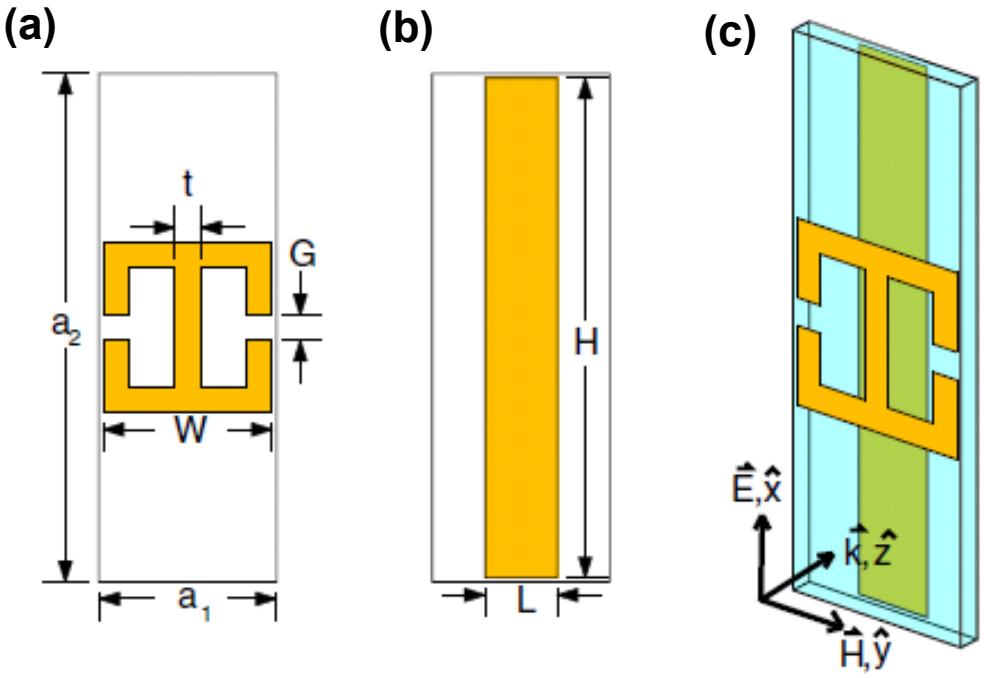

Figure 4.2: *Electric resonator (a) and cut wire (b). Dimension notations are listed in (a) and (b). The unit cell is shown in (c) with axes indicating the propagation direction [31]. (Figure adapted with permission. Copyright 2008, American Physical Society.)*

4.2.4 Theoretical consideration

The theory of the metamaterial absorber is presented thoroughly in the progress report by Padilla and co-workers [32] and herein we briefly summarize the general theoretical background in this section. Based on Fresnel equation, the reflectivity at the air interface of a medium with refractive index n ($(n = \sqrt{\mu.\epsilon})$ [142]) for transverse electric (TE) and transverse magnetic (TM) polarized waves are as follow [32]:

$$R_{TE} = \left| \frac{\cos\theta - \dfrac{\sqrt{n^2 - \sin^2\theta}}{\mu_r}}{\cos\theta + \dfrac{\sqrt{n^2 - \sin^2\theta}}{\mu_r}} \right|^2 \tag{4.1}$$

$$R_{TE} = \left| \frac{\epsilon_r \cos\theta - \sqrt{n^2 - \sin^2\theta}}{\epsilon_r \cos\theta + \sqrt{n^2 - \sin^2\theta}} \right|^2 \tag{4.2}$$

in which θ is the angle of incidence, n is the refractive index, ϵ and μ are permittivity and permeability of the of the medium (Metamaterial), respectively. In case of normal incidence angle ($\theta = 0$), the above equation reduces to [32]:

$$R_{TE} = \left| \frac{1 - \dfrac{n}{\mu_r}}{1 + \dfrac{n}{\mu_r}} \right|^2 \tag{4.3}$$

$$R_{TE} = \left| \frac{\epsilon_r - n}{\epsilon_r - n} \right|^2 \tag{4.4}$$

If it is intended to have no reflectivity for both polarisations, both of the above terms should equal to zero which is equivalent to $\mu_r = \epsilon_r$. This means impedance of the metamaterial should match that of air in order to reduce the reflection loss down to zero. According to Kirchhoffs rule, the sum of the transmittance T, reflectance R, and absorbance A should be equal to 1 in the absence of scattering and diffraction [50]. Taking both mentioned facts into consideration, it can be concluded that if the impedance of a metamaterial matches to that of the free space and the medium is opaque (zero light transmission) the light can be absorbed totally [48]. Note that if the medium is not sufficiently thick and not enough lossy, the wave which is bounced back off the base mirror can reflect back into free space [32]. Although the satisfaction of the impedance matching is rather hard, by using an optically thick metal plate, the zero transmission condition can be provided. Therefore, the challenge is to design and manufacture a structure with impedance matching the free space for a single or wide

range of frequency. Usually, in multi-layer structures, impedance matching is accomplished either by using anti-reflection coating or by a dielectric film (certain thickness) flanked by partially reflecting mirrors (i.e. Fabry-Perot interferometer) [143]. In both mentioned cases, an additional lossy medium is required in order to absorb the light and dissipate the incidence energy.

It is known that metals are *lossier* in high frequency, in particular at optical realm, due to electron transitions from the filled d bands into the sp conduction bands (absorption) [144]. However, at lower frequency (longer wavelengths), one can assume that most metals act as a perfect conductor with small loss, since the corresponding ohmic loss fraction (the ratio of the skin depth over wavelength) is only 0.1% or less [143]. This means that for the metamaterials designed for IR, the source of the main loss is the dielectric. This is the main reason why lossy dielectric is incorporated in metamaterial design. In other words, lowering the reflectivity by impedance matching is not sufficient and presence of lossy materials is obligatory for realization of high absorptivity. In contrast to low frequency, contribution of metallic absorption (e.g. ohmic loss and surface plasmon decay) is more than dielectric when the operating frequency is NIR or visible. Therefore, absorption within the metallic part in metamaterials absorber for visible reduces the role of dielectric absorption, and hence relatively thinner dielectric is sufficient for high frequency purposes. By taking into consideration all the mentioned facts, recently a new perfect absorber was designed and fabricated which is orders of magnitude thinner than conventional cermet while its absorption, bandwidth and intensity is surpassing that of conventional metamaterial absorber and traditional cermet. Here, the top layer is replaced by ultra thin ($\sim 20nm$) plasmonic nanocomposite made of metal nanoparticles dispersed randomly in polymeric (or generally dielectric) matrix. In spite of the early consideration of graded refractive index layers as beneficial method for higher absorption, it is shown that thin film of a highly dispersive material (plasmonic nanocomposite) [145] with a high refractive index contrast to the second layer (interlayer) could give rise to perfect absorption of light in a broad range of frequency from deep UV [146] up to visible and NIR [147, 148]. The key feature of this metamaterial absorber is reversing the traditional arrangement of layers where the refractive indices ascend in consecutive layers. Impedance matching of the medium to free space, multi-reflection of light between the layers and light trapping and absorption by the tiny metallic particles enable realization of almost unity absorption of light in wide range of spectrum from UV to NIR.

4.3 Metal-dielectric nanocomposites with tailored plasmonic response

Many approaches have been reported to prepare metal-dielectric nanocomposites containing metallic nanoparticles embedded in a dielectric organic or ceramic matrix due to their unique functional properties with hosts of applications (for recent reviews see [149, 150]). For the present application of metaldielectric composites in plasmonic metamaterial absorbers, two revere restrictions apply. First, a high filling factor of the metallic nanoparticles close to the percolation threshold is required to take advantage of the interaction of plasmon resonances

localized at individual nanoparticles. Second, large area coverage is indispensable in most applications which rules out electron beam lithography and rather calls for self-organized formation of the nanostructures. This is why vapor phase deposition techniques are particularly attractive for tailoring the nanostructure and the resulting properties [149]. Vapor phase deposition, *inter alia*, allows excellent control of the metallic filling factor and its depth profile as well as the incorporation of alloy nanoparticles with well-defined composition [151]. The metallic nanoparticles typically form via a self-organization during co-deposition of the metallic and matrix components due to the high cohesive energy of the metals and the low metal-matrix interaction energy [149, 152]. Various methods such as sputtering [110, 153], evaporation [154], and plasma polymerization [155] have been applied for the deposition of the matrix component, while the metallic component has mostly been sputter-deposited or evaporated. Moreover, gas aggregation cluster sources were utilized to obtain independent control of filling factor and size of the embedded nanoparticles [156]. Examples of plasmonic metal-dielectric composites are given in [134, 146–148, 151, 155, 157].

4.3.1 Fabrication procedure

For all types of nanocomposites discussed in this review, the same fabrication procedure was used [147] which is summarized as follows. Magnetron sputtering was carried out for deposition of all the films and composite of various types and compositions. The machine was a cylindrical custom-build stainless steel vacuum chamber located in a cleanroom. Argon was used as inert gas for sputtering. During the deposition process, samples were rotating with a constant speed by means of a speed controlled motor in order to assure the uniformity of the deposited film. For metallic film preparation (e.g. gold or silver), a DC magnetron was used where the distance between the center of sample holder and head of the magnetron was 14 cm. The initial base pressure of the chamber and sputtering pressure were $10^{-6} mbar$ and $2.5 \times 10^{-3} mbar$, respectively. For sputtering of the insulating materials ($PTFE$, TiO_2 and SiO_2), RF sputtering was applied to neutralize the charge accumulation at the surface of the substrate during the deposition59. For nanocomposite deposition, co-sputtering method was applied. Both targets (DC and RF sources) were installed opposite of each other except for the case of co-sputtering of copper and $PTFE$ where the targets were not opposing. For preparation of nanocomposite with different filling factor, the rate of each of the materials (metal and dielectric) were determined separately at the same pressure and gas flow rate which was used for co-deposition. The filling factor was estimated by considering the equivalent film thickness of each component within the time scale of deposition. Then, the ratio of metallic film to overall thickness was considered as the filling factor of the nanocomposite. To confirm the mentioned estimation, EDX analysis of the typical composite with different filling factor was performed which agrees quite well with the value determined by thickness consideration.

4.3.2 Results and Discussion

Since the type of metallic constituent in the nanocomposite is the most influential parameter on the optical properties of the system, in the following, three different nanocomposite perfect absorbers based on gold, copper and silver will be presented.

4.3.3 Gold nanocomposite

Though gold is one of the known primeval noble metals and has been the subject of investigation in science for ages [158], the current state-of-the-art nanofabrication methods reorient the studies of this metal for a host of new application in electronics and optics. Au NPs are among the most stable metal nanoparticles with some unique features and properties such as size-related electronic, optical and magnetic properties as well as application in catalysis and biologic systems [158]. In the field of plasmonic materials, the gold (in particular in nanoparticles form) is also the leading building block not only because of its stability but also due to its plasmon resonance and unique optical properties in visible. Forasmuch as the mean free path in gold and silver is 50 nm, particles smaller than this size do not experience any bulk scattering and surface effect is dominating. Therefore, the light in resonance with the surface plasmon oscillation causes the free-electrons in the metal (d electrons in silver and gold) to oscillate. Since the resonance occurs at the surface, it is called surface plasmon resonance (SPR). Consequently, any effect which changes the surface geometry of the particle (e.g. size or shape) causing a shift in the electric field density on the surface which results in the alteration of oscillation frequency of the electrons (i.e. SPR shift) [159]. Changing the surrounding environment of the NPs could also affect the resonance frequency which is the basic principles of plasmonic sensor (for details see the review by Stewart et al. [160] and the references therein).

It is well known that the interacting metallic particles and film could considerably absorb light. Inspired with earlier works on metal-polymer nanocomposite [157, 161] and recent developments in the field of metamaterials, the authors of the present article found that ultra-thin nanocomposite as a top of dielectric coated metal film could result in complete absorption of light in broad spectrum. Similar to the older works, a three-layered structure was developed. However, the main difference was the use of ultrathin metal-dielectric nanocomposite (highly dispersive material [145]) as top roof film (Figure 4.3a). Gold was selected as a prime metallic constituent of the proposed structure due to its great stability and unique optical properties. Experimental data verified that 20 nm nanocomposite (Au-SiO_2) deposited on 25 nm SiO_2 coated gold film (100 nm) is the optimum condition for realization of broad-band perfect absorber in visible frequency. It was found that the volume fraction (filling factor) of the gold in composite significantly alters the optical response of the designed metamaterials. By optimization, it was found that 40% filling factor is the optimum value for high absorption in a wide range of wavelengths making the surface appearance black (Figure 4.3b-c). The authors postulated that the huge absorption originated from several factors as follows. Impedance matching in these metamaterials as well as dipoleimage (polarized particle and its image in the base mirror) interaction which

causes an electromagnetic confinement in the spacer layer, alleviates reflection [147]. The broad resonance of the absorber stem, due to the fact that the broad Mie resonance of the nanoparticles ensembles (which originates from the large size distribution of the particles with random shapes), and the plasmon polariton of the base metal film overlap. A study of the optical data measured at a higher angle of incidence confirmed the mentioned reasoning in which the broad plasmonic resonance peak splits into two peaks along with a slight drop in absorption in grazing incidence [147]. Changing the thickness of the spacer layer (interlayer) revealed that the dipole-image interaction is one of the reasons for light trapping in the nanocomposite perfect absorber. For instance, thickening the interlayer results in a drop of the absorption intensity, which can be interpreted as weaker dipole-image interactions due to weaker coupling [147].

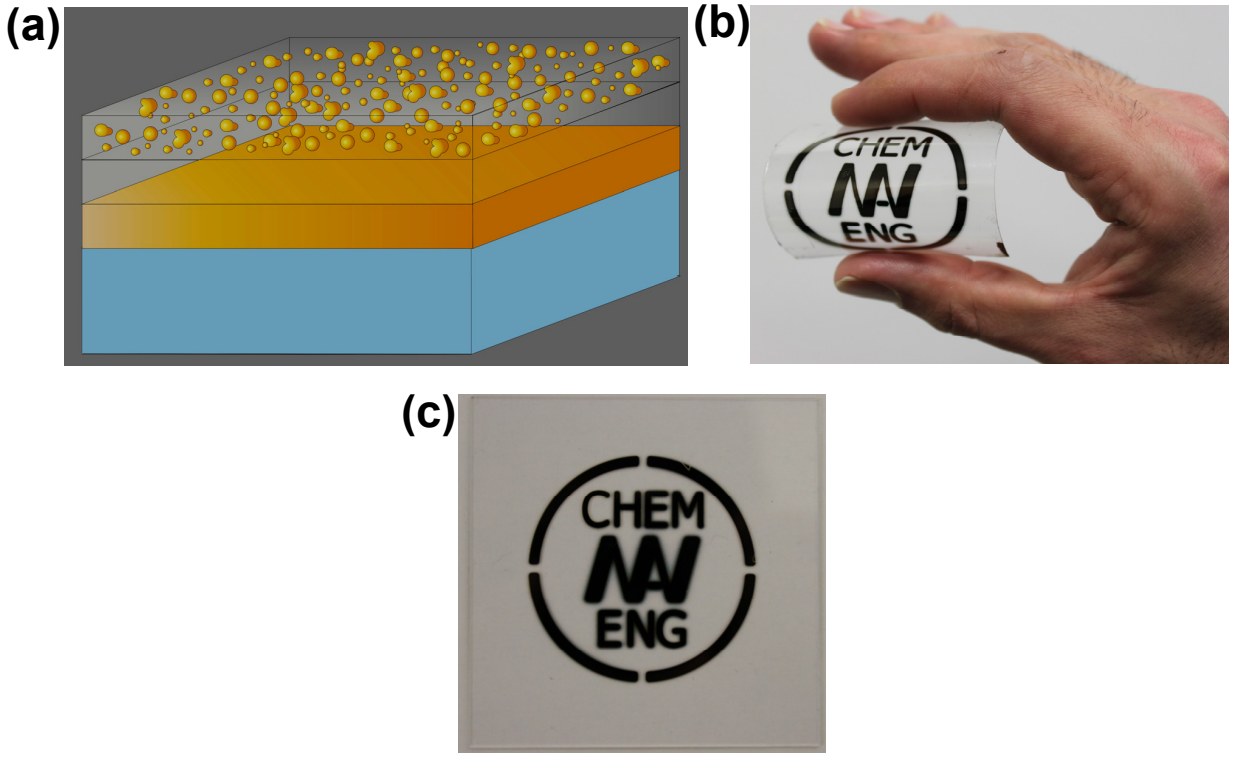

Figure 4.3: *((a) Schematic of the perfect absorber structure fabricated by sputtering. The thickness of the layers from top to down are (i.e. nanocomposites, SiO_2 spacer, and the gold mirror) 20, 25, and 100 nm, respectively. Perfect absorber (blackbody) coated via a mask on (b) flexible polymer foil and (c) glass. This example shows the potential of the coating for application on different substrates. (Figure 4.3b adapted with permission. Copyright 2011, WILEY-VCH Verlag GmbH Co. KGaA, Weinheim [147].)*

Tuning the optical response of any metamaterials is desired. It was shown that alteration of the filling factor could provide the possibility of adjusting the resonance position. As it is shown in Figure 4.4a, the absorption peak either shifts towards the NIR when increasing or towards the blue when decreasing the filling factor [147]. Since the resonance of the plasmonic structure is strongly influenced by any changes in the surrounding envi-

ronment, the peak position of absorption in the plasmonic nanocomposite perfect absorber is also altered by changing the matrix. Figure 4.4b depicts the absorption of the absorber with three different matrices of the composite ($PTFE$, TiO_2, and SiO_2). In the case of the matrix with lower refractive index ($PTFE$) compared to the SiO_2, the resonance blue shift, while having a higher refractive index material (TiO_2), shifts the peak to a longer wavelength. It seems that the retardation effect of the higher refractiveindex matrix (TiO_2) on the resonance of the metallic particles is shifting the absorption band to a longer wavelength while the polymer matrix with less dielectric constant (than that of silicon dioxide matrix) provides the condition for higher resonance frequency.

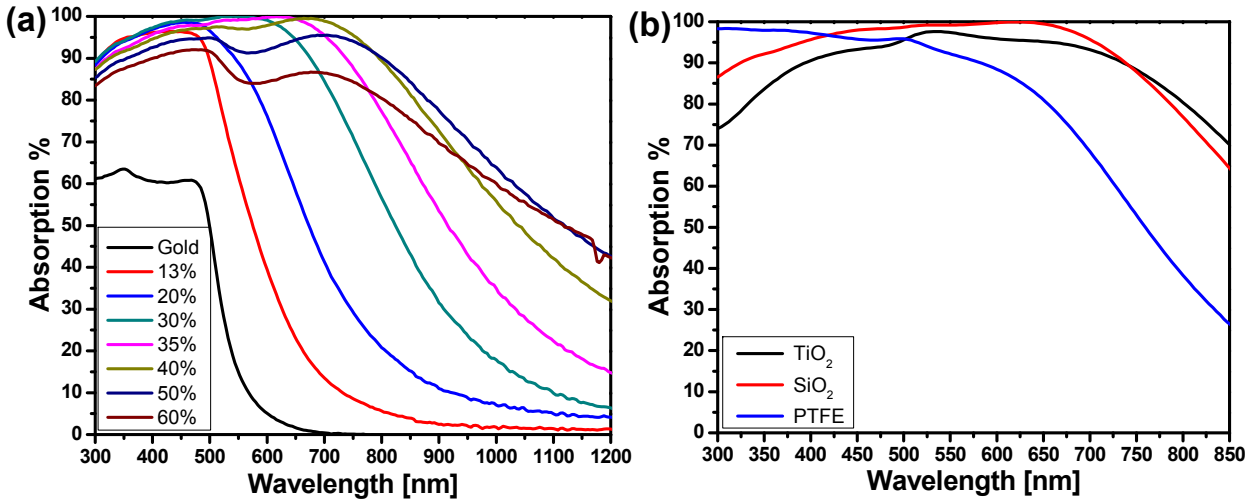

Figure 4.4: *(a) Absorption spectra of a 20 nm Au-SiO_2 nanocomposite with different filling factor sputter-deposited on a 100 nm gold film which has been coated with a 25 nm SiO_2 spacer layer. The absorption calculated by measuring the reflection (at a 6° angle of incidence) using A% = 100 - R% while assuming the scattering is negligible. (b) Absorption spectra of a 20 nm Au-SiO_2 (circles), 20 nm Au-TiO_2 (triangles) and 20 nm Au-PTFE (squares) nanocomposite on a 100 nm gold film with a 25 nm SiO_2 at a 6° angle of incidence (Figure 4.4b adapted with permission. Copyright 2011, WILEY-VCH Verlag GmbH Co. KGaA, Weinheim [147].)*

4.3.4 Copper nanocomposite

Copper has been in use by humans from early civilization since people could simply cold-hammer native copper for building tools [162]. Similar to gold, copper soon found its way toward decorative applications (beside its extensive types of mechanical usefulness). The ruby color of some glasses nowadays is attributed to the existence of nanoparticles of copper immersed in a silica matrix [163, 164]. In the field of metamaterials, and in particular perfect absorbers, copper is a promising candidate due to its significant loss in visible range, though it has been implemented and used for realization of high absorber devices in other frequencies, too.

One of the first copper metamaterial perfect absorbers was demonstrated by Soukoulis and coworkers [165] in both numerical simulations and experimental measurements for GHz in the form of chiral metamaterial. A material is considered to be chiral if it lacks any planes of mirror symmetry. They were inspired by early works on chiral metamaterials [166] where significant loss is originated from dielectric loss in the FR-4 board at microwave [165]. Hence, they selected lossy elements (copper) in their design to achieve higher absorption. After Soukoulis's work, numerous perfect absorbers which have copper as their constituent were presented for GHz. The majority of the works were based on the three-layer absorber where a dielectric is sandwiched between two metallic structures and/or films. In the majority of the available literatures, FR4 (lossy dielectric) film were used for copper absorber [167–174]. Indeed, the role of dielectric seems to be more significant than the metal itself. Based on the two studies in which the dielectric contribution to the absorption is analyzed, the role of dielectric loss in absorption is considerably larger than that of the ohmic losses in metal [174, 175]. Although the majority of the works were limited to the three layer

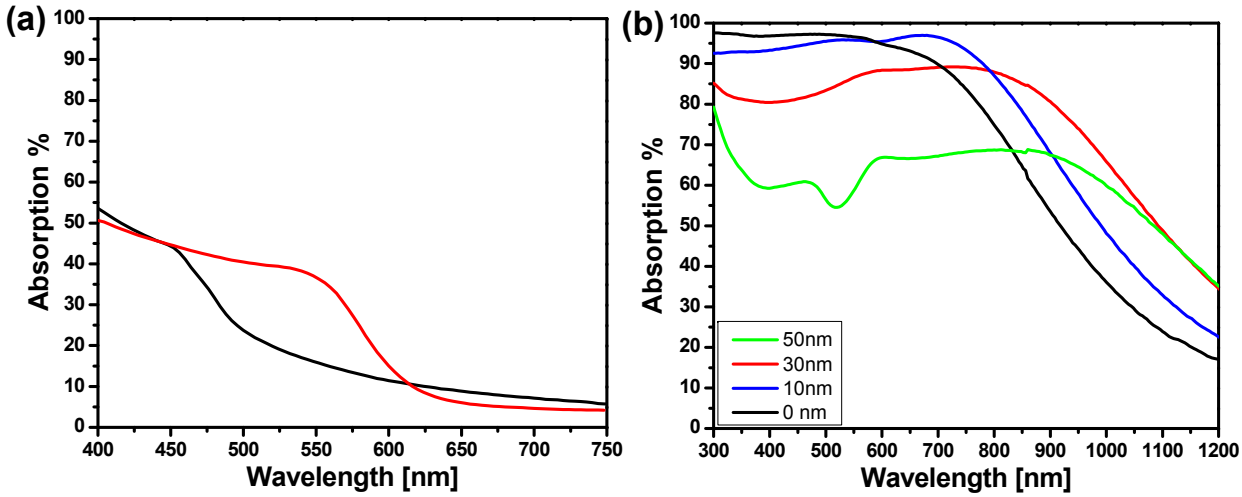

Figure 4.5: *((a) Absorption spectra of 20 nm Cu-PTFE composite (black) with a sputtering ratio of 2.0 on 20 nm PTFE on glass in comparison of 100 nm copper film (red). (adapted with permission. Copyright 2011, Springer Science and Business Media [148].)(b) Absorption spectra of a 20 nm Cu-PTFE nanocomposite sputter-deposited on a 100 nm copper film which has been coated with different thickness of spacer layer. The absorption calculated by measuring the reflection (at a 6° angle of incidence) using A% = 100 - R% while it assumes that scattering is negligible.*

system with lossy dielectric, there have been some more innovative designs and proposed structures in which other possible influential parameters are changed in order to improve the absorption efficiency in terms of band-width and tunability. One of the unique works in the field of copper base metamaterial absorber is the work by Sun et *al.* [176] which showed that by means of destructive interference, broadband absorption of light can be realized. They showed that the choice of proper refractive index dispersion enables the designer to produce a consecutive anti-reflection which may widen the bandwidth of the absorber significantly. To achieve such a goal, multilayer of SRRs with different dimension

stacked over each other to provide a dispersive refractive index required for anti-reflection (high absorption). In other words, their proposed structure shows high absorption not because of resonant loss of SRRs but rather due to the antireflectivity of the dispersive coating [176]. Integrating resistors into resonators while maintaining an impedance-matched material at normal incidence was another innovative method used by Gu et *al.* [177] in order to have a broader absorption band. With that strategy, they could realize an absorber with a peak absorption of 99.9% at 2.4 GHz, and a full width at half maximum (FWHM) of 700 MHz. Similarly, to broaden the bandwidth of the metamaterial absorber, Cheng et *al.* [178] incorporated lumped elements (resistance and capacitance) into a typical three layer structure (dielectric substrate sandwiched with metal split-coin resonators (SCR)) by welding. In such a system, which is in analogy with an RLC4 circuit, the incidental EM energy can be converted into electric energy in the circuit, and then electric energy can be subsequently consumed by lumped resistances [178].

The trends to turn metamaterial devices from passive performers to active (tunable) ones increased considerably. Accordingly, the same interest holds for absorbers based on copper elements. Wen et *al.* [179] incorporated VO_2 to the traditional multilayer absorber to enable the resonance tunability by temperature variation. Since the vanadium dioxide phase transition between from metallic to insulating occurs around 330 K, its refractive index changes correspondingly. Therefore, the resonance condition inside the structure would change by heating or cooling the sample at this temperature range, giving rise to the realization of a tunable perfect absorber [179].

In spite of all the reported highly absorbent metamaterials in which the top layers are patterned metallic structures, Shu et *al.* [49] recently showed numerically that the triple absorber consisted of metallic film (nonstructured) as the top and bottom layers surrounding a dielectric film, which could act as the perfect absorber for visible and IR frequency. However, their design is based on Fabry-Perot interferometer principles and therefore the thickness of the interlayer and its refractive index is relatively high. The ease of fabrication of such a class of absorber is beneficial, but its narrow bandwidth and its rather bulky thickness would be its limiting factors for application in nano-optics.

Generally, the metamaterial absorbers made of copper suffer from one or some of the following limitations; fabrication complexity, cost of production, narrow band of resonance and angular/polarization sensitivity. In our recent work, we tried to fabricate an ultra thin triple-layer perfect absorber with copper as its metallic constituents in which a straightforward fabrication process is used and a wide absorption band with marginal sensitivity to the angle of incidence demonstrated for visible and NIR [148]. As discussed earlier, metal-dielectric nanocomposite in a stack with metallic and dielectric film could confine the light and results in broad-band perfect absorber. Analogous to gold nanocomposite, copper nanocomposite were fabricated but by using an organic matrix. In the copperbased absorber, the bandwidth is broader and given that the copper is cheaper than gold, the new developed absorber could be more cost effective for practical application. The average absorption intensity of copper absorber in visible frequency is above 97%, which makes it, to the best of our knowledge, the most intense reported broadband plasmonic perfect absorber so far. Note that the absorption of bare copper film or single layer $Cu\text{-}PTFE$ nanocomposite are

rather poor and their average intensity in visible is below 30% [148] as shown in Figure 4.5a.

As dielectric, $PTFE$ was used which has a low refractive index (1.3) to assess the role of dielectric type on the optical properties of absorber. In spite of Au-SiO_2 absorber where 25 nm SiO_2 interlayer showed the best performance, 20 nm spacer layer of $PTFE$ resulted into the maximum absorption in copper system [148]. Thickening the spacer layer to 50 nm whilst the other parameters kept the same, the absorption intensity drops considerably (Figure 4.5b). Additionally, in spite of gold absorber which was shown in the previous section, deposition of nanocomposite on bare copper (with no spacer layer) could lead also to very high absorption intensity (Figure 4.5b). These evidences prove that both coupling and interference contribute to the high absorption of such a structure. However, it seems that copper particles act as stronger light absorber than gold which can be the cause of the high absorption of structure even without any spacer film.

The absorption intensity and broadness of copper perfect absorber is greater than that of its gold counterpart. The TEM image of typical Cu-$PTFE$ composite used in [148] is shown in Figure 4.6a. The electron diffraction pattern (Figure 4.6b) shows that Cu similar to Au is formed as nanocrystallites in the matrix, as confirmed by the rings with diffuse intensity representing the various Miller planes [180]. It seems that the differences in the absorption properties of copper and gold base absorber is routed mainly from the fact that copper is more lossy in visible frequency than gold. Nevertheless, the overall behavior of the two mentioned systems shows some similar tendencies where the absorption intensity in entire visible spectrum is high.

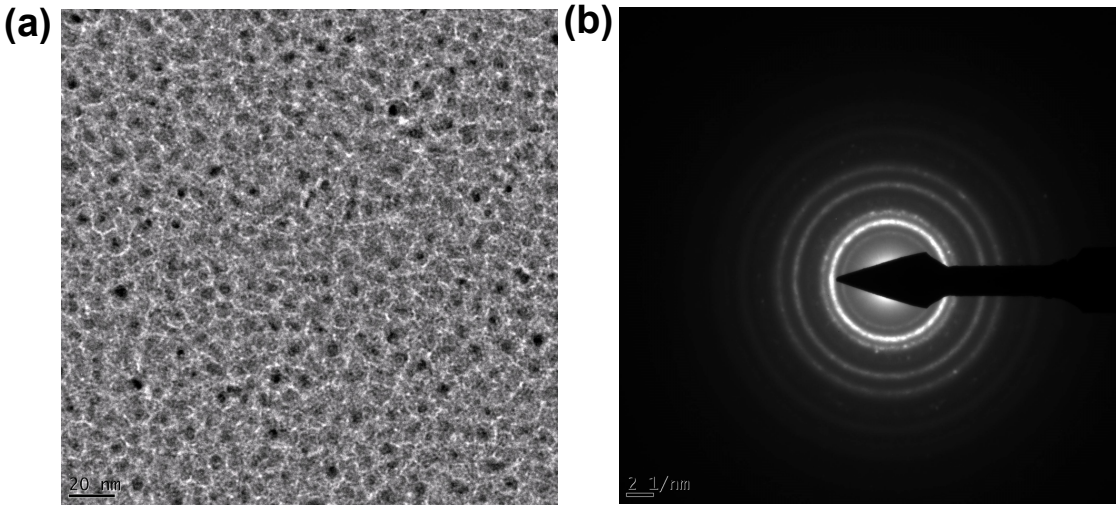

Figure 4.6: *(a) Top-view TEM image of the near percolated copper-PTFE nanocomposite. (b) The selected area diffraction pattern of the structure shown in (a).*

In addition to the dipole-image interaction and light trapping between the particles gap, one can explain macroscopically the optical behavior of such metamaterials by interference theory [181]. In other words, not only plasmon coupling but rather interference and multi-excitation of resonance because of the mirror nature of the base layer contribute to the high absorption (low reflection) of the multi-stacks. By changing the thickness of the spacer

layer, the resonance frequency and intensity of the peak vary which shows that not only the plasmon absorption of the particles but also the interaction of the particles and the film contribute to the absorption of the current metamaterial.

Even though huge absorption was realized in copper based metamaterials' absorber, the structure and optical properties vary by time mainly due to the probable oxidation of particles via interpenetration of oxygen to the particles surface. Generally, the main difficulty in utilizing copper nanoparticles is their inherent tendency to oxidize in ambient conditions. Applying different barrier layer is known as the major solution to that issue [182]. However, the polymeric ($PTFE$) matrix which was used as the dielectric could not provide the efficient protective layer and avoid copper NPs oxidation. Further works are needed to encapsulate copper nanoparticles in an oxygen impenetrable matrix to guarantee the long term stability of the final device.

4.3.5 Silver nanocomposite

Silver in different forms being used for curing of burns, wounds and several bacterial infections for thousands of the years. In the current century and thanks to the advances in nanofabrication techniques, the range of silver applications has broadened, especially silver NPs which are now known as a potential antimicrobial agent [183]. In spite of extensive work on silver nanostructure as the main metallic constituents of metamaterials [184–190], metamaterial perfect absorbers are mainly composed of gold. It seems that gold have been in use in the mentioned field because of ease of fabrication, stability and high absorption in the middle of visible spectrum. In spite of high damping losses of gold and copper, silver is known as the lowest damping metal in the visible frequency [191] and hence consideration of silver as the constituent of perfect absorber sounds unreasonable. In other words, silver has been implemented in metamaterials for high frequency because of its low loss [192–196]. It is known that the interband transition from occupied d states to unoccupied p and s states above Fermi level appear at 310 nm and 350 nm in bulk silver, respectively. However, for silver nanostructures such electron transitions could occur above 350 nm wavelengths and depend on nanostructure geometry [55]. Therefore, high optical absorption in silver particles is likely to occur at 350 nm wavelengths and above. On the other hand, silver's reflection is close to unity over the whole visible region and hence the absorption of optically thick Ag film is usually below 5% in that region.

In comparison with bare silver film, nanocomposite shows higher absorption and its intensity is around 30% in the visible frequency. In spite of the expected low absorption of silver in visible frequency, our experimental data demonstrated that the high absorption span for the UV up until the green part of spectrum can be realized by silver base plasmonic metamaterial absorber [146]. This is coming from the fact that the resonance of plasmonic materials moves to longer wavelengths when the dielectric constant of the adjacent environment enlarges. This is more prominent if the particle is in proximity to a metallic substrate. Particularly, as a dielectric encloses the metallic nanoparticle, the induced screening charges on the metaldielectric boundary reduce the plasmon excitation energy resulting in a redshifting of the resonance. Likewise, for nanoparticles ensembles, the dielectric materials

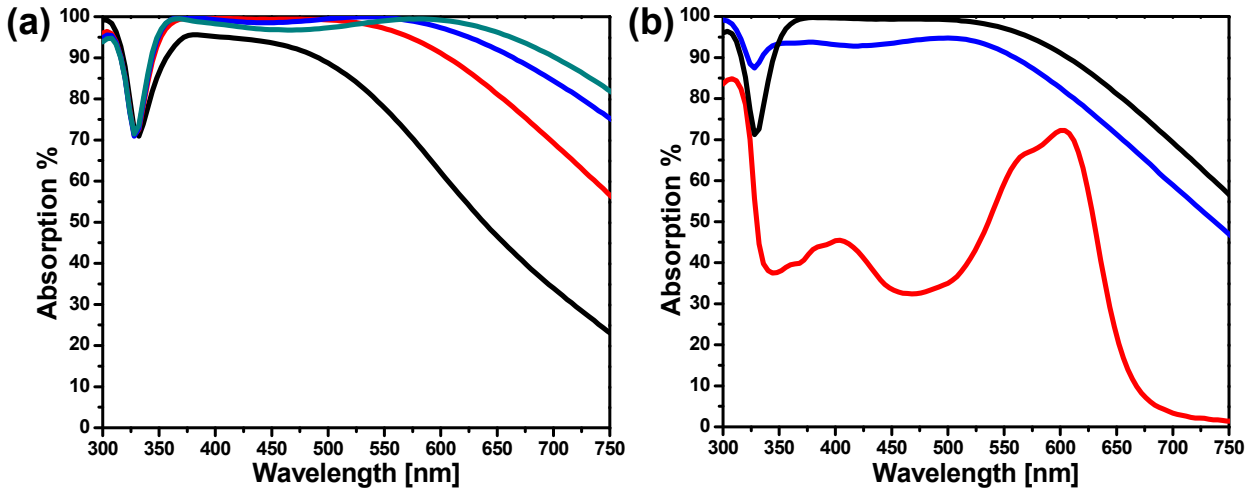

Figure 4.7: *(a) Absorption spectra of silver-SiO_2 nanocomposite with 15 nm (black curve), 20 nm (red curve), 25 nm (blue curve), and 30 nm (green curve) thickness deposited on 15 nm SiO_2 coated silver mirror. (b) Absorption spectra 200 nm silver film coated with 40 nm polystyrene-SPO composite (red curve) and 20 nm silver-SiO_2 nanocomposite with 42% filling factor deposited on 10 nm (blue curve) and 15 nm(black curve) SiO_2 film. The organic film is UV illuminated prior to measurement. (Figure adapted with permission. Copyright 2014, AIP [146].)*

screen and weaken the interaction between the NPs and lessen the shift of the coupled plasmon [197]. Accordingly, the absorption band of the silver absorber moves to the visible range due to the interaction of the composite and the base silver mirror. It is worth mentioning that part of the red-shift originated from the particle dipole which is anti-symmetrically coupled to its image inside the silver mirror (substrate) [128].

In analogy with copper perfect absorber system, low reflectivity of the silver absorber is partially routed from the interference [198]. In such layered stacks, the Fabry-Perot cavity is built-up between the top composite and the bottom mirror, and results in a strong interference of the incident and the reflected wave. Specifically, the bounced-back rays from the mirror destructively interfere with the direct reflection from the top (air-composite) interface. If the thickness of the spacer layer is properly selected, the reflected waves cancel each other out which results in negligible reflection. Given that the base silver film is thicker than the skin depth, no light transmits through the layers and thus perfect absorption is achieved [146].

One of the major differences of the silver absorber and the two other types of absorbers (gold and copper based absorbers) which were discussed above is the appearance of an absorption dip at higher frequency (around 325 nm). This dip cannot simply stem from transmission of silver film at 320 nm (5% transmission) because the intensity drops around 30% which is much more than the probable absorption loss due to transmission. The dip is routed from overlapping of two other resonances. One is the surface plasmon resonance of silver film excited either by diffraction via particles or from the roughness of the film itself.

The other is, the plasma frequency of silver which appears at 320 nm. In other words, at high frequency two mentioned absorption peaks appear while their center resonance is apart. Therefore, the gap between the two peaks appears as a dip of absorption [146].

The effect of filling factor and thickness of the film or composite on the optical properties of silver perfect absorber was in accordance with the copper or gold system. The only difference came from the initial peak position which was discussed above. For instance, by increasing the thickness of the composite (while keeping the other parameters constant), the absorption band can be widened extensively. Indeed, metamaterial silver absorber which spans the whole visible frequency can be made by increasing the thickness of nanocomposite with 46% filling factor to 30 nm (Figure 4.7a).

The interestingly high absorption of the silver system in deep UV range shows its potential as UV protection film. Comparative study of the absorption performance of silver nanocomposite absorber with typical UV absorber (Spirooxazine molecules) showed that the absorption intensity of the presented metamaterials is higher than the inorganic absorber (Figure 4.7b). Hence, one can see the potential application of perfect absorber as a highly efficient UV protective layer [146].

In short, nanocomposite perfect absorber (i.e. nanocomposite-dielectric-metal film stack) shows almost unity absorption in a broad range of frequencies with marginal angular dependency. The absorption peak position and intensity can be tuned by changing the type of nanocomposite, filling factor, and the host matrix, and the thickness of the layers which demonstrate the flexibility of the proposed method from both a fabrication and application point of view. The implementation of perfect absorbing structures on a variety of substrate is a new idea which could be implemented into the new generation of thin film solar cells for clothing (textile industry) [199]. Accordingly, we showed that nanocomposite with high filling factor can be deposited even on aluminum kitchen foil, turning it into a black absorber or any other color (Figure 4.8). This idea can push the field of metamaterials absorber one step forward for novel energy applications.

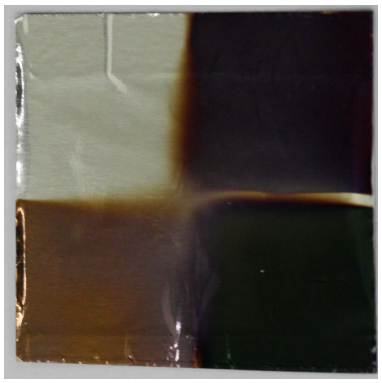

Figure 4.8: *True photograph of 50 nm gold nanocomposite with (13%), (20%) and (30%) filling factor on aluminum foil resulting in different color. The white are (top left) is the bare aluminum foil.*

4.4 Innovative design of light weight broadband nanocomposite perfect absorbers

As discussed above, majority of metamaterials absorbers (narrow or broadband) consist of three or multiple layers out of metals and dielectric assembled in a way to provide light confinement either by electric/magnetic resonance or via interference and localization. Moreover, physical vapor deposition (PVD) is the prime technique for production of metamaterials absorber for high frequency. Nonetheless, innovative design for realization of broadband perfect absorber have been developed while it is not made through PVD nor designed by triple layers. It is known that ensemble of nanoparticles can strongly confine the light. This

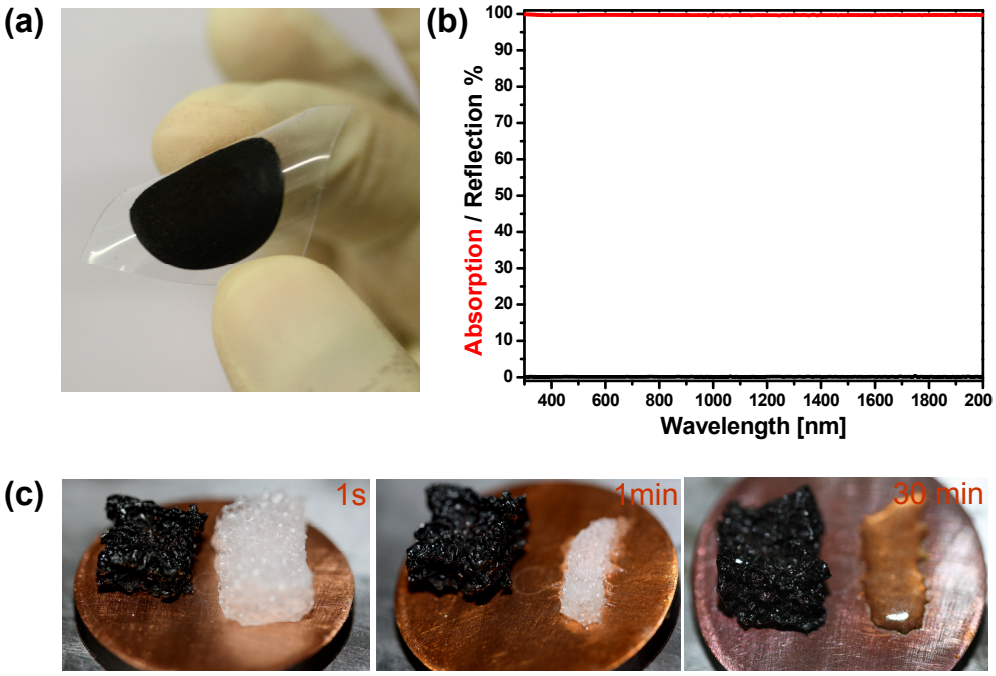

Figure 4.9: *(a) A flexible polymeric substrate coated with the black spongy gold. (b) Reflection and absorption spectra of black spongy gold in the visible and near-infrared frequency. (c) Heating stages of coated (black) and neat foam (white) on a hot plate after (bottom-left)1 s, (bottom-middle) 1 min and (botoom-right) 30 min at 150 °C. (Figure adapted with permission. Copyright 2013, Nature Publishing Group [64].)*

.

trapping is more intensified when the particles' inner-distance shrinks down to the diameter of the particles. Porous metals are among those structures which provide the small inter particles distance and enable localization of electromagnetic field (via localized surface plasmon resonance). Hence, the tuning of the resonance is directly correlated with the size at dimension of the porosity and the structure itself [200]. This fact was the base of the new design of perfect absorber which has been recently developed by Elbahri and co-workers [64]. They use the Leidenfrost drop to create a nanoporous gold hybrid structure as well as black plasmonic foam, which absorb the whole visible and NIR electromagnetic waves resulting in

a very broadband, perfect plasmonic absorber (Figure 4.9).

When a water drop touches a plate which is hotter than the boiling point of the drop, the part in contact with the substrate vaporizes and the drop levitates on its own vapor. Interestingly, remnant solid is left on the surface over which the drop has levitated. Based on Elbahri´s group finding, overheating, thermal gradients and charge separation are fundamental to Leidenfrost condition. In addition to the great possibility of nanofabrication under Leidenfrost condition such as nanoparticles formation, coating *etc.*, the authors demonstrated that such an approach can be used for fabrication of 3D metamaterial broadband absorber (400-2500 nm) in a very simple, cost effective and an environmentally friendly manner (Figure 4.9a-b). In this approach, a drop of (1 ml $HAuCl4$, 20 mM + 700 ml Sod. citrate 1% + 150 ml NaOH 0.5 M, pH 8.5) was placed on a preheated hot plate (with a constant temperature of 270°C) which provide a suspension of the desire black porous structure in less than a minute. The black suspension can turn a flexible polymeric substrate to a super absorber by a simple casting method (Figure 4.9a). To realize a macro-scale three dimensional porous metamaterial, a commercial packaging polymer foam is introduced in a levitated black pool out of the porous gold. Thanks to the dynamic covering potential of Leidenfrost drop, the foam was coated with the metallic spongy structures and a millimeter size black 3D metamaterials is realized (Figure 4.9c). In such a complex polymer-metal structure, the suppression of light reflection is attributed to consolidation of light scattering by the sample roughness, localized and de-localized excitation of plasmons within and on the surface of pores [201], as well as light trapping inside the gaps. Although broadband absorbers are critical in energy harvesting applications, for more effective use of solar energy it is desirable to develop cost-effective, durable and lightweight systems [202] with improved ability to absorb solar radiation energy particularly at wavelengths below 3 μm (c.f. Figure 4.9b) [203]. This chemically developed metamaterial absorber can withstand high temperatures, which demonstrates its potential application in energy collecting purposes. Figure 4.9c shows the black coated foam on a hot plate in comparison to uncoated foam. It can be clearly seen that the black metamaterial could stand high temperatures in which the neat foam melts. The bioinspired fabrication approach is another novel and cost effective method

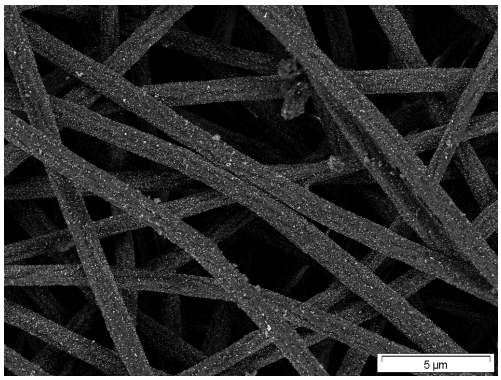

Figure 4.10: *Formation of a bionanohybrid structure through adsorption of Au nanoparticles onto the BSA/PANGMA nanofibers. (Figure adapted with permission. Copyright 2012, WILEY-VCH Verlag GmbH Co. KGaA, Weinheim [65].)*

for development of 3D metamaterials perfect absorber. Biological materials are inherently and naturally multifunctional and even smart. For instance, chameleons are well-known for their ability to change color. This stems from the fact that chromatophores (organocell) could either spread the pigment particles all over the cell or concentrate them into a small lump [204].A quite similar concept is applied for humidity based color change (light blue to black) in Cryptoglossa verrucosa. The color phases are formed by "waxfilaments" that spread from the tips of miniature tubercles that cover the cuticle surface [205]. Elbahri and co-workers [65] mimicked the beetles to achieve a broadband and lightweight perfect absorber using nanocomposites as a standalone matrix. Recently, they have shown a macro-porous membrane consisting of polymeric nanofibers and proteins able to filter out tiny nano-scaled particles present in aqueous solutions. A nanofluid (i.e. a colloidal suspension of metal nanoparticles in water) can pass through a macro-porous nano-fibrous membrane unless the membranes nanofibers are biofunctionalized by a globular protein. It was found

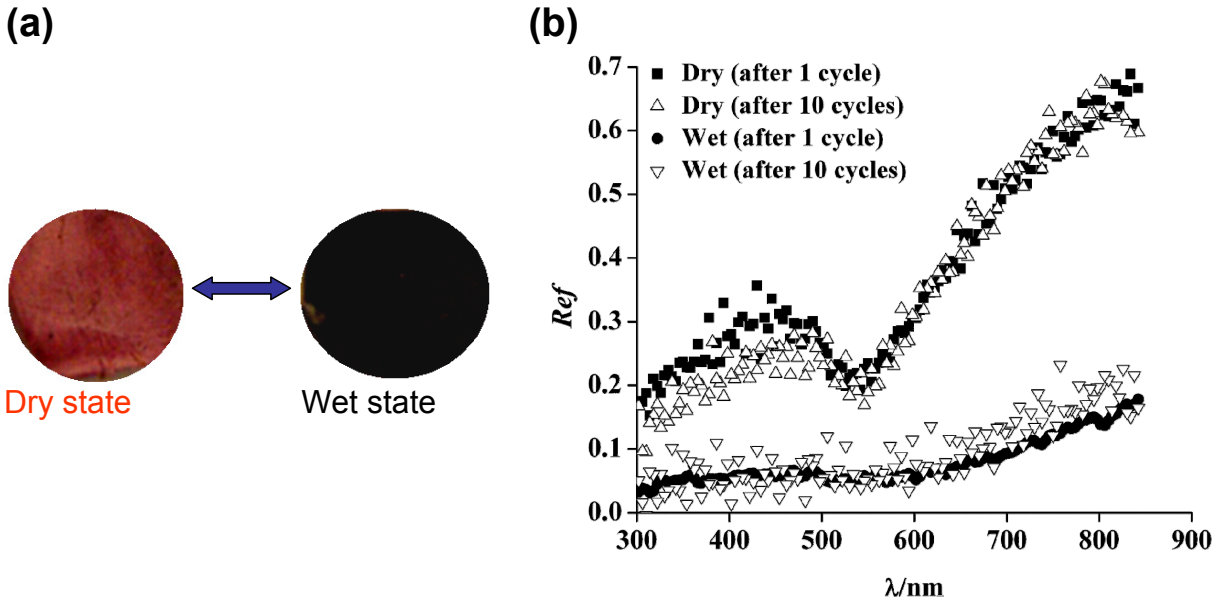

Figure 4.11: *(a) Tunable coloration of the surface of the membrane at dry (red) and wet (black) states. (b) The reflection spectra of the nanocomposite in dry and wet (completely water soaked) states. (Figure adapted with permission. Copyright 2012, WILEY-VCH Verlag GmbH Co. KGaA, Weinheim [65].)*

out that the biofunctional agent (bovine serum albumin) could undergo a conformational change thereby capturing all the metal nanoparticles during the filtration process. Accordingly, a novel method for bio-nanocomposite fabrication has been introduced (Figure 4.10) wherein the surface color changes (Figure 4.11a) from red to black upon wetting thereby enabling realization of an omni-directional wideband perfect absorber [65]. In dry state, the sample looks red while the average reflection of the sample is about 35%. On the other hand, by wetting the sample, it turns black while showing low reflectivity (Figure 4.11b) and it acts as a swollen, open, porous nanostructure foam. The resulting porous structure give rise to the localization of the incident electromagnetic field (in analogy to the nanoporous

structures). Therefore, the sample turns black and absorbs the visible energy [65]. Nevertheless, this bio-nanocomposite structure is in its infancy and further studies are required to explore the mechanism behind the high absorption. These mentioned examples shows that chemically routed fabrication methods could also provide the possibility for design and fabrication of new metamaterial absorber. However, wet chemical fabrication techniques are less considered and their pros and cons need to be explored.

4.5 Prospects and Future

The field of metamaterial perfect absorbers is still immature. Much more effort must be made to bridge the gap between the lab-scale fabrication and industrial application. Nevertheless, current achievements both in theory and experiments showed the immense potential of this new type of metamaterials for a variety of applications.

As the prime utility of highly absorptive structures, photovoltaic and solar cells are the fields of interest. Very recently, the effect of typical, perfect absorbing structures (i.e. metallic nanostructure and film separated by a dielectric) on the absorbing efficiency of organic photovoltaic materials was investigated. The authors demonstrated numerically that absorption augmentation up to 2.88 can be achieved in a 40 nm thick $P3HT : PC60BM$ film sandwich by Aluminum nanostructure and film due to critical coupling into the magnetic resonant mode [206,207]. Other uses of metamaterial perfect absorbers are in the fields where huge light confinement is desired. Li et *al.* [208] making use of such potential of plasmonic absorber, demonstrate its applicability in surface enhanced molecular spectroscopy (SEMS). Due to the localized field within the nanostructure and its tunability, the resonance could match the molecular vibrational modes of interest in the analyte which provides the possibility to identify chemical stretches. They showed that by using a cross-shaped nanoscale structure separated from a gold film by alumina, Parylene C molecular vibrational stretches in very thin film can be revealed [208]. Microbolometer thermal sensors is another general application of metamaterial absorbers [209]. Aluminum nano-pattern and aluminum plate with SiO_2 spacer layer was the design demonstrated by Kearney et *al.* [209].

Gigantic field enhancement achieved by perfect absorber can be applied for Raman spectroscopy of single molecules, too. Wang et *al.* [210] showed this in a structure composed of silver particles (average radius size of around 20 nm) dispersed on a surface of SiO_2 coated silver mirror. In such a structure , in which they called "metasurface", surface-enhanced Raman scattering (SERS) enhancement factors which is one order of magnitude higher than those of silver nanoparticle islands on glass can be achieved. They attributed this enhancement to the improvement in the coupling between the incident light and plasmon resonance of the developed metasurface [210].

Cloaking an object by perfect absorber (in reflection mode) is another potential application of this class of material. Alaee et *al.* [211] numerically showed that any object which can be wrapped by a perfect absorber would be cloaked and turn invisible in reflection due to the suppression of back-scattered light from the wrapped object. Their proposed structure is also composed of metallic pattern and film but on a curved surface. Perfect absorbers

designed for low frequency have been shown to be acoustic metamaterials which absorb the airborne sound in the frequency range of 100-1000 Hz. The designed and fabricated structure comprises an elastic membrane decorated with asymmetric rigid platelets. This intelligently designed metamaterial can have a broad range of applications such as reducing the cabin noise in airliners and ships, regulating the acoustic quality of music halls, and environmental noise abatement along highways and railways, amongst others [212].

Similar to other plasmonic structures, application of metamaterial perfect absorbers as a sensor [213] is also promising, in particular when the absorber is narrowband. In all reported works, tri-layer absorber is designed and it is shown that the resonance band of such structures can be tuned upon exposure to different liquids [43, 214] or vapor [215] because of the refractive index change of the surrounding environment.

Taking into consideration all the illustrated applicability of metamaterial perfect absorbers, one could see the progress in this new and fast growing field. However, none of the proposed structures have been used in the currently industrialized solar cells or collectors and therefore their long term performance and stability needs to be examined. Moreover, up-scaling of the nano-lithographically fabricated system (which is the major fabrication method in meatamaterial) in a cost-effective and reproducible way is also in doubt and requires the invention and development of some new robust and cheaper alternatives. Nevertheless, the future of this field is very bright and mass production and implementation of metamaterial perfect absorbers for everyday life is not out of reach in the current decade.

4.6 Acknowledgments

Authors gratefully acknowledge the financial support by the German Research Foundation (DFG) through the projects EL 554/1-1 and SFB 677 (C1,C9). M.E. would like to thank the Initiative and Networking Fund of the Helmholtz Association's (grant No. VH-NG-523) for providing the financial base for the start-up of his research group.

4.7 Conflicts of Interest

The authors declare no conflict of interest.

Chapter 5

Design of a perfect black absorber at visible frequencies using plasmonic metamaterials

M. K. Hedayati, M. Javaherirahim, B. Mozooni, R. Abdelaziz, A. Tavassolizadeh, V. S. K. Chakravadhanula, V. Zaporojtchenko, T. Strunkus, F. Faupel, M. Elbahri, Design of a perfect black absorber at visible frequencies using plasmonic metamaterials, *Advanced Materials 2011*, 23, 5410-5414.

5.1 Main text

During the course of the last decade, trends to achieve perfect absorbers increased tremendously due to the huge interest in development of the materials for harvesting solar energy. However up to date all of the applied methods (perforated metallic films [44, 45, 51], grating structured systems [41, 42, 50, 216], and metamaterials [31, 36–38, 40, 174, 217] are costly and suffer from a lack of flexibility. Furthermore their absorbance is limited to a narrow spectral range which makes their application for a broad range of frequencies impossible.

Here we demonstrate design, fabrication and characterization of a perfect plasmonic absorber in a stack of metal and nanocomposite showing almost 100% absorbance spanning a broad range of frequencies from ultraviolet to the near infrared. The fabrication technique of our metamaterial is cost effective and compatible with current industrial methods of MEMS which make our proposed system an outstanding candidate for high efficiency absorber materials.

Thick metallic film are known as an excellent mirror but when they are structured, the reflectance fades away because the light gets absorbed by the excitation of the conduction electrons by electromagnetic waves which is generally known as plasmon resonance [44]. This concept has been used in the last few decades to realize highly absorbing systems in diverse areas of the electromagnetic spectrum but these works were either successful only for a very

narrow range of frequencies [50], [37, 43, 218] or the absorbance was distant from that of blackbody materials [38].

Not only the metallic film supports plasmon resonances but also the metallic nanoparticles show high absorption due to its localized particle plasmon resonance (Mie resonance) [6, 219]. Indeed, the resonance of these particles embedded in different matrices has been extensively studied within the last decade and it is well known that the resonance band-width depends on the size, shape, density and distribution of the nanoparticles [6, 219]. Indeed, a highly dense nanocomposite gives rise to a very broad-band absorption due to the excitation of the localized plasmon resonance of the nanoparticles by visible light. In contrast to the expectation for the absorption behavior of a metal/polymer nanocomposite, we have recently shown that nanocomposites with low filling factor in a proximity to a thin metallic film can even enhance the optical transmission of the system due to the plasmonic coupling of the film and the nanoparticles which mainly result in a reflection/scattering reduction of the system by dipole/image interaction [134]. However, rising the distance between the metallic film and the nanoparticles by adding a spacer layer confines and traps the electromagnetic field in the small gap and consequently intensify the absorption. For this arrangement the absorption value typically does not exceed 60% and the absorption band is limited to a narrow frequency range.

Here we modified the concept by the use of a nearly percolated nanocomposite (possessing both localized and delocalized plasmon modes) as top layer and an optically thick metallic film as the base mirror separated from each other by a spacer layer where the light is trapped. Figure 5.1 shows the schematic geometry of the black absorber realized in this work (left) along with HRTEM image of the nanocomposite with 40% filling factor (right). The

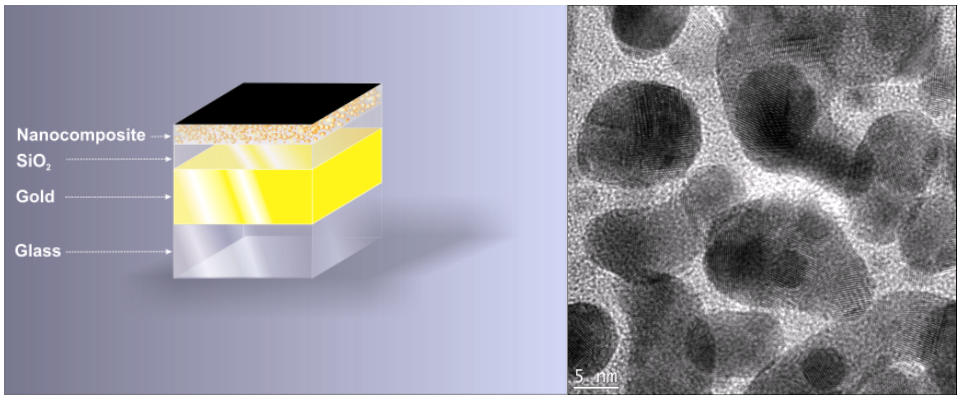

Figure 5.1: *Schematic of the perfect absorber structure manufactured by sputtering. The thickness of the nanocomposites, SiO_2 spacer and the gold mirror are 20, 25 and 100 nm respectively. The whole structure resides on a glass substrate (left) and the top view TEM image of the nanocomposite film (right).*

structure is composed of (from bottom to the top) a glass substrate coated with an optically thick metallic film (Au) followed by a thin dielectric layer (SiO_2) acting as a spacer layer and at the very top, a thin (20 nm) nearly percolated film of nanocomposite (Au/SiO_2).

Indeed, this coating can be applied onto any kind of substrate even on flexible ones. Figure 5.2 illustrates visually a blackbody made of gold showing the logo of our group either on a gold film (as background) (left) or directly on a flexible polymer (Figure 5.2(right)) demonstrating the versatility and applicability of this system on any kind of substrates.

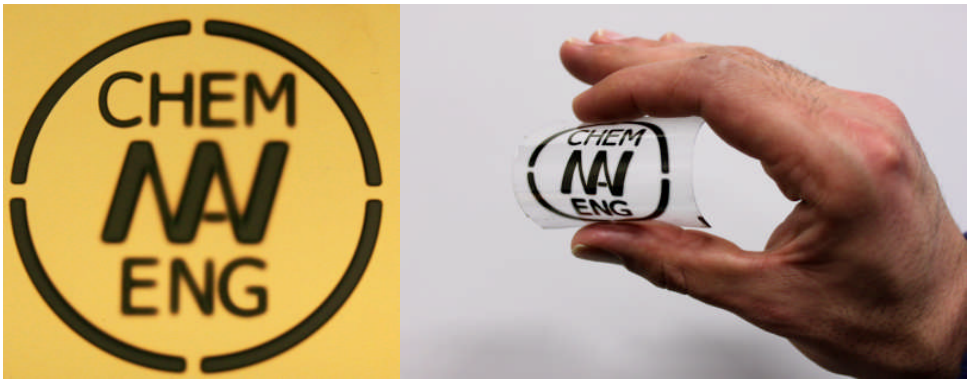

Figure 5.2: *Perfect absorber (blackbody) coated via a mask on a gold coated glass (left) and on a flexible polymer foil (right). It shows the potential of the coating for application onto a flexible substrate.*

Figure 5.3a shows the absorption and reflection spectra of our plasmonic metamaterial. One can see that the absorption of the system is almost 100% in most part of the visible. Indeed, corresponding reflectivity of the structure is negligible (almost zero) which is attributed to impedance matching of the device to the vacuum [43]. Impedance calculations were done to evaluate the matching behavior of the films. These data (inset in Figure 5.3a) were calculated from reflection measurements and showed that the impedance of our plasmonic metamaterials in most part of the visible spectrum is unity which is corresponding to the spectral region of minimum reflection.

Impedance matching of plasmonic metamaterials is owing to the magnetic optical resonance, which is induced by dipole-image interaction and causing an electromagnetic confinement in the spacer layer and thereby alleviate the reflection [31,37,43]. It is known that anti-parallel currents will be excited in the nanoparticles (embedded within the nanocomposite) and the bottom layer [43], [134,220]. Essentially, this is called a magnetic resonance for the reason that the circulating currents result in a magnetic moment which can robustly interact with the magnetic field of the incident light. Therefore, a strong enhancement of the localized electromagnetic field is established in the spacer layer and consequently no light is reflected back [43]. Having used a base layer with sufficiently large thickness to block the light from passing through along with the trapping of the light and suppressing reflection, the incident light will be obstructed completely and this makes the system a perfect absorber (Figure 5.3a). The role of magnetic resonance in the high absorption of the structure is further proved by measuring the optical spectra with polarized light. Figure 5.3b shows TE polarized absorption spectra of the device in the angles ranging from 15 to 60 degrees. Although the reflectance for TE polarization is larger than for TM polarization at higher incidence angle [43], (as expected, owing to the weak induction of the circulating current

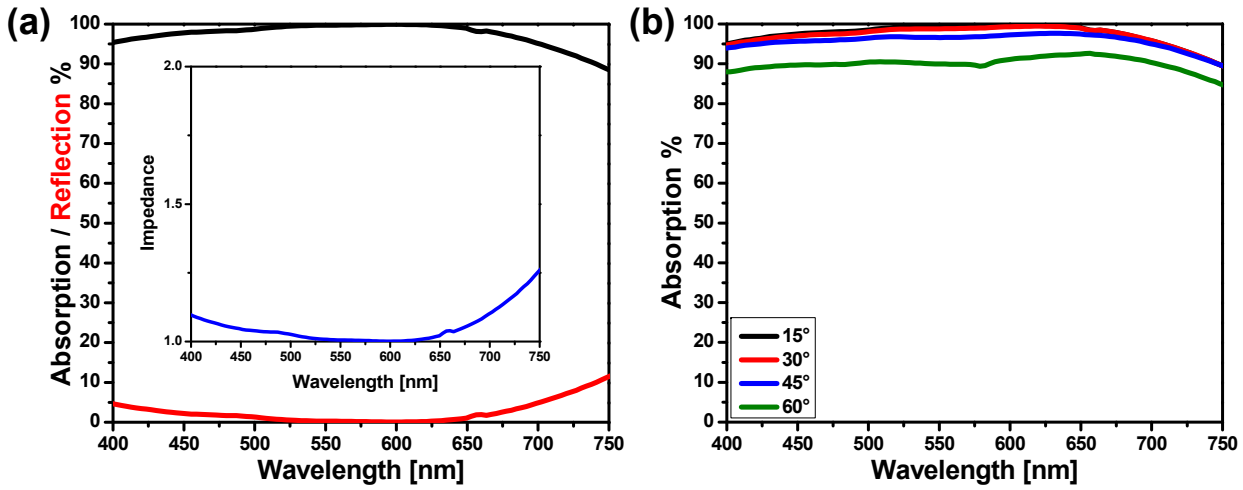

Figure 5.3: *(a)Absorption (black) and reflection (red) spectra of 20 nm Au/SiO_2 nanocomposite deposited on a 100 nm Au film with 25 nm SiO_2 spacer layer (black curves) measured at 6 degree angle of incidence. The inset shows the impedance data of 20 nm Au/SiO_2 nanocomposite deposited on a 100 nm Au film with 25 nm SiO_2 spacer layer. (b) Absorption spectra of gold based perfect absorber composed of 20 nm Au/SiO_2 nanocomposite deposited on a 100 nm Au film with a 25 nm SiO_2 spacer layer with TE polarization at 15 (black) 30 (red) 45 (blue) 60 (olive) degree of incidence, respectively.*

.

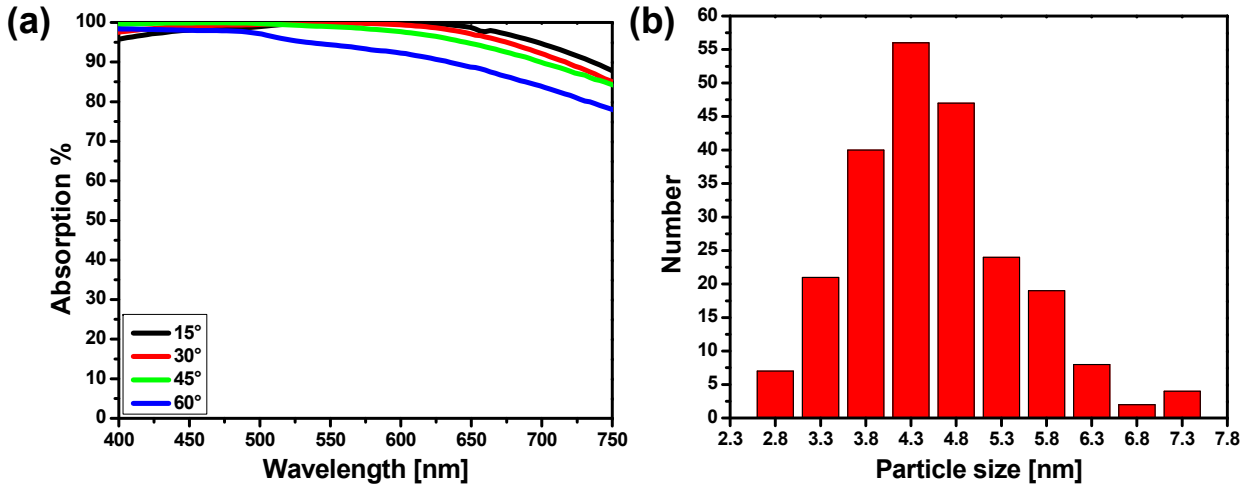

Figure 5.4: *(a) Absorption spectra of gold based perfect absorber composed of 20 nm Au/SiO_2 nanocomposite deposited on a 100 nm Au film with a 25 nm SiO_2 spacer layer with TM polarization at 15 (black) 30 (red) 45 (blue) 60 (Magenta) degree of incidence, respectively. (b) The typical size distribution of the nanoparticles of the nanocomposite used as the top layer.*

.

between the top nanoparticles (dipoles) and the bottom metallic film (mirror)), in the TM mode (Figure 5.4a), the magnitude of resonance peak does not change so much with angle [37]. In fact, we attribute the broad resonance of our structure to two effects. The first is the hybrid plasmonic coupling between the broad Mie resonance of the nanoparticles (which is originated from the large size distribution of the particles (Figure 5.4b) with random shapes [221]) and the plasmon polariton of the metal film whereas the induced plasmonic magnetic resonance within the spacer layer (owing to the interaction within nanoparticle plasmon resonances in the composite and their dipole images on the gold mirror) is another reason which gives rise to a very broad resonance of the system. These facts can be better understood when the sample is illuminated at higher incidence angle ((Figure 5.3b Figure 5.4a). In that case the broad plasmonic resonance peak splits into two peaks along with a drop in absorption (especially in TE polarization). In other words, the broadness of the absorption peak originates from the overlap of two resonances inside our plasmonic metamaterials [222].

Even thought there is a drop in absorption up to 60 degree angle, the drop is not so large and the overall absorption still remains around 90% in a broad range of the spectrum which shows the potential of using this system as a solar absorber [223]. Indeed the angular dependence reflectance for both polarizations show a negligible change which indicates that our plasmonic metamaterials are effective for both light propagating directions, in contrast to known split-ring resonators (SRR) which are highly angle-dependent [37]. To further prove the role of dipole-image interaction, the thickness of the spacer layer changed while keeping the other parameter constant (Figure 5.5a). Changing the thickness of the spacer layer influences the interference of the plasmon waves and results in a change of the resonances. Indeed, raising the distance between the metal film and the nanocomposite by adding a thick interlayer, disturbs the resonant condition and results in a weaker coupling. (Figure 5.5a). Our results gave critical spacer layer of 25 nm where the absorption width and intensity is maximized and slight changes in the mentioned spacer thickness values lead to an absorption reduction due to the lack of efficient dipole-dipole interaction [224] and shows that the absorption of the device is not based on Fabry-Perot resonance [225]. Besides the high absorption of this structure, its band-width can be tuned by adjusting the filling factor of the nanocomposite. To study the effect of the filling factor on the optical properties of our absorber, gold based absorbers with different filling factors were prepared and examined. It was observed that changing the filling factor of the nanocomposite from its optimum value (40%) shifts the resonance peak either towards the NIR upon raising or blue shift the resonance upon decreasing the filling factor (Figure 5.5b). This is indeed attributed to the mismatching of the SPPs resonances [226]. However, the structure with very high filling factors (i.e. already percolated nanocomposites) result in intensive reflectivity which is accompanied by a drop of the absorption. Figure 5.6a shows the spectrum of a fully percolated composite deposited on a spacer coated gold film. As mentioned above, the reflectivity of the system is enhanced dramatically compared to the near percolated one which leads to the drastic reduction of the absorption. Not only the filling factor of the composite changes the absorption of the structure but the type of the dielectric matrix will also affect the overall absorption of the system. Figure 5.6b shows the absorption of the absorber with three different matrices of the composite (TiO_2, SiO_2 and $PTFE$).

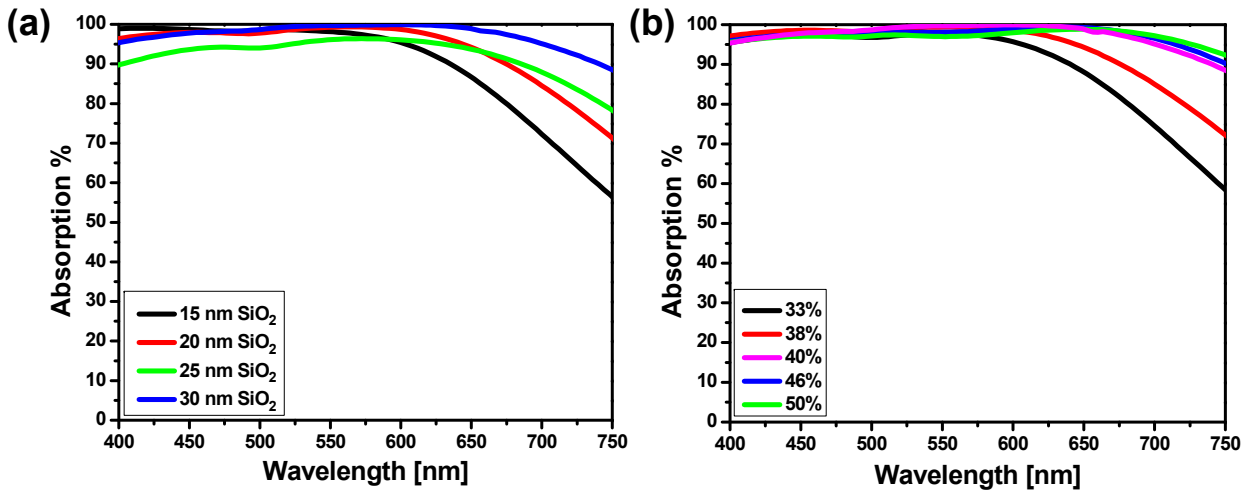

Figure 5.5: *(a) Absorption spectra of Au based perfect absorber composed of 20 nm Au/SiO_2 nanocomposite deposited on a 100 nm Au film with different thickness of inter-layer. (b) Absorption spectra of 20 nm Au/SiO_2 nanocomposite with different filling factor sputtered on a 100 nm Au film with a 25 nm SiO_2 spacer layer at 6 degree angle of incidence.*

One can clearly see that using TiO_2 (refractive index = 2.5) instead of SiO_2 (refractive index = 1.5), the absorption shifts to the lower frequency and its intensity drops. This can be attributed to the retardation effect of the higher refractive index matrix on the resonance of the metallic particles. In addition, the high value of the dielectric constant of the corresponding nanocomposite, disturbs the condition of impedance matching to the vacuum and thus the absorption (reflection) of the system drops (goes up). On the other hand, when a composite composed of gold and a low dielectric constant matrix ($PTFE$ with refractive index of 1.35) is used, the resonance of the system is significantly blue shifted which we attribute to the higher resonance frequency of the metallic particles in low dielectric constant environment [218]. This is indeed another sign of the plasmonic origin of our device which changes its resonance upon changing the dielectric constant of the environment [6].

Indeed study of the both filling factor as well as the spacer layer along with the angular dependence measurements showed that the 100% absorption could only be realized under certain condition while slightly changes in the optimum condition causing a drop in the absorption intensity. However better understanding of this fact needs in depth investigation which is far above the scope of this work. Our concept is simple, cost effective, straightforward and applicable to all plasmonic materials. To prove the concept, we have also designed and fabricated a copper based perfect absorber which also exhibits a broad absorption resonance in the visible (not shown here).

5.2 Summary

In summary, we have developed a new plasmonic metamaterial with almost perfect absorption of light within the whole visible spectrum. Its fabrication technique is cost effective

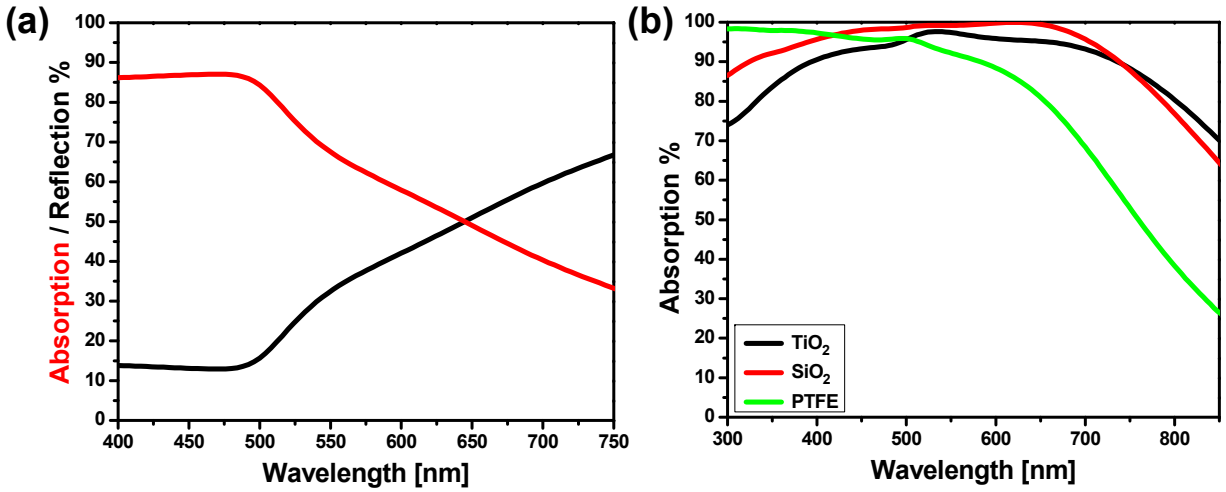

Figure 5.6: *(a) Absorption/Reflection spectra of 20 nm of a fully percolated composite on a 100 nm Au film with a 25 nm SiO_2 spacer layer at 6 degree angle of incidence. (b) Absorption spectra of a 20 nm Au/SiO_2 (circles), 20 nm Au/TiO_2 (traingles) and 20 nm $Au/PTFE$ (squares) nanocomposite on a 100 nm Au film with a 25 nm SiO_2 at a 6° angle of incidence.*

and compatible with current MEMS industry. In addition the small thickness of the whole film and its potential to be deposited onto flexible substrates makes it an excellent candidate for absorber and/or anti-reflector coatings. We have shown that this method can be used for different noble metals and the high absorption achieved is slightly sensitive to the polarization and does not change significantly with the angle of incidence.

5.3 Experimental

All experiments were carried out in a home made metal vacuum chamber, which was initially evacuated to below $10^{-6} mbar$. Two magnetron sources was installed inside the chamber which allows synthesis of nanocomposite films as well as multilayer systems with different metal filling factors. We used an RF magnetron system for sputtering of SiO_2 and a DC magnetron sputter source for gold. The magnetrons were arranged in opposite directions relative to the sample holder both with an angle of 50° to the substrate plane. A rotatable sample holder was used to obtain films with a uniform thickness and metal distribution. The thickness of the films was measured with a profilometer (Dektak 8000 surface profile measuring system). Energy dispersive x-ray spectroscopy (EDX) mounted in a scanning electron microscope (SEM) (Philips X L30) was used to determine the metal amount and distribution in the composite films. Details of the EDX measurement for filling factor calculation can be found in ref. [218]. For UV-vis measurements the layers were deposited onto glass slides. The optical properties were studied using a UV/Vis/NIR spectrometer (Lambda900, Perkin Elmer) and for the angular dependent measurements an Ellipsometer was used Polarization dependent measurements were also done in Mads Clausen Institute (University of Southern

Denmark) with an adjustable polarizer supplied with the Ellipsometer.

5.4 Acknowledgements

The authors would like to thank Prof. Ruhbanh (University of Southern Denmark) for providing the possibility for doing the ellipsometer measurements and S. Rehders for his technical help regarding the set up and operation of the sputter chamber. Financial support was partly provided through SFB 677 funded by the German Research Foundation (DFG). M. Elbahri would like to thank the Initiative and Networking Fund of the Helmholtz Association's (grant No. VH-NG-523) for providing the financial base for the start-up of his research group.

Chapter 6

Tunable broadband plasmonic perfect absorber at visible frequency

M. K. Hedayati, F. Faupel, M. Elbahri, Tunable broadband plasmonic perfect absorber at visible frequency, *Applied Physics A 2012*, 109, 769-773.

6.1 Abstract

Metamaterials and plasmonics as a new pioneering field in photonics joins the features of photonics and electronics by coupling photons to conduction electrons of a metal as surface plasmons (SP). This concept has been implemented for a variety of applications including negative index of refraction, magnetism at visible frequency, cloaking devices amongst others. In the present work, we used plasmonic hybrid material in order to design and fabricate a broad-band perfect plasmonic metamaterial absorber in a stack of metal and Copper-$PTFE$ (Polytetrafluoroethylene) nanocomposite showing an average absorbance of 97.5% in the whole visible spectrum. Our experimental results showed that the absorption peak of the stacks can be tuned upon varying the thickness and type of the spacer layer due to the sensitivity of plasmon resonance to its environment. To the best of our knowledge, this is the first report of a plasmonic metamaterial absorber based on copper with absorption around 100% in the entire visible and near-Infrared (NIR).

6.2 Introduction

The general interest in solar use was raised fast in the mid-70^s due to the renewed interest in substitute energy resources, which resulted from the "oil crisis" [120]. Graded structure made of a metal-dielectric composite along with anti-reflectors were one of the basics of the developed structure for solar absorption, which were fabricated by the electroplating or vacuum deposition methods (details can be found in [120]). Nowadays, due to the fast growing field of nanotechnology and the great demand for a nanoscale system, the trends to realize

a system showing black absorption for solar and sensoric purposes with sub-wavelength dimension increased. However, so far most of the applied techniques (e.g., perforated metallic films [44], grating structured systems [42] and metamaterials [31, 36, 43] are either costly or has low fabrication tolerance and their absorption resonance is a narrow-band, which limits their utility for energy harvesting. Recently, we showed experimentally for the first time fabrication of a broadband perfect plasmonic absorber in a stack of gold and Au-SiO_2 nanocomposite showing nearly 100 % absorbance at the visible spectrum [147, 227]. In this report, we implemented the same idea but in a polymeric nanocomposite and replaced gold with a copper to significantly reduce the material cost. In the copper-based absorber, the bandwidth is broader and since the copper is cheaper than gold, the new developed absorber is more cost effective for practical application. In addition, the average value of absorption in visible is above 97 %, which is the best reported broadband plasmonic perfect absorber so far.

6.3 Experimental procedure

A cylindrical vacuum chamber was used for sputtering of the metal and polymeric film. By installing two magnetrons with an angle of 50°, co-sputtering was done in order to make a nanocomposite out of a copper and $PTFE$ targets. Simultaneous sputtering from different sources allows deposition of nanocomposites with different filling factors (ff) and thicknesses. For acquiring a uniform thickness for the film and homogeneous metal distribution for the composite, all depositions were done on the samples attaching to a rotatable sample holder. For dielectric deposition ($PTFE$ in this case), a RF power and for conductive targets (Copper) a DC power supply were used. The details of co-sputtering methods can be found in our former reports [228]. Thickness measurements were performed using the Dectak 8000 profilometer. Optical analysis carried out by a UV-Vis-NIR spectrometer (Lambda 900, Perkin Elmer). Although aluminum was used as a mirror for reflection measurement, the data was normalized to a perfect reflector in order to achieve absolute value of reflection. Since all the base film thickness was 100 nm, which is far greater than the skin depth of copper, it was assumed that the transmission is zero. Therefore, all calculation of absorbance is based on: $A+R = 100$ %, where A stands for absorption and R is reflection.

6.4 Results and discussion

A schematic of the structure, which was used in this work is shown in Figure 6.1a. It is composed of an optically thick copper film as base layer (100 nm) and a nearly percolated Copper-$PTFE$ nanocomposite as a top layer, which are separated by a dielectric interlayer ($PTFE$). Transmission Electron Microscopy (TEM) of the nanocomposite used in this work presented in Figure 6.1b. One can see that the distance between the particles is very small and the composite is near-percolation. Figure 6.2a shows the photograph of the optimized sample compared to the bare copper film where one can see the black appearance of the highly absorber system compared to the shiny surface of metallic film. Optical measurements

showed that a 20 nm spacer layer of $PTFE$ gives the best performance of the device and thickening or thinning the thickness of interlayer reduced (increases) the absorption (the reflection) of the system. Figure 6.2b shows the absorption spectra of 20 nm Cu-$PTFE$

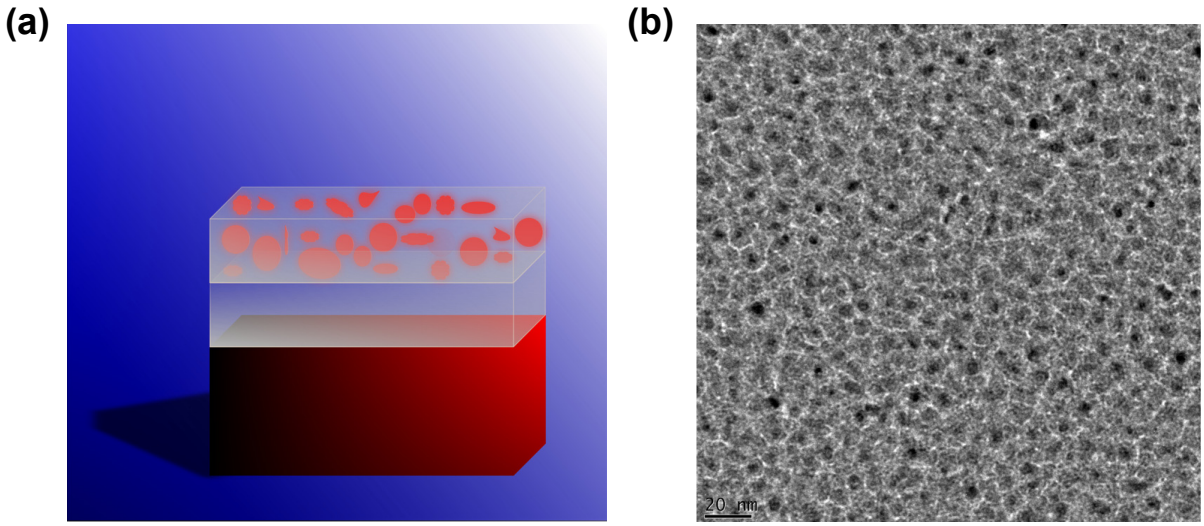

Figure 6.1: *(a) Schematic drawing of the perfect absorber structure, which is composed of the Cu-PTFE nanocomposite deposited on the PTFE coated copper film. (b) Top-view TEM image of the near percolated Copper-PTFE nanocomposite.*

composite on 100 nm copper-base layer separated with different thickness of interlayer. It is obvious that changing the spacer layer thickness from the optimum value of 20 nm will alter the efficiency of the device and the absorption drop. We attributed the drop to the lack of coupling of the top nanoparticles and the base layer. Indeed, in such a system, excitation of anti-parallel currents between nanoparticles (embedded within the nanocomposite) and base layer (known as magnetic resonance) induced by dipole-image interaction will trap the light within the interlayer. However, it seems that upon increment or decrease of spacer-layer thickness, dipole-image interaction becomes less efficient and results in a drop in absorption [43, 147]. Deposition of the composite on a bare base layer further supports the mentioned idea in a sense that when there is no distance between the film and nanoparticles, no light can be confined and, therefore, the reflection enhances (Figure 6.2b (green curve)). The optical response of such a stack is not only dependent on the spacer layer thickness rather than the filling factor of the composite plays a crucial role in the efficiency of film. UV-vis measurement of the samples prepared with different filling factor showed that the best performance achieved when the ratio of the sputtering rate of copper to PTFE is 2.33. On the other hand, changing the sputtering ratio to 2.0 or 2.66 reduces the overall absorption of the device. Figure 6.3a shows the absorption spectra of the stacks with a different sputtering ratio of copper and $PTFE$. It is obvious the highest absorption occurs when the ratio is 2.33. When the ff rises far above the percolation threshold, the reflectivity of the upper layer goes up, and consequently the optical response of the stacks becomes similar to thick copper film. In other words, as soon as the composite starts turning to a continuous metal film, the light cannot pass through the top layer anymore and it acts as

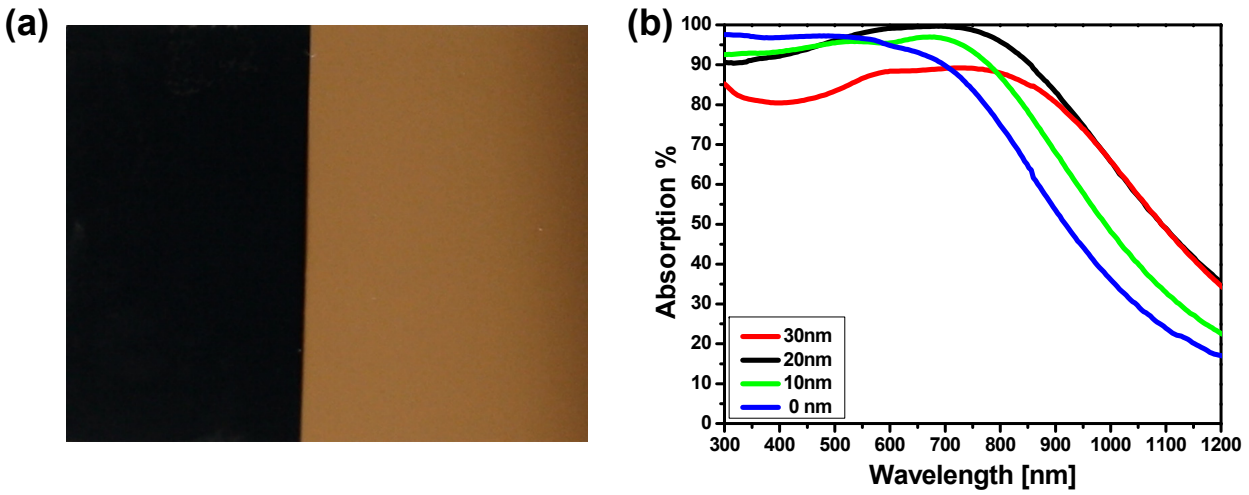

Figure 6.2: *(a) Photo of the perfect black absorber (left) in comparison with bare copper film (right). (b) Absorption spectra of 20 nm $Cu-PTFE$ composite on $PTFE$ spacer layer with different thicknesses on a 100 nm Cu. The green curve shows the composite on a base layer without any inter-layer for comparison.*

a metal reflector. Therefore, the absorption of the structure dramatically drops. Comparing the current results with our previous report on the gold base perfect absorber [147], one can see that the broadness of the peak in the copper-base perfect absorber is more than the gold base one. In other words, the average value of absorption in the visible range (400 - 750 nm) is around 97%, which shows the higher efficiency of the copper-absorber compared to its gold counterpart. In fact, the filling factor of the optimized condition in the copper system (70%) is far above that of gold (40%) and, therefore, it is expected to be highly reflective. However, a broader resonance and perfect absorption was observed, which we attributed to the plasmonic damping of copper, which occurs due to interband processes via the electron photon as well as electron-electron scattering [229]. The role of magnetic resonance in the high absorption of the structure was shown in our last work [147], however, one cannot roll out the significance of interference in the low reflectivity of such a structure. The influence of interference in a perfect absorber has been recently proposed by Chen [181]. He showed in a typical metamaterial absorber there is minor near-field interaction or magnetic response among the neighboring metal structures. In addition, the surface currents with anti-parallel directions originated from the interference and superposition, rather than excited by the magnetic component of the incident electromagnetic fields [181]. It seems that interference can also play a role as a contributor to the observed low reflection of our system besides other mentioned phenomena. In other words, not only plasmon coupling rather than interference and multi-excitation of resonance because of the mirror nature of the base layer contribute to the high absorption (low reflection) of the multi-stacks. However, further theoretical works are required to explore the real mechanism of the high absorption in our multi-stack structure.

Measuring the optical response of the metal alone as well as the composite film with the same condition deposited on glass substrate showed that the high absorption of the

system is originated neither from the composite alone nor from the metal. Figure 6.3b shows the absorption spectra of the composite and bare copper film on glass. It is clear that the average absorption value in both cases is less than 30%, which is far below the 97% of the copper-perfect absorber. These results further support the idea of plasmon coupling in the highly absorber structures and show that the Ohmic losses of the device within the metallic particles due to the localized particles plasmon resonance of copper nanoparticles is not the dominating process of the overall absorption. In addition, the optical study of the system with a different spacer layer thickness further supports the significant role of dipole-image interaction in perfect absorption of our developed system (Figure 6.2b). As it was mentioned above, increasing the distance between the metal film and the nanocomposite by adding a thick spacer layer, disturbs the resonant condition and results in a weaker coupling. Different to our previous report [147], a critical spacer layer of 20 nm was observed where the absorption width and intensity is maximized. The significant drop in the absorption observed when the thickness of the spacer layer exceeds 50 nm, which we attributed to the lack of efficient dipole-dipole interaction. Indeed, the difference of the spacer layer in the gold and copper system can be attributed to two effects. First, the refractive index of $PTFE$ is less than that of SiO_2. Secondly, the plasmon resonance of gold and copper respond differently to the certain dielectric [6]. Besides the two mentioned parameters, the ratio of gold to SiO_2 matrix in the gold-perfect absorber was less than the ratio of copper in $PTFE$ in copper-one. Indeed, all of the difference originated from the different plasmon resonance of gold and copper.

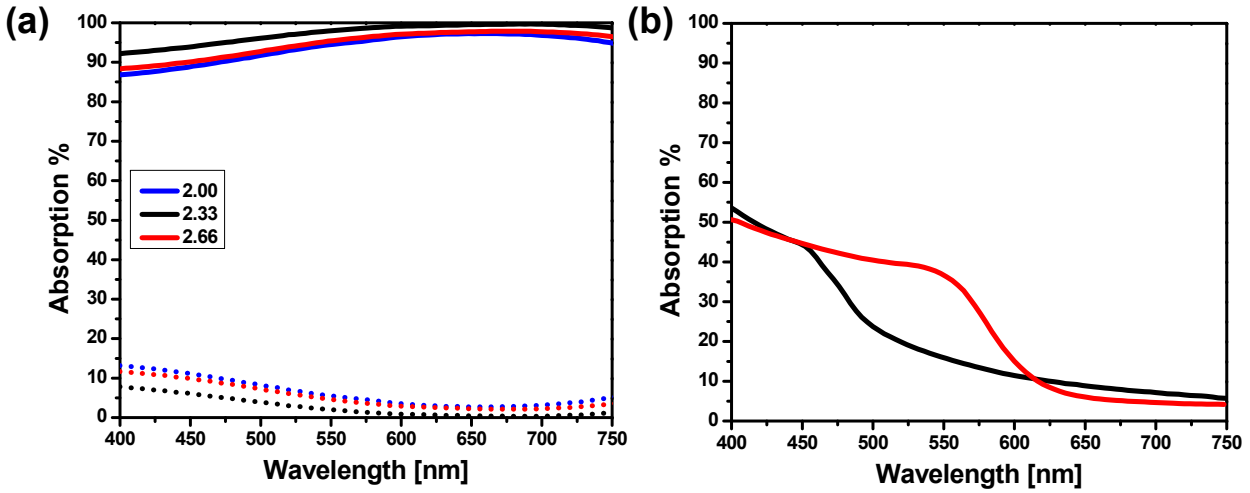

Figure 6.3: *(a) Absorption (solid lines) and reflection (dot lines) spectra of the near percolation nanocomposite with three different sputtering ratios of polymer and metal on a 100 nm Au film coated with 20 nm PTFE layer as a spacer. (b) Absorption spectra of 20 nm Cu-PTFE composite (black) with a sputtering ratio of 2.0 on 20 nm PTFE on glass in comparison of 100 nm copper film (red).*

6.5 Conclusions

In summary, we have developed and studied a new plasmonic metamaterial with almost perfect absorption of light in visible frequency. Structure out of the polymer matrix of composite and spacer layer and copper as a metallic component showed that the perfect absorption can be achieved with another system rather than gold. However, the thickness of the interlayer and the filling fraction of metal should be varied and depends on its dielectric function. We concluded that the only interference theory cannot explain the broadband perfect absorption of our developed system and in parallel plasmonic coupling and multi-excitation of plasmon resonance of particles due to the reflective nature of copper base film, which also contribute to the high absorption of the structure. Due to the simple fabrication technique that we employed, the production cost is very low compared to the competitive methods such as e-beam lithography. In addition, the higher fabrication tolerance of our highly absorber structure makes it an outstanding candidate for future application in photovoltaic and sensors.

6.6 Acknowledgements

Funding by the German Research Foundation (DFG) through the projects EL 554/1-1 and SFB 677 (C1, C9) are acknowledged. M.E. would like to thank the Initiative and Networking Fund of the Helmholtz Association (grant No. VH-NG-523) for providing the financial base for the start-up of his research group. The authors acknowledge V.S.K. Chakravadhanula for taking the TEM image.

Chapter 7

Plasmonic tunable metamaterial absorber as ultraviolet protection film

M. K. Hedayati, A. U. Zillohu, T. Strunskus, F. Faupel, M. Elbahri, Plasmonic tunable metamaterial absorber as ultraviolet protection film, *Applied Physics Letters 2014*, 104, 041103, doi: 10.1063/1.4863202.

7.1 Abstract

Plasmonic metamaterials designed for optical frequency have to be shrunk down to few 10^{th} of nanometer which turns their manufacturing cumbersome. Here, we shift the performance of metamaterial down to ultraviolet (UV) by using ultrathin nanocomposite as a tunable plasmonic metamaterial fabricated with tandem co-deposition. It provides the possibility to realize a plasmonic metamaterial absorber for UV frequency with marginal angle sensitivity. Its resonance frequency and intensity can be adjusted by changing thickness and filling factor of the composite. Presented approach for tunable metamaterials for high frequency could pave the way for their application for thermo-photovoltaic, stealth technology, and UV-protective coating.

7.2 Introduction

Plasmonic Metamaterials (PM) as a class of materials with some exotic properties drawn the attention considerably in the last decade due to non-limited potential for vast number of applications such as negative refractive index [230], nano-laser [231] and photovoltaics [5] amongst others. Metals, as a core of majority of PM suffer from losses especially when it is supposed to be contrived for ultraviolet (UV)-visible frequencies [232]. For a metal surrounded by an ideal dielectric, loss is originated by free-electron scattering in the metal and, at high frequencies, through absorption via inter-band transitions [233]. In spite of early consideration of loss as a foremost drawback of PM, the absorptivity is started to be

considered as one of the new potential application of PM following the first experimental demonstration of PM perfect absorber (MPA) [31] (For detail see the review by Padilla and co-workers [32]). Thick film of metal-dielectric [234–236] or semiconductor-dielectric [237] composite have been used as spectrally selective absorber since late 70th for solar thermal absorber whereas the high absorption in metallic composite was attributed to the interband transition of metal and small particle resonance [234–236]. Because of the large thickness of these films, their application in miniaturized device of 21st century is limited. Replacing small inclusion of nanocomposite with lithographically fabricated nanostructure have been the main trend in development of recent MPA. This approach could realize perfect absorber but due to the narrow band-width, sensitivity to the angle of incidence and low production tolerance of this complicated structure, their performance could not exceed that of old hybrid films. We have shown recently that instead of using very thick composite, ultra thin film deposited on highly reflecting mirror where the two layers separated with a dielectric layer could act as a perfect absorber for different frequency [147, 148]. This approach is enjoying ease of fabrication, low production cost and possessing high efficiency in the sense of absorption intensity, band-width and angular sensitivity while being ultrathin (20 nm). In such a plasmonic metamaterial super absorber (PMSA), the absorption is routed from several sources: multi-reflection of light from the base mirror which results in multi-excitation of plasmon resonance in particles, destructive interference between the thin layer which (increases) reduces the reflectivity (absorption) [198] and strong light confinement (creation of hot spot) between the small gaps of particles [147]. . In general, excluding

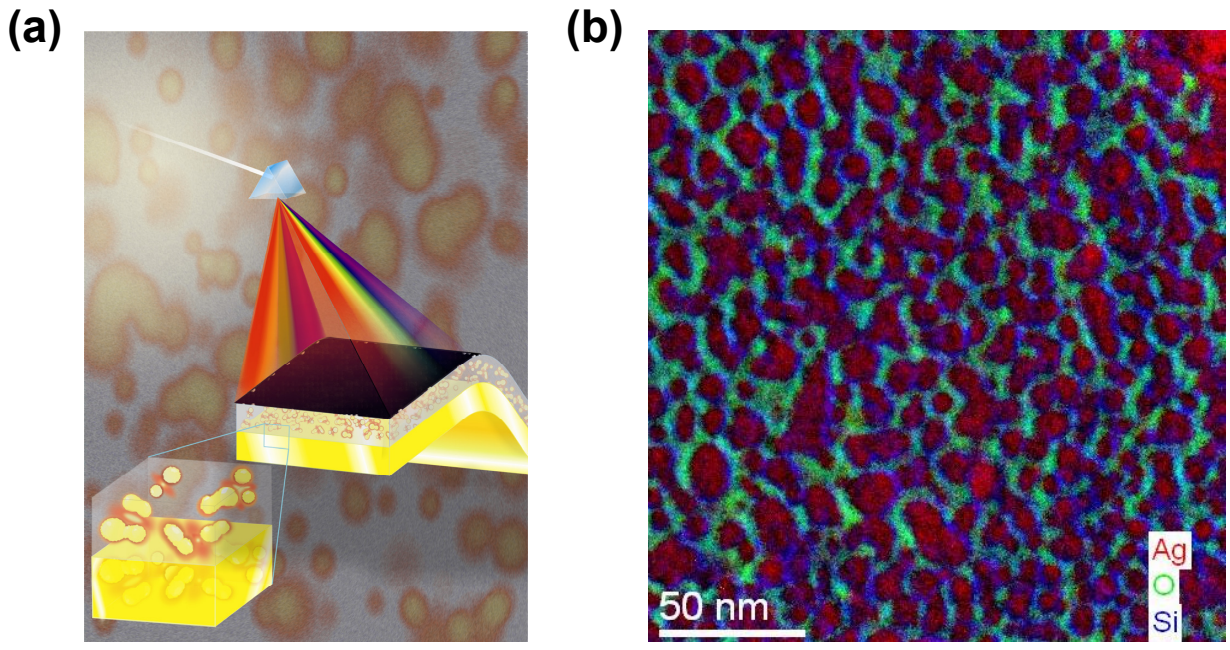

Figure 7.1: *(a) Schematic of the geometry of the metamaterials where the base layer is a optically thick silver covered with 15nm SiO_2 film. Atop, 15nm Ag-SiO_2 composite with near percolation filling factor is deposited. (b) TEM elemental map of the optimized silver-SiO_2 nanocomposite for perfect absorption.*

few exceptions, gold is the leading metallic components of metamaterials in general and metamaterial absorber, in particular, because of its large (plasmonic) absorption in green part of visible [45, 51, 60, 147, 238, 239]. However, the perfect absorption frequency is mainly limited to visible/near infrared [63] and shifting the resonance to shorter wavelength (e.g. UV) remains as a challenge. Because of interband transitions frequency of silver (in UV region) and its short-wavelength plasmon resonance, silver based perfect absorber can be a promising candidate for high efficient inorganic UV protection layer. In fact, any surface plasmon wave (SPW) propagating along the surface of gold is more attenuated and exhibits higher localization of electromagnetic field in the dielectric than an SPW supported by silver [19]. Therefore, the silver base PM can not only be more practical for energy absorption but also the light can propagate in metal/dielectric interface for larger distance than that of gold [240]. UV radiation is typically categorized into 3 bands in sequence of rising energy: UV-A (320-400 nm), UV-B (280-320 nm) and UV-C (100-280 nm). This division was put forward by the Commission Interntionale de l'Eclairage (CIE), and corresponds broadly to the effects of UV radiation on biological tissue. Indeed, approximately 5% of the ground-level solar radiation is ultraviolet radiation, mostly in the UV-A range [241]. Accordingly, a practical UV coating layer should be more absorbing in UV-A frequencies. Here in this report, we design and fabricate a tunable silver-SiO_2 nanocomposite following our recent works [147, 148] on a highly reflecting substrate by tandem co-deposition to realize a PMSA which operates through the visible up to UV-A frequency. SiO_2 film as a dielectric used to separate the composite from the base mirror. In this configuration, the huge absorption of light in a broad range of frequency (in visible and UV) can be achieved which surpassing the absorption intensity of recently reported silver absorber [55, 61, 242]. The absorption of presented PM is almost invariant to the angle of incident and its broadband peak can be tuned throughout the UV-visible frequencies which shows its great potential in sensing applications, too [243]. To demonstrate the feasibility of our absorber functioning as a UV protective layer, we compare the performance of current design with organic counterpart. For that purpose, a dye-molecule incorporated in polymer matrix film [132] was deposited on optically thick silver film as UV absorber and the absorption intensity and band-width of the both film were collated. It turns out that the absorption intensity of PMSA system is twice of organic one. Not only the absorption intensity of silver base absorber is higher but also the its bandwidth cover broader range of frequency than the single-band dye absorber showing its advantage over traditional absorbers [244].

7.3 Experimental Procedure

A cylindrical custom-build vacuum chamber was used for sputtering of the metal and dielectric. By two magnetrons with an angle of 50°, co-sputtering was done in order to make a nanocomposite. Simultaneous sputtering from different sources allows deposition of nanocomposites with different filling factors (ff) and thicknesses. For acquiring a homogeneous thickness for the film and uniform dispersion of metals, all depositions were carried out on the samples attaching to a rotatable holder [134]. Spirophenanthrooxazine (SPO) molecules ($1,3-Dihydro-1,3,3-trimethylspiro[2H-124indole-2,30-$

$[3H]phenanthr[9,10-b](1,4)oxazine]$), which was used as a photochromic dye, was obtained from Sigma Aldrich. For spin coating a thin layer of SPO doped Polystyrene (PS), 1.2 wt% of solute, consisting of equal amounts of PS and SPO, was dissolved in toluene. Substrate was hold in vacuum chuck of the spin coater and $70\mu l$ of the desired solution was injected on its surface. The spinning speed of 2000 rpm used for samples to yield a uniform thin film. . Thickness measurements were performed using the Dectak 8000 profilometer and optical

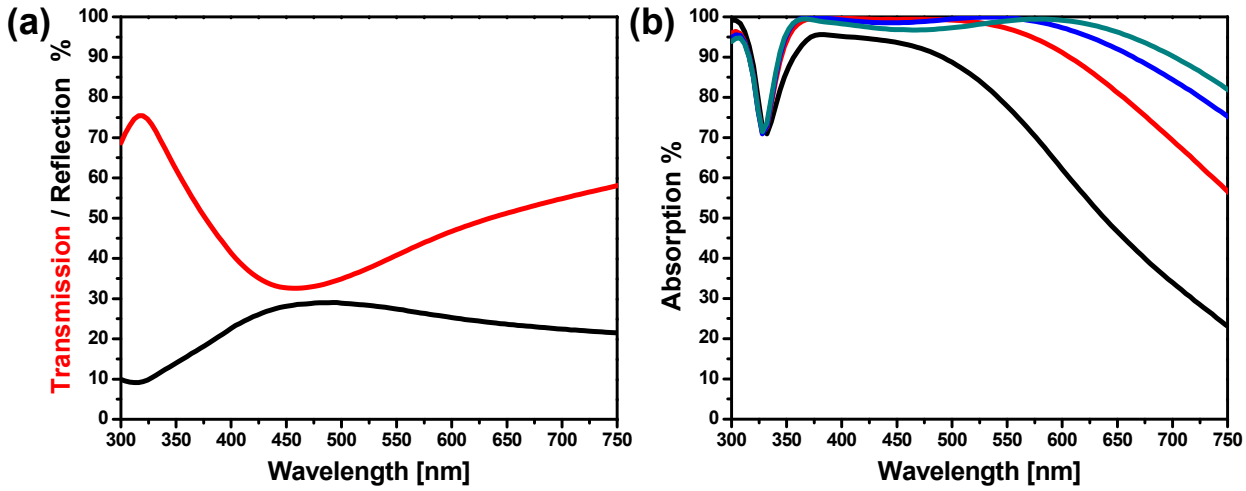

Figure 7.2: *(a) Reflection spectra of 20nm silver-SiO_2 nanocomposite with 40% filling factor deposited on glass substrate. (b) Absorption spectra of silver-SiO_2 nanocomposite with 15 nm (black curve), 20 nm (red curve), 25 nm (blue curve) and 30 nm (green curve) thickness deposited on 15 nm SiO_2 coated silver mirror.*

analysis was done by a UV-Vis-NIR spectrometer (Lambda900, Perkin Elmer). Angular reflection measurements of the films was carried out with J. Woolam M-2000 (spectroscopic ellipsometer).

7.4 Results and Discussion

The elemental map of the real sample measured with HRTEM and the schematic geometry of the designed PMSA are presented in Figure 7.1. The stack is composed of 4 layers. From bottom to up, glass, 200 nm silver film, 10-30 nm SiO_2 and 20 nm Silver-SiO_2 composite, respectively. The gap between the nanoparticles (NPs) is very small because of high filling factor of particles. Indeed, the inter-particle distance is varying between 2 nm to 5 nm which guarantees the strong confinement of electric field in such a system. Since the base layer is optically thick (200 nm silver), the transmission is nearly zero and hence reducing the reflectivity to very negligible amount would provide the condition for super absorption. It is known that silver's reflection is close to 100% over the entire visible region but it reduces to less than 10% in 320 nm due to a surface plasmon resonance [245]. Hence, the absorption of optically thick Ag film is usually below 5% in the visible region [55]. On the other hand, the transparency of silver-SiO_2 composite with 30-40% filling factor is

around 44% in visible, but its average reflection is 25%. In Figure 7.2a, transmission and reflection spectra of the 20 nm silver-SiO_2 composite with 40% filling fraction of metallic particles are depicted. The dissimilarity between the transmission and reflection spectra in Figure 7.2a could be due to the fact that the transmission spectra which reflect the morphology of the films throughout their depth are more affected by particle aggregation, but reflection spectra are more sensitive to surface structures in the film [246]. The drop in the transmission of composite film stem from the localized particle plasmon resonance (LPPR) of silver particles which revealed at 450 nm. In spite of known sharp resonance peak of silver particle, the dip in spectra of nanocomposite is relatively wide which originate from different shape and size (distribution of particles in sizes) [55] of the particles as well as dipole-dipole interaction within the matrix [147]. The reflection spectra show a broad resonance, too. The appearance of a wide reflection peak at the plasmon frequency illustrate that the composite reflect the light at near resonance wavelength. This can be ascribed to the semi-metallic structure (surface morphology) of high filling factor composite which reflect the light through the visible. This intrinsic reflection of composite film provide the condition of Fabry-Perot cavity formation when they are come to proximity of a reflective mirror (which is discussed in the following). It is known that metallic particles in air have a different optical properties than of metal-dielectric nanocomposite. The resonance wavelength of plasmonic red-shift when the refractive index of the adjacent dielectric increases. This effect is more pronounced once the particle is come within reach of a metallic substrate [128]. In other words, when a dielectric envelop the isolated metallic nanoparticle, the induced screening charges on the metal-dielectric interface lower the plasmon excitation energy ensuing in red-shifting of the resonance. Similarly, for coupled nanoparticles, the dielectric materials also screen and weaken the interaction between metal nanoparticles and decrease the shift of the coupled plasmon [197]. According to the mentioned reason, we are able to shift the resonance peak of Ag from UV to visible by depositing silver-SiO_2 nanocomposite atop of a mirror. Beside the particles coupling inside the composite, the resonance further red-shifts due to the fact that the particle dipole is anti-symmetrically coupled to its image inside the silver mirror [128]. In addition to the plasmonic absorption of ensembles of particles (i.e. nanocomposite), interference also contribute to its low reflectivity [198]. In such a stack of layers (nanostructure and continuous metallic film), the reflection reduction is achieved due the impedance matching of the system and air. On other hand, the Fabry-Perot cavity is created between the top composite and the bottom mirror leading to strong interference between the incident and the reflected wave. In other words, the superposition of the multiple reflections from the base layer destructively interferes with the direct reflection from the air-composite interface. With the optimized interlayer thickness, these two waves counteract each other ensuing in zero reflection; whereas with other spacer thicknesses (Figure 7.2b) the amplitude and phase do not or partially match, leading to a less intense absorption peak and subsequent frequency shift [48]. As mentioned above, in spite of the narrow resonance band of silver, the composite has a broad resonance width due to the dispersive size of the particles and particle-particle (dipole-dipole) interaction within the layer. Apart from these effects, deviation from perfect spherical shape could profoundly influence the large broadening [247]. Therefore, the cavity resonance is occurred at several wavelength leading to vanishing of reflection in a broad range of frequency. Since the base layer is optically

thick, no light transmit through the layers and consequently perfect absorption is achieved. In contrast to other reported composite-based super absorbers, the presented silver base PMSA is unique since its absorption intensity reachs 100% in UV (up to green part of visible) which is the first PMSA reported for such a high frequency (UV-A wavelength). The film appearance is dark-red demonstrating that this PMSA is highly reflecting at red part of spectra (Figure 7.3a). Macroscopically consideration of the system show that the

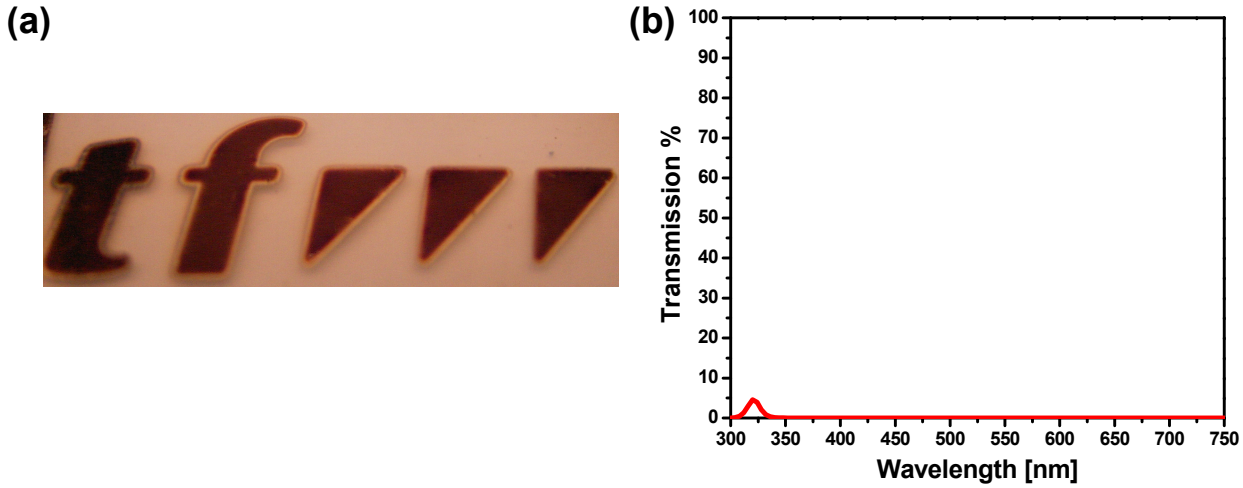

Figure 7.3: *(a) True color photograph of the perfect absorber coated on transparent polymeric substrate presenting the logo of Technical Faculty (TF) of University of Kiel. (b) Transmission spectra of typical perfect absorber.*

absorption band is split into two separate (broad) peaks similar to the stacks of silver cluster and mirror [198]. We attribute the resonance at shorter wavelength (around 360 nm) to the silver interband transition. Indeed, the interband transition from occupied d states to unoccupied "p" and "s" states above Fermi level appear at 310 nm and 350 nm in bulk silver, correspondingly. But, for silver nanostructures such an electron transitions could occur above 350 nm wavelength and depend on nanostructure geometry [55]. The second broad peak which appears at longer wavelength might stem from localized surface plasmon resonance of the silver particles (370 nm) and interference (550-600 nm). This becomes more apparent when the thickness of the composite changes. In Figure 7.2b, the absorption spectra of silver-SiO_2 nanocomposite with 15 nm, 20 nm, 25 nm, and 30 nm thickness is shown. The low frequency peak position red-shift with thickening the film which is a sign that the peak is interference routed [198]. Moreover, the peak itself split into two parts as long as the composite thickness raises from 10 to 30 nm. However, further thickening of the composite results in a drop in the absorption in visible and hence reduce the efficiency of the system, though it further broaden the spectra. Beside of the two mentioned wide-band peak, a dip in absorption spectra reveals at very short wavelength (around 325 nm). From the first glance, it might be concluded that this dip is routed from the small transmission of silver film at 320 nm (Figure 7.3b). But the drop intensity is around 30% meaning 10 times bigger than the transmission intensity of film.

It is known that surface plasmon resonance can be excited on the silver film at around

340 *nm* due the roughness originated from deposition [248, 249]. Therefore, the reflection spectra of the stacks will show two dips at higher frequency; One at 320 *nm* associated with the plasma frequency of silver and the second one at around 340 *nm* corresponding to the surface plasmon resonance of the bulk silver. In other words, two reflection dips reveal in the spectra of silver mirror one at 340 and the other one at 320 *nm*. Therefore, the mentioned drop (reflection peak) in the absorption is the boundary of two resonance phenomenon which occurred in the present multi-stack [220]. Reflection measurement at different angle of incidence with two different polarization (-s and -p) (Figure 7.4) showed that the current PMSA is almost angle and polarization invariant. The reflection intensity stay low for both polarization even at high incidence angle (60°) demonstrating that the performance of such a PMSA is not being influenced considerably by angle of incidence. Nevertheless, there is a slight difference in s- and p-polarization that we attributed to the Brewster angle. Generally, the s-polarized reflection in a metamaterials can reach to zero at higher angle of incidence provided that the permeability of the materials is non-unity [250]. Since the permeability of current metamaterial is not unity in visible regime [147]; therefore, the reflection is vanishing for s-polarization at certain frequency while p-polarized light slightly reflect-off the surface. Alteration of filling factor is a other fundamental parameters which

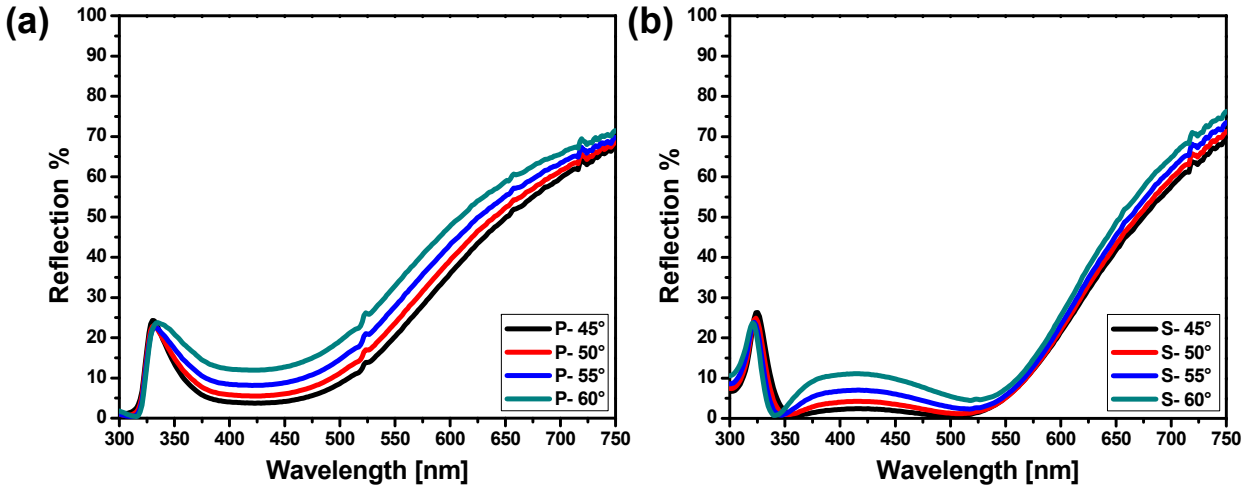

Figure 7.4: *Reflection spectra of 20 nm silver-SiO_2 nanocomposite with 30% filling factor deposited on 20 nm SiO_2 coated silver film (200 nm thick). (a) -p and (b) -s polarization at different angle of incidence.*

can tune the optical response of this PMSA. Figure 7.5a, shows the absorption spectra of the silver-SiO_2 nanocomposite with different filling factor while the other parameters kept constant. As long as the filling factor increases, the spectra red-shift and its band broadens. However above the certain composition (optimized value), the absorption band start to shrink again. The above shift could be attributed to the amplified electromagnetic interaction among the particles in addition to the change in the effective permittivity of the surrounding medium as predicted by Maxwell-Garnett theory [247]. For our developed system, it seems that 42% filling factor show the best performance and the width of the absorption peak (with intensity higher than 95%) becomes 220 *nm* (Figure 7.5b). In the

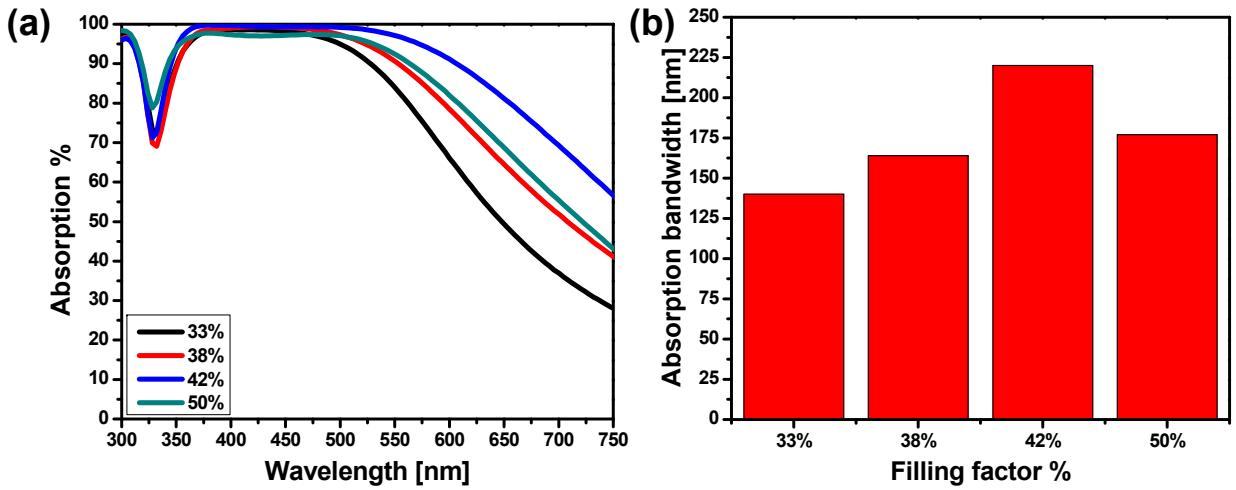

Figure 7.5: *(a) Absorption spectra of silver-SiO_2 nanocomposite with different filling factor. (b) Absorption band-width with intensity greater than 95% for different PMSA with variety of filling factor shown in (a).*

current PMSA, the sensitivity of the absorption intensity to the filling factor variation is less than the thickness. We attribute the mentioned difference to the limited range of filling factor variation. On other hand, the region of near percolation is very restricted and a little increment of the metal ratio lead to the metallic behavior of composite and therefore the reflection increment (absorption drop) of the stack [147]. Around the percolation threshold (around 50%) the peak broadening starts to decrease (Figure 7.5a (olive curve)) prior to dropping sharply after percolation. This is owing to the decline in scattering of the conduction electrons by surfaces and discontinuities [251]. In other words, the high filling factor only could give rise to high absorption provided that the particles are discontinuous and do not make any metallic chains in the matrix. In fact, incorporation of solid dielectric between the particles (for formation of composite) provide the chance to keep them distant from others and delay the interconnection up to relatively high filling fraction of metals. In order to prove the better performance of the current PMSA compared to the known dye UV absorber, Polystyrene film doped with Spirooxazine molecules were spin coated on 200 *nm* thick silver film. Based on the optimization experiments, the most intense absorption can be realized when the thickness of the coating is around 40 *nm* and its highly concentrated ($\sim$ 50% SPO). The absorption spectra of the silver absorber and UV irradiated organic coating is depicted in Figure 7.6. It is clear that the absorption intensity as well as band-width of silver PMSA is larger than its organic counterpart. Indeed, the average absorption of the doped polystyrene in the UV-A range is (45%) half of the absorption intensity of the silver absorber (92%) further showing that the PMSA can be a higher efficiency alternative for organic UV protection layer. It is worth mentioning that the absorption dip in high frequency (in PMSA) can be reduced by thinning the spacer layer down to 10 *nm* but in the expense of overall absorption reduction (in otherwise wavelengths). In other words, one can compensate the drop and increase the absorption intensity up to 90% at 325 *nm* by thinning the spacer layer (Figure 7.6(blue curve)). We believe that the presented perfect

absorber might pave the way of metamaterials application for Thermo-photovoltaic [252], stealth technology [253] and UV-protective coating [241]. Note that the long-term stability of silver is rather poor [19, 254]. Indeed, oxygen or water could penetrates even dense silica matrices on a scale of days, not only through pores but even through the matrix network and deteriorate its optical properties [255]. Therefore, more efforts and improvements is needed to upscale the fabrication of the present PMSA for long term performance.

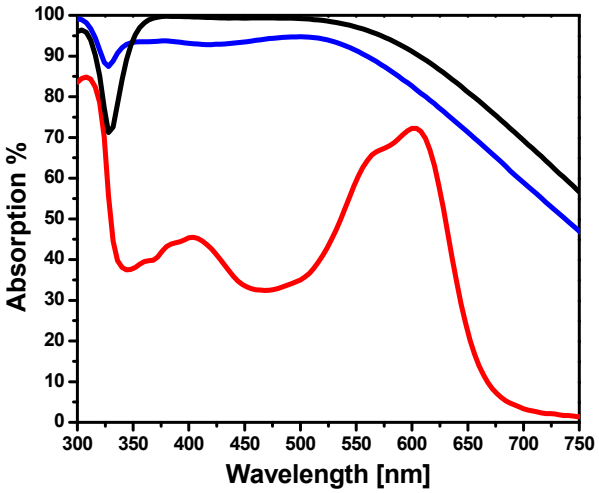

Figure 7.6: *Absorption spectra 200 nm silver film coated with 40 nm polystyrene-SPO composite (red curve) and 20 nm silver-SiO_2 nanocomposite with 42% filling factor deposited on 10 nm (blue curve) and 15 nm (black curve) SiO_2 film. The organic film is UV illuminated prior to measurement.*

7.5 Conclusion

In summary, a plasmonic tunable metamaterial absorber is presented for UV part of spectrum. The absorption frequency and intensity of the metamaterial is considerably tuned throughout the UV-visible wavelengths. We achieved this unprecedented level of wavelength and intensity agility by varying the nanoparticle volume fraction, composite and spacer layer thickness. It was shown that the absorption of silver PMSA is twice of organic absorber in UV and visible range. Therefore, this class of metamaterial could be a promising candidate for highly UV and visible absorbing coatings.

7.6 Acknowledgements

We would like to acknowledge C.V.S. Chakravadhanula for TEM imaging and A. Tavassolizadeh for drawing the sketch. We gratefully acknowledge the financial support by the German Research Foundation (DFG) through the projects SFB 677 (C1,C9) and EL 554/1-1.

M. E. would like to thank the Initiative and Networking Fund of the Helmholtz Association's (grant No. VH-NG-523) for providing the financial base for the start-up of his research group.

Chapter 8

The hybrid concept for realization of an ultra-thin plasmonic metamaterial antireflection coating and plasmonic rainbow

M. K. Hedayati, S. Fahr, C. Etrich, F. Faupel, C. Rockstuhl, M. Elbahri, The hybrid concept for realization of an ultra-thin plasmonic metamaterial antireflection coating and plasmonic rainbow *Nanoscale 2014*, 6, 6037-6045.

8.1 Abstract

We report on the design, the simulation, the fabrication, and the characterization of a novel two layers antireflective coating (ARC) based on a plasmonic metamaterial and a dielectric. Promoted by the strong material dispersion of the plasmonic metamaterial, our novel concept (called hybrid ARC) combines two possible arrangements for layers in an anti-reflection coating into a single structure; albeit at two different wavelengths. This, however, causes a broadband reduction of reflection that is less sensitive against oblique incidence when compared to traditional antireflective coatings. Furthermore, we show that the current metamaterial on metal reflector can be used for the visualization of different coloration such as plasmonic rainbow despite its sub-wavelength thickness.

8.2 Introduction

The finite reflectivity from the interface of two disparate media with dispersive material properties is an obstacle that often denies the design of efficient photonic and opto-electronic devices [256]. Traditionally, the problem can be diminished while incorporating anti-reflection

coatings (ARCs) [71] that base on graded index layers [105, 257–259], gradient-index coatings [260, 261], or nanostructured textures [79, 81]. However, these approaches usually suffer from one or multiple severe drawbacks such as a narrow spectral domain of operation, sensitivity against oblique incidence, complexity, or a lack of applicability to extremely thin films. Here, we mitigate these problems by introducing and verifying a new class of ultra thin two-layer antireflection coating with a metamaterial as a top and a dielectric material as a second layer; demonstrating therewith an entire novel concept names as "hybrid ARC". The key feature of this hybrid ARC is using (quasi) two arrangement for the dielectric layers in one design where the refractive indices ascend or descend in consecutive layers with a descending order, albeit at a different wavelength. This is only possible by exploiting the strongly dispersive character of metamaterials. High ARC performance on silicon substrate is shown to be possible by plasmonic nanocomposites with a strong dispersion in the permittivity around its plasmonic resonance. Below the plasmon resonance wavelength the layer acts as traditional graded-index coating while it performs as Fabry-Perot interferometer at longer wavelengths. This provides the opportunity to considerably lower the reflection across a broad range of wavelengths with only a marginal angular sensitivity. Moreover, the hybrid concept can be applied on metals where the tunability of the plasmonic nanocomposite enable realization of plasmonic rainbow colors by a sub-wavelength coating.

The consideration of anti-reflective coatings (ARCs) as being very important is justified from their integration in nearly all photonic devices [94, 262–265]. Optical elements where they find use range from ordinary lenses over any laser system up to advanced photonic devices for disruptive technologies. Traditional ARCs made from an individual non-absorbing layer can usually be optimized to operate perfectly at an isolated design wavelength. Then, the refractive index (RI) of the ARC (being directly linked to the square root of the permittivity for non-magnetic, homogenous, isotropic, local materials as considered here) has to be the geometric mean of the RIs of the materials on both sides of the respective interface from which the spurious reflection is encountered, i.e. herein called a substrate and the incident medium. By no means of restriction, we consider in the following the RI of the substrate to be larger than the RI of the incident material (coating). The thickness of the ARC ought to be a quarter of the desired wavelength. However, and quite detrimental, the vanishing reflectivity only occurs at normal incidence and only at the isolated design wavelength. Nevertheless, wider-band ARCs are possible by relying on innovative designs [93, 266], plasmonic and metamaterials layers [267, 268] or multilayer coatings [269]. For instance, two-layer ARCs [270], i.e. "V" coat, could result in a wide-band ARC by a proper selection of films. In such a case the RI of the top layer should be smaller than the second layer and each layer thickness shall equal a quarter of the desired wavelength. The first suggestion for such a traditional arrangement of the layer materials is linked to the name of Lord Rayleigh; hence hereafter we call it the Rayleigh configuration. In fact, the order of ARC film is very crucial in such a technique and once the order of layers is inversed (i.e. low and high RI placing as spacer and top layer, respectively), the reflection of the device increases and could even turn the substrate (in certain circumstances) into a mirror (Bragg-mirror) [271, 272]. We wish to call such arrangement in the following the reverse-Rayleigh configuration. Note that the in the reverse-Rayleigh configuration at least two reflection dips surround the central reflection peak [273]. Recently, a new class of ARCs

has been introduced, specifically for metallic substrates where the coating acts as an absorbing element to reduce the light reflection. In such a configuration, the reflection drops not only due to the interference [48] but also by exploiting the absorbing character of the coating combined with losses in the metallic substrate [36, 43, 146–148, 274–277]. The strong optical attenuation through the highly absorbing coating or the strong resonant behavior in layers [275] give rise to low reflection from the metal substrate, although the thickness of the coating is much less than the wavelength of light. This concept works well on gold films which could sustain a plasmonic response at certain condition as well as a broad intrinsic absorption (i.e. minimum reflection) in the visible range because of interband transition. The question arises whether this concept is equally applicable to semi-conductors as the substrate material. It is known that semi-conductors like silicon exhibit strongly dispersive material properties that complicate the design of efficient ARC. Therefore, it remains a challenge to perceive an ARC that operates over the entire range of the visible and near-IR for semi-conductors [278]. Here, we introduce an ultra-thin bi-layer coating as ARC. The key-feature of our coatings is the use of a material with a high RI for the layer that faces the incident medium, i.e. the top layer. Moreover, the thicknesses of all involved layers are considerably thinner than a half or even a quarter of a wavelength. By a systematic analysis we show that an excellent anti-reflection performance is possible. While demonstrating the concept in a first stage with a pair of dielectric materials possessing only a weak dispersion, i.e. TiO_2 / SiO_2, we exploit the strong dispersive nature of metamaterials in a second stage to demonstrate the hybrid-concept and eventually achieve a broad-band ARC with only a marginal angular sensitivity.

8.3 Results and Discussion

The metamaterial we will use consists of an ultrathin plasmonic nanocomposite made from ultra-fine metallic nanoparticles (diameter D $< 5\ nm$). Figure 8.1a-b, show the cross sectional and top view TEM image of the sample. It is apparent that the particles diameters are around 5 nanometers and randomly distributed into the matrix. It possesses a dispersive permittivity with a Lorentzian profile centered at the particle plasmon resonance. The homogenous isotropic metamaterial is characterized by a strongly dispersive RI that takes high values at long wavelengths and small values at short wavelengths, taken with respect to the particle plasmon resonance. Such material can therefore beneficially be used to perceive an ARC that combines the reverse-Rayleigh and the Rayleigh ARC in the same structure, albeit at different wavelengths. Therefore, we call out structure a "Hybrid-Antireflection" structure. We postulate that the broadband anti-reflection performance of the presented metamaterial is facilitated by the anomalous material dispersion around the plasmon resonance. The dispersive refractive index of composite varies in a way that at wavelengths longer than the resonance the coating serves in a reverse-Rayleigh configuration but at smaller wavelengths the composite's RI is smaller than the second layer and hence the Rayleigh condition is satisfied. In other words, by overlapping the reflection dip of traditional ARC with that of Fabry-Perot interferometer, the corresponding reflection dip of our two layers coating is very broad despite of its low thickness. This unique dispersive RI of the presented

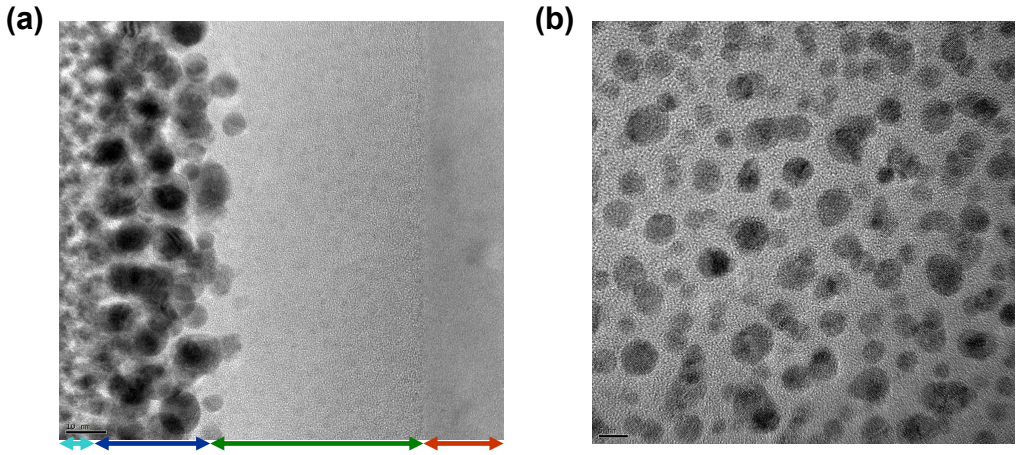

Figure 8.1: *(a) Cross sectional of plasmonic nanocomposite in which the arrows indicate each are of the samples. Light blue, blue, green and red arrows represent the platinum (top adhesion layer for cutting of the sample), nanocomposite, SiO_2 layer and silicon wafer, respectively. (b) Top view TEM image of plasmonic nanocomposite wherein the dark sphere are the silver particles.*

metamaterial leads to the opportunity to observe a hybrid wide-band ARC encompassing the Rayleigh/reverse-Rayleigh configurations. Full wave electro-magnetic simulations of the metamaterial verify that it acts as a homogenous medium rather than an ensemble of plasmonic absorbers. This entails their description in terms of effective material properties which paves the way to consider such a structure in the design of many high efficient ARC devices. To start with, we consider a bi-layer ARC where the top layer facing air as the incident medium is an ultrathin film of a high RI material. With the final device in mind, the thickness is chosen to be 20 nm. This adheres to the desire to have an ultra-thin and compact ARC. We leave here the exact value of the RI as a free parameter. The second layer shall be made from a low RI material. Silicon dioxide is selected as the low RI film since it is a common material in silicon industry and it can be either deposited or grown on the silicon substrate with good adhesion. We leave as a degree of freedom the thickness of this layer. In such a scheme, the substrate, i.e. silicon wafer, has the highest RI in the stack. To identify on analytical grounds the conditions where the ARC operates optimal, a thin-film transfer matrix technique is applied to calculate the reflection. Results are shown in Figure 8.2a. There, the reflectivity at a design wavelength (in this case at 600 nm) is calculated depending on the RI of the top layer and the thickness of the SiO_2 layer. It is apparent that the reflection is suppressed for a rather high value of RI of the ultrathin top layer and a thin SiO_2 layer. To suppress reflectivity at longer design wavelengths, the RI should be approximately the same but the thickness of the SiO_2 layer should be slightly increased. However, it can always be assured that the reflection can be reduced to a negligible quantity, even though the coating is sub-wavelength in its thickness, i.e. far below the quarter of the design wavelength. According to the calculated reflection contour (Figure 8.2a), a high RI material which suitably matches the required RI is TiO_2 (its average RI in visible is 2.4 [279]). The oxide films were prepared by sputtering of a dielectric target (namely SiO_2

or TiO_2) and the thicknesses were measured with a profilometer. Based on the simulation, 20 nm TiO_2 layer and a 50 nm SiO_2 coated on silicon could realize low reflection at 570 nm. Indeed, the fabricated stacks with the mentioned geometry and thicknesses provide a broad reflection reduction with a reflection minimum at 570 nm wavelength for silicon as shown in Figure 8.2b which agrees well with simulation. By resorting to a traditional order for the

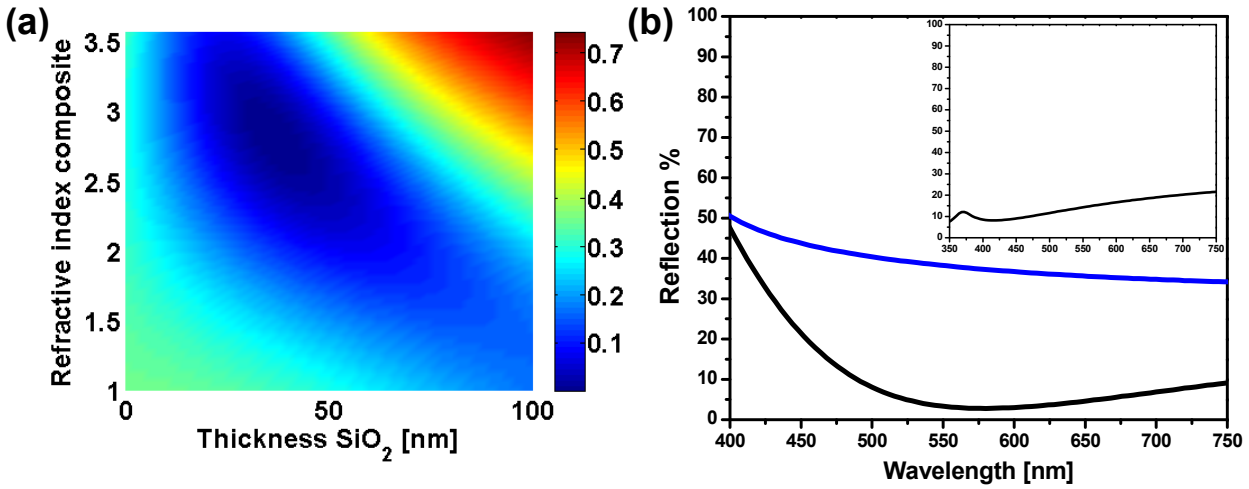

Figure 8.2: *(a) Reflection of a 20 nm film with varying RI on a SiO_2 film with varying thickness on top of a silicon substrate at a wavelength of 600 nm. (b) (black) Reflection spectrum of a typical reverse-Rayleigh configuration (20 nm TiO_2 atop of 50 nm SiO_2 coated Silicon) in comparison with bare silicon (blue). The inset shows the reflection spectrum of 50 nm SiO_2 atop of 20 nm TiO_2 coated Silicon (Rayleigh configuration).*

layers, i.e. an ordinary Rayleigh configuration where the materials are arranged in ascending order of their RI, it was observed that the reflection minimum occurs at 410 nm Figure 8.2b (inset), in agreement with Rayleigh's postulation but it does not vanish totally since its thickness is far below the quarter-wavelength which is required for anti-reflectivity. It can be seen that the ARC in Rayleigh configuration is spectrally narrower than the reverse-Rayleigh configuration and its remaining reflection almost doubled. However, since those results might be affected by experimental uncertainties, we would like to stress the major advantage of the reverse-Rayleigh concept that can be better appreciated while comparing the angular dependency of both configurations (i.e. Rayleigh and reverse-Rayleigh). The average reflection at higher incidence angles for the case of Rayleigh configuration is almost twice the intensity of similar film but in reverse order (Figure 8.3a). In fact, the reflection drop considerably red-shifts upon changing the geometry from traditional to the reverse-one which proves that the performance of ultra-thin reverse-Rayleigh ARC is more promising for an operation in the visible spectrum. The more pronounced reflection drop and red-shift of the curve in reverse-Rayleigh compared to Rayleigh configuration can be well explained by interference [280]. In principle, destructive interference of the direct reflected light and the light reflected at consecutive interfaces requires a phase accumulation of π by the wave traversing the layers back and forth. This easily explains the dogma on using quarter wavelength layers with a small RI as the first (top) layer. However, in the case of a top-film

with high RI (reverse-Rayleigh), the light which travels through the low RI layer and the reflected wave have a π phase difference [281] which ends up with a destructive interference. In other words, in the case of a top-film with high RI, π phase accumulation comes for free as the impinging light reflected at the various interfaces experiences π -0- π phase shifts. The phase difference of the incoming and reflected light in the cavity is $\Delta(\Phi) = ((2\pi)/\Lambda)+\pi$ [282] where n, d and Λ are the RI, thickness of the spacer layer and the wavelength of interest, respectively. By inserting the values of thickness and RI of SiO_2 in the mentioned equation, it ends up with $(3\pi)/2$ which provides the condition of destructive interference. Color changes of the coating by changing the thickness of spacer layer (i.e. SiO_2 film) from 10 to 50 nm, further prove interference role in the reverse-Rayleigh coating. Figure 8.3b, shows the true color photograph of the silicon samples coated with 30 nm TiO_2 film atop of 10, 30 and 50 nm SiO_2 on silicon substrate. Nevertheless, neither ARC based on reverse-Rayleigh concept

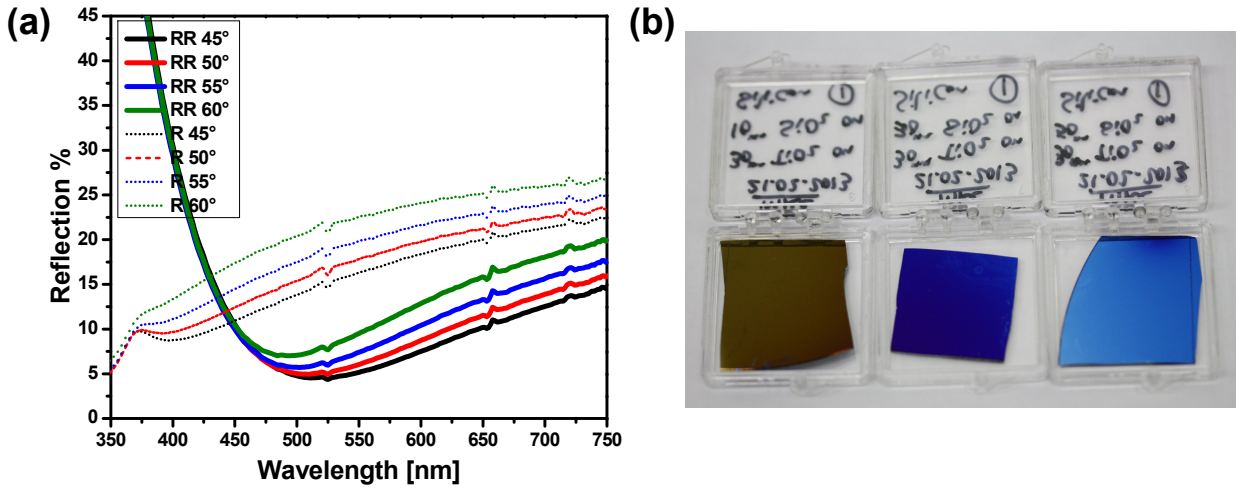

Figure 8.3: *(a) Reflection spectra of 20 nm TiO_2 atop of 50 nm SiO_2 coated on silicon (solid line) and 50 nm SiO_2 on 20 nm TiO_2 coated on silicon (dashed line) at different angle of incidence. (b) True photograph of Silicon samples coated with 30 nm TiO_2 film atop of (from left to right) 10, 30 and 50 nm SiO_2 film, respectively.*

nor Rayleigh provide the desired properties of a wide-band ARC (i.e. whole solar spectrum range) owing to high reflection that appears at short and long wavelengths of the visible for both configurations. Additionally, for shifting the reflection dip to NIR, increasing the layer thickness and/or using a high RI materials is needed. Note that there are only a limited number of materials with high refractive index which could fulfill the required RI contrast for reverse-Rayleigh configuration. In our opinion, and from technological point of view, the field is revolutionized if a coating is used that would enable both Rayleigh and reverse-Rayleigh configurations simultaneously, at different wavelengths though. Suppressing the reflections at multiple wavelengths would automatically enable a broad band ARC based on ultrathin films. However, this requires the use of strongly dispersive materials in the design of the ARC. Ideally, the geometrical dispersion that degrades the anti-reflection action beyond the target wavelength in an ARC design where non-dispersive materials are used has to be compensated by a suitable material dispersion. This perfect balancing, however, requires

an anomalous dispersion in the material properties which is always accompanied by absorption. Nonetheless, motivated by the recent work on ARC coatings on metals using weakly absorbing materials [275], we may conclude that if the ARC coating is sufficiently thin and contain ultrafine plasmonic nanoparticles (in the range of quantum dots) the absorption might not be detrimental. To evaluate the potential of this idea, we sought out a way to design a new concept for a coating that considers artificial materials (metamaterial) in their design that possesses a strong chromatic anomalous dispersion. Accordingly, we consider a plasmonic nanocomposite of tiny metallic nanoparticles embedded in a dielectric host as a metamaterial with the required highly dispersive refractive index. The properties of the nanocomposite can be tuned by many parameters which constitutes a great degree of freedom. They constitute an extraordinary material platform with many intriguing advantages. The fabrication of these nanocomposites is based on self-assembly processes using sputter techniques, which is well established [149], and they can be deposited on large surface in short time and at low costs (for more details see the methods section). This metamaterial derives its unique properties from the excitation of localized plasmon polaritons in the metallic nanoparticles [8]. The nanoparticles are sufficiently small and arranged sufficiently dense, such that the material can be considered as effectively homogenous and isotropic. The material is characterized by a Lorentzian resonance in the effective permittivity which is centered at the plasmon resonance wavelength. Due to the isotropy of the material and the vanishing of any magnetic response, the permittivity uniquely defines the effective refractive index. The material can be perceived as a strongly dispersive dielectric with some finite absorption in resonance.

It is known that, with filling fractions for the metallic nanoparticles between 20% and 40%, the effective properties cannot be derived from canonical effective medium theories such as Clausius-Mossotti [283]. Instead, we used finite-difference time-domain (FDTD) simulations of a sufficiently large super-cell and calculated the dispersive complex reflection and transmission coefficient [284] (c.f. Methods section). From these coefficients effective properties were retrieved for the composite. These parameters were afterwards fueled into a thin-film transfer matrix technique to simulate all quantities of interest. Selected configurations were equally simulated by the $FDTD$ method to cross-check the predictive power of the effective properties. Identical results were always predicted, justifying the treatment of the nanocomposite as an effective medium. (For more details see the methods section). The dispersive RIs of the nanocomposites with different filling factors are shown in Figure 8.4a. It is apparent from this dispersion graph that at resonance the absorption is maximal and the real part of the RI undergoes anomalous dispersion. At wavelengths longer than the resonance wavelength the material is characterized by a large RI (large permittivity) and hence would be suitable to serve in the reverse-Rayleigh configuration as the top material ($n_{top}>n_{spacer}$). In contrast, at wavelengths smaller than the resonance wavelength, the medium is characterized by a rather small RI (small permittivity) and accordingly would be appropriate to be used in the Rayleigh configuration as the top material ($n_{top}<n_{spacer}$). Therefore, plasmonic nanocomposites can be considered as the hybrid ARC that meets the condition of both Rayleigh and reverse-Rayleigh geometries resulting in a broad-band ARC coating. We demonstrate the hybrid concept by coating a polished silicon wafer with 20 nm silver-silicon dioxide nanocomposite separated from the substrate by a thin layer (50 nm) of

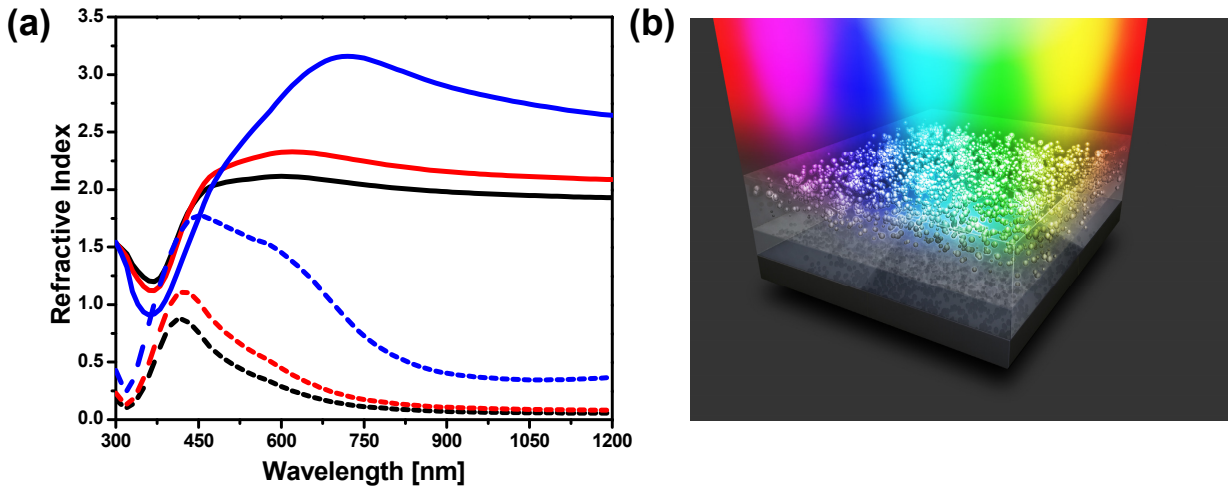

Figure 8.4: *(a) Complex refractive index of Ag-SiO_2 nanocomposite with 15% (black), 20% (red) and 40% (blue) filling factor. Solid and dotted-lines represents the real and imaginary part of RI, correspondingly. (b) Geometry of the Anti-Rayleigh hybrid ARC which is composed of 20nm nanocomposite atop of SiO_2 coated silicon.*

silicon dioxide as shown schematically in Figure 8.4b. Such a stack gives rise to the realization of a black silicon with a homogeneous ultrathin layer coating. Figure 8.5a shows the reflection spectra of 20% and 30% nanocomposite deposited on 50 nm SiO_2 coated silicon and the inset is the true color photograph of the sample with 30% which looks black indeed. Angular reflectance measurement of the coating with 30% filling factor (Figure 8.5b) shows the marginal angular and polarization dependency of the plasmonic hybrid ARC. More details on the angular behavior [146], especially for the angular domain that is not shown here, can be found in the literature [147]. The spectra possess two main dips in the reflection spectra. The small wavelength dip is attributed to the graded ARC (i.e. in analogue to a configuration where 50 nm SiO_2 is deposited atop of 20 nm TiO_2 (c.f. Figure 8.2b (inset)) and the second reflection dip originates from the destructive interference of the reflected field (i.e. in analogy with TiO_2 film atop of SiO_2 (c.f. Figure 8.2b(black curve)). In spite of the expected wavelength shifts of the antireflection dips (c.f. Figure 8.5b (inset)), one peak at 450 nm (i.e. where the plasmon of the nanocomposite arise) is also revealed that is invariant against the angle of incidence and hence we attribute it to the plasmon resonance of the composite. Indeed, the wavelength of the peak remains unchanged by angle variation which confirms the localized nature of the (particle plasmon) resonance. To demonstrate the tunability of the hybrid ARC and meanwhile to gain more understanding about the role of plasmon in the observed phenomena, the effect of the spacer layer on the optical responses was examined. Keeping the top layer thickness and composition constant while increasing thickness of SiO_2 from 50 nm to 100 nm, a red-shift of the reverse-Rayleigh as well as Rayleigh antireflection dips were observed (Figure 8.6a). This behavior is in good agreement with our simulation (Figure 8.6b-c) which shows that an increasing of the spacer results in a broad ARC in NIR (800-900 nm) for the case of reverse-Rayleigh configuration. On the other hand, ARC performance of the graded configuration (small wavelength regime) in the

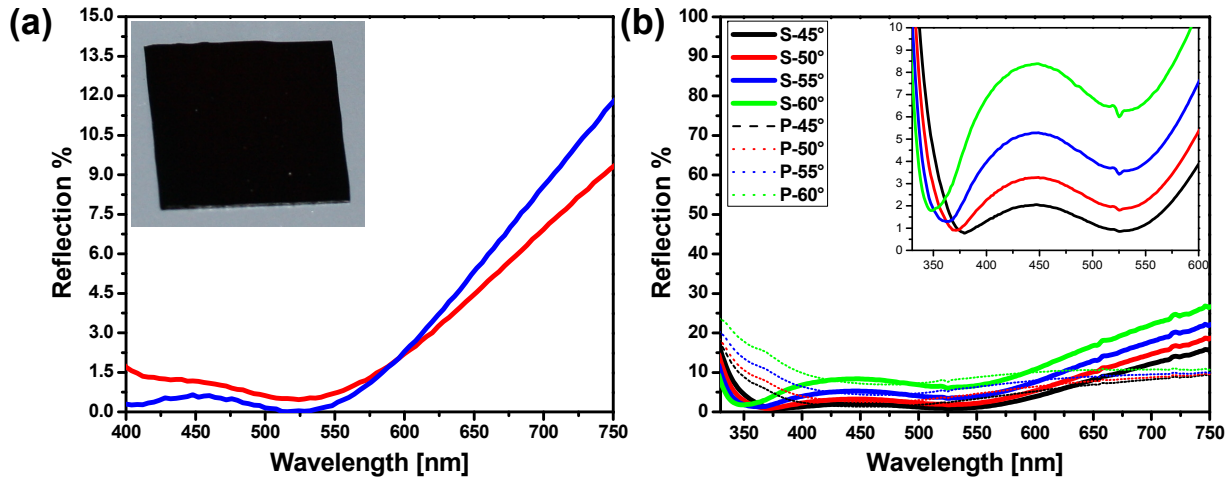

Figure 8.5: *(a) Reflection spectra of 20nm Ag-SiO_2 with 20% (red) and 30% (blue) filling factor deposited atop of 50 nm SiO_2 coated silicon. The inset shows the true color photograph of the silicon coated with the optimized film which turn its appearance black. (b) Reflection spectra of film as in (a) measured at different angle of incidence with s- (solid lines) and p-polarization (dotted lines), respectively. Inset shows the magnified image of s-polarization.*

hybrid is deteriorated by thickening the spacer layer. Indeed, the origin of the mentioned high reflection with thicker inter-layer could be attributed to two phenomena; firstly the constructive interference of the incident and the reflected light. Secondly, the spectral overlap of the plasmonic resonance of nanocomposite and the Rayleigh antireflection dip. Such an overlap occurred because of the red-shift of the Rayleigh originated dip via thickening of the spacer layer. Indeed, integrating plasmonic structure as a hybrid ARC coating provides an additional degree of freedom for tuning the performance of ARCs coating. In other words, by using hybrid plasmonic ARC, the designer can reach the desired optical properties not only by alteration of layers thickness but also by adjusting the filling factor (RI) and type of the metallic constituents of nanocomposite. Generally, the performance of hybrid ARC depends on the contrast of the RIs between the layers. At the wavelengths where the top layer showing higher RI, reverse-Rayleigh condition is satisfied but the traditional Rayleigh would be realized once the top film possesses the lower RI in the stack. The presented plasmonic anti-reflector shows such low and tunable reflectivity due to the extreme dispersive RI of metamaterial (cf. Figure 8.4a) which have been shown formerly [285–288]. The RI of nanocomposite with 40% filling factor changes from 0.9 up to 3.15 from small to long wavelengths. In other word, the relative RI changes of the host matrix before and after embedding of the nanoparticles can vary from -30% to +140%. In fact, the tunability of the plasmon resonance and correspondingly the reflection change [275] by changing the filling factor of nanocomposite provide the possibility for the coloring of metals using our hybrid concept. Figure 8.7 shows a true photograph of samples of 25 *nm* SiO_2 gold film coated with 20 *nm* gold-SiO_2 nanocomposite with variety of filling factor, creating a spectrum of colors including yellow, orange, blue and green. The colors originated from the different reflection drop associated with each filling factor demonstrating the potential of hybrid concept for realization of plasmonic rainbow colors [289]. Note that demonstration of various

color on silicon substrate is not possible under the same conditions (i.e. constant thickness of layers while varying the filling factor). It seems that, the surface plasmon of the gold film (which is absent on silicon) in parallel with the hybrid ARC contribute to the rainbow colors. We believe that the hybrid concept could pave the way for new highly efficient ARC for a variety of applications ranging from photovoltaics [89] and optics to solar absorber and stealth technology [252,253] as well as other fields where high reflection is undesired. But for energy applications, not only the low reflectance rather than high transmission is desired. Calculation showed that the light transmission into the substrate (silicon) is enhanced by using the plasmonic coating. Figure 8.8 shows the light absorbed by silicon (i.e. light transmitted into silicon) by means of current plasmonic coating. The light reaching the substrate is apparently increased through the coating which shows the potential of such an approach for energy harvesting purposes. However, the preliminary results on photocurrent measurements of presented coating on p-silicon showed some current loss that we attributed to the poor interface of the prepared films which acts as the sites for electron-hole recombination. Nevertheless, a more sophisticated design is required to better explore the role of present ARC for electron-hole generation which is beyond the scope of this manuscript.

8.4 Conclusion

In summary, we demonstrated a new concept for antireflection coatings and experimentally showed an ultra-thin tunable plasmonic anti-reflector by using a routine technique of MEMS/NEMS technology. The developed hybrid ARC, which is based on a continuous plasmonic medium, acts as a consolidation of graded-index and interferometer (reverse-Rayleigh) providing a wide-band reflection drop throughout the visible spectrum. Due to the simplicity of our production approach, the concept can be further extended to other substrates/applications where broadband ultra-thin anti-reflective coatings are required.

8.5 Methods

8.5.1 Fabrication

All depositions were carried out in a cylindrical vacuum chamber, which was primarily evacuated to $10^{-6} mbar$. We used a RF magnetron for sputtering of SiO_2 and a DC magnetron sputter source for silver and gold. Both sources were oriented in reverse directions relative to the sample holder at 50° angle to the substrate plane. All the coating was done while the rotatable sample holder was spinning in order to end up with a uniform thickness and composition (details in [221]). In order to keep the filling factor below the percolation threshold, the deposition rate of the metal was adjusted to be less than that of dielectric during codeposition. In other words, to avoid the coalesce of nanoparticles in the matrix, i.e. the formation of fractal aggregates of NPs, the deposition rate of SiO_2 was set to be 10 nm/s while the rate of silver was adjusted to be around 3 nm/s. However, for the creation of the plasmonic Rainbow, the mentioned constrain was actually not necessary. Therefore,

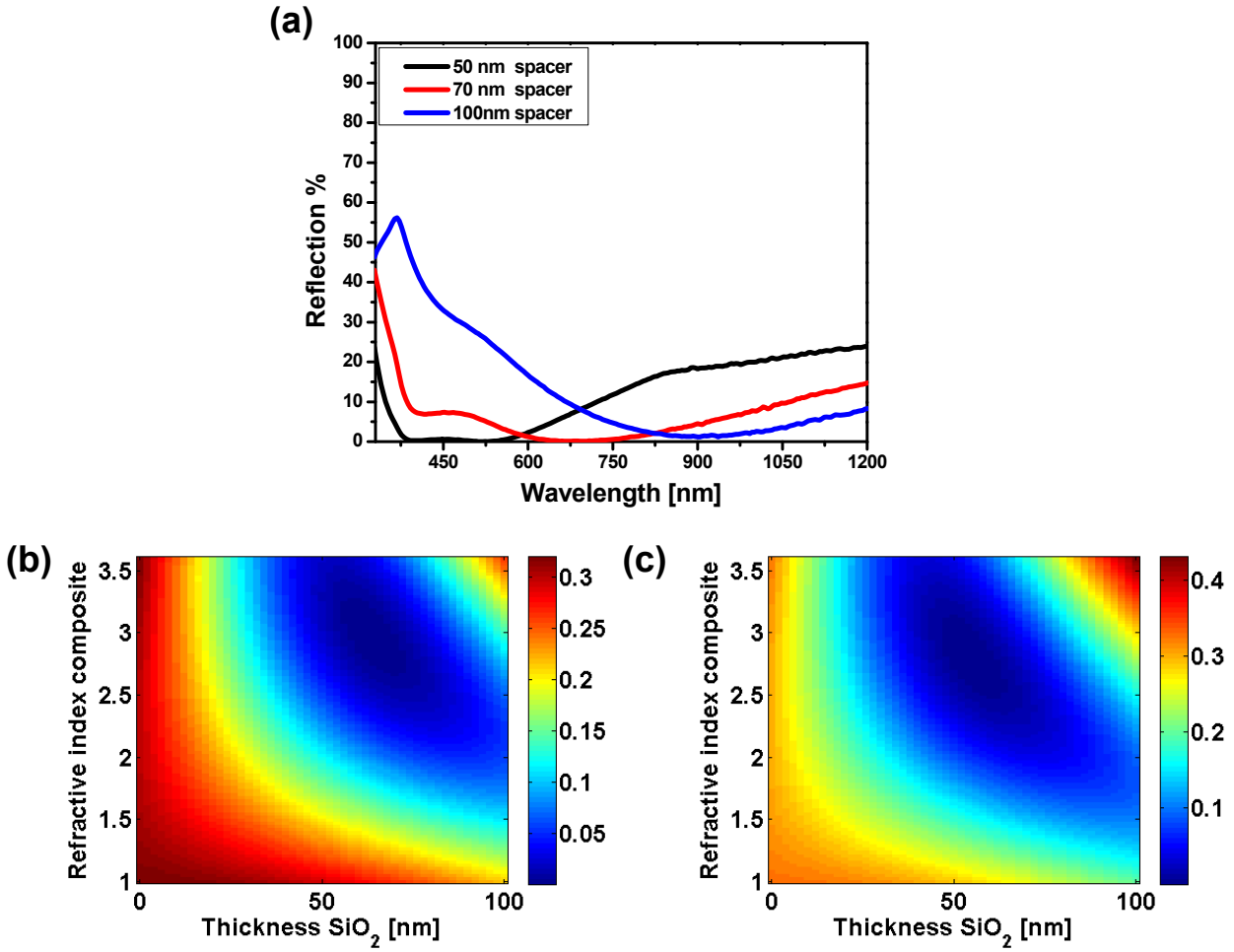

Figure 8.6: *(a) Reflection spectra of hybrid ARC with 30% filling fraction of metal in the top layer deposited on spacer layers with three different thicknesses. The ARC is deposited again on silicon. Black, red and blue curves showing the spectra of 50, 70 and 100 nm thick spacer layer,correspondingly. Reflection contour of 20 nm film with various RI on SiO_2 film with different thickness at (b) 800 nm and (c) 900 nm wavelengths.*

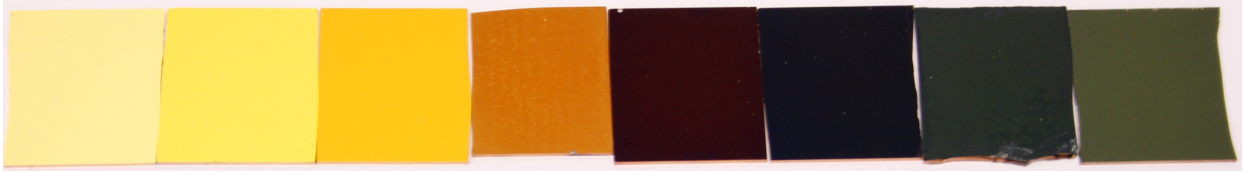

Figure 8.7: *True photograph of 25 nm SiO2 coated gold film covered by 20 nm Au-SiO_2 nanocomposite with different filling factor. From left to right the filling factor of nanocomposite increased (13%, 20%, 30%, 40%, 50% and 60%, correspondingly) while the first and second samples are bare gold and 45 nm SiO_2 coated gold, respectively.*

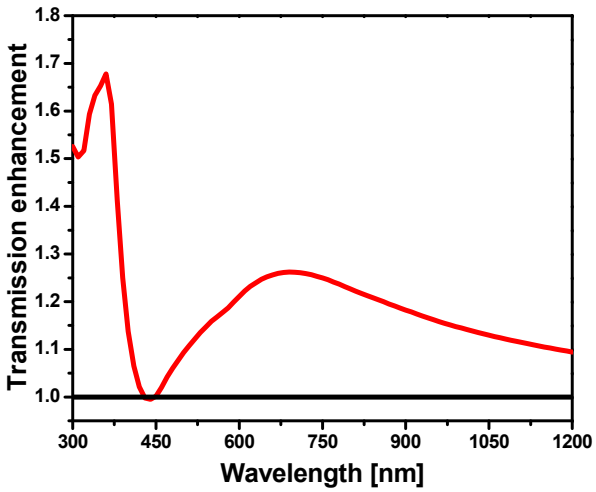

Figure 8.8: *Calculated transmission enhancement of silicon by plasmonic coating which is calculated by normalization of the transmission of coated silicon by that of bare one. The black line shows the normalized transmission of bare silicon while the red curve is the normalized transmission of Ag-SiO_2 nanocomposite deposited on SiO_2 coated silicon.*

the gold deposition rate was varied between 3 to 13 nm/s. This enabled us to fabricate gold nanocomposite with a wider range of filling factors (below and above percolation threshold). Nevertheless, we increased the rate of deposited gold only to an extent such that we avoid the formation of a continuous gold film instead of particles. For the formation of a gold film no localized plasmon resonance would appear which has to be avoided. From final TEM investigation data we could eventually observe that the particles do not coalesce and they are mainly spherical which further simplified the theoretical modeling.

The thickness of the films was measured with a profilometer (Dektak 8000 surface profile measuring system) and the thickness of dielectric was further measured with ellipsometer (M2000 (J.A. Woollam Co., Inc.)). Optical properties of the samples at normal incidence were measured with a UV/vis/NIR spectrometer (Lambda900, PerkinElmer). For transmission measurements, the base line was collected by measuring the empty compartment (i.e. air considered as the reference) while for reflection measurements, the mirror provided by the company was used. To extract the absolute value of reflection, the measured reflection spectra of the samples were normalized to the tabulated data of the mirror provided by the manufacturing company (PerkinElmer). In all types of measurement, the scan step was fixed to 4 nm and the base line was collected twice by a full sweep across the spectral domain of interest while the integration and acquisition time were kept constant. Polarization-dependent and variable angle spectroscopic Ellipsometry reflection measurements of the films was carried out with J.A. Woollam Co., Inc. M2000 UI (spectroscopic ellipsometer) with a dual lamp system with Deuterium and Quartz Tungsten Halogen (QTH) lamps as light sources (Data provide by LOT catalogue Europe). Angle sweep step was selected to be 5° or 10° and the angle variation from 45° to 85° was performed. In order to have a comparable study and achieving the best signal-to-noise, 5 seconds acquisition time was applied for all experiments. Accordingly, the measurement did not take more than few seconds. For analyzing the data,

CompleteEASE® software package provided by the company was used.

8.5.2 Simulations

FDTD simulations were made with an in-house developed code on a sufficient large cluster [284]. The considered structure consists to a nominal implementation of the experimental geometry. For this purpose a random arrangement of spherical metallic nanoparticles with a diameter corresponding to the mean diameter as extracted from the TEM samples has been generated. The filling fraction has been adjusted according to the experimental values and we only enforced an isolation of all spherical nanoparticles, i.e. their interpenetration has been excluded. The spatial domain considered in the simulation was $100nm \times 100nm$ in lateral directions. In these directions periodic boundaries were enforced to eventually mimic an infinitely extended space. The chosen spatial domain was sufficiently large to exclude any notable effect from the periodicity. In the propagation direction the sequence of layers and their respective thicknesses has been considered in full analogy with the experimental situations. Permittivity of SiO_2 has been taken as non-dispersive and equal to 2.25. Permittivity of gold was taken as tabulated in the literature [144] but with an additional correction term to accommodate the finite and small size of the nanoparticles [290]. The intrinsic dispersion of the material has been fully taken into account by performing at each wavelength an individual simulation and adjusting the free parameters in a Drude model to provide a material with the respective properties at the considered wavelength. Spatial discretization in the FDTD was 1 nm and perfectly matched layers were used in the propagation direction. To retrieve the effective properties the complex reflection and transmission coefficients have been extracted from the FDTD simulations and a parameter retrieval has been applied [291].

8.6 Acknowledgements

M.K.H., F.F. and M.E. gratefully acknowledge the financial support by the German Research Foundation (DFG) through the projects EL 554/1-1 and SFB 677 (C1,C9). M.E. would like to thank the Initiative and Networking Fund of the Helmholtz Association's (grant No. VHNG- 523) for providing the financial base for the start-up of his research group. The authors also gratefully acknowledge Dr. U. Schürmann and Prof. Kienle for TEM measurements. This work was supported by the German Federal Ministry of Education and Research (PhoNa) and by the Thuringian State Government (MeMa). We thank Karsten Verch (www.karstenverch.com) for his artistic view of the concept in Figure 8.4b.

Chapter 9

Photo-driven perfect absorber as active metamaterial with a tunable molecular-plasmonic coupling

M. K. Hedayati, M. Javaherirahim, A. U. Zillohu, H. J. El-Khozondar, M. Bawa'aneh, A. Lavrinenko, F. Faupel, M. Elbahri, Photo-driven super absorber as active metamaterial with a tunable molecular-plasmonic coupling *Advanced Optical Materials 2014*, doi: 10.1002/adom.201400105.

9.1 Abstract

Active optical materials in which the properties controlled by an external stimulus have found applications in memories [292–295] opto-electronic devices [296], smart windows [297–299] drug delivery [300], bio-analytics [301] and surgery [302] amongst others. Beside the traditionally used transition metal-oxides, semiconductors and smart polymers as switchable materials [303] molecular switching elements [304] spurred considerable attention, in particular molecule-plasmon interacting systems [305–308]. In a molecule-plasmon hybrid system, the plasmon resonance peak can be shifted, split or its intensity can be tuned by changing by the induced changes in the molecule. Even though this concept has been extensively studied, the gap between the concept and its applications still exist. Recently, we showed that consolidation of the absorbing nature of the photoswitchable dye molecules and plasmon resonance enable realization of new class of optical device, in which the transparency can be optically adjusted by light [132]. Here, we show that an optically driven super absorbing system can be realized in a stack composed of a thin polymer-photoswitchable film and a metal mirror. In such a system, the reflectivity of the metal mirror could be dropped down to few percent or recovered to more than 95% by UV or visible illumination, respectively.

9.2 Main text

Metamaterials are known as artificial structures, where the desired exotic properties can be achieved by special structural composition of their building blocks (unit cells) [309]. Perfect (super) absorber systems are also among the structure that initially were introduced through the concept of metamaterials [31]. Even though, various strategies and techniques have been made in order to have high absorption in a wide range of frequencies from GHz to UV [32, 277], the real-time tunability of the resonance band remains a challenge [310]. Through the concept of metamaterials, there are few reports on an active perfect (super) absorber, where the resonance band tuned electrically [70, 311–313] or by heat induce phase change [274]. However, the concept of absorption/reflection modulation was introduced earlier than the birth of metamaterial absorbers, when *Tennant* proposed using of an active layer (screen) in front of a conducting target [314]. The active surface that he proposed is a microwave screen that can be switched between totally reflective and totally transparent states as demonstrated earlier [315, 316]. Although he did not verify his speculation experimentally, his theoretical calculations showed that in a single and in a multilayer screens narrow and wideband modulations of the reflection/absorption can be realized. This idea inspired researchers and, indeed, it is the basic idea behind the recently demonstrated electrically tunable metamaterials [70, 311–313] which switch between highly reflecting and highly absorbing states [68]. Nevertheless, to the best of our knowledge, active metamaterials absorbers wherein the optical properties are adjusted by light have not been reported so far.

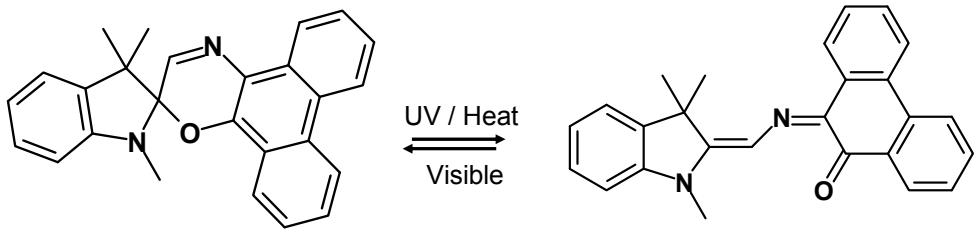

Figure 9.1: *Schematic illustration of photochromism of the SPO molecule used in this work.*

In this work, we demonstrate the first optically driven reflector/absorber switching in a molecular-plasmonic hybrid system which acts as a super absorber. The absorption band of this structure can be broadened or squeezed by UV or visible illumination, respectively. Our optically driven system is realized in a stack composed of a thin polymer-photoswitchable film (composite) and a metal mirror. The stack is fabricated by spin coating a thin layer of $1,3-Dihydro-1,3,3-trimethylspiro[2H-indole-2,3-[3H]phenanthr[9,10-b](1,4)oxazine$ (SPO) doped polystyrene (PS) on an optically thick gold film (the substrate of the stacks is glass). In such a system, the reflectivity of the metal mirror, which is typically very high, could be remarkably dropped down to few percent only or recovered to more than 95% by UV or visible illumination, correspondingly. As a specific highlight, we further demonstrate a new platform for the photoswitchable plasmonic modulator by incorporation the PS-SPO composite in a cavity inside the plasmonic [146–148, 277] in which a switching between weak

and strong plasmon-molecular coupling (hybridization) can be realized by light. The current approach could find applications in remote sensing and plasmonic switches amongst others.

Photochromic materials in which light-induced rearrangements occur drawn significant interest because of their practical applications. In this material, reversible transformations between two states with different absorption spectra happens by electro-magnetic radiation [317]. Spirooxazines belongs to the family of molecules displaying photochromic properties. Immediately after irradiation, the colorless molecules undergo a heterolytic CMO ring cleavage, producing colored forms of merocyanines [318]. In other words, the close form (off) of the molecule has absorption in the UV region while the open form (on) absorption is in the visible region. Note that the initial structure can be recovered in this class of materials by bleaching via visible light illumination or heating [319].

Figure 9.1 presents a schematic illustration of the molecular structure of SPO, which is used in this work. In this molecule, the C-O bond in the close form (Figure 9.1 (left)) breaks upon illumination, and the molecule turns to its planar photomerocyanine (PMC) state (open form in (Figure 9.1 (right))). This process is reversible and the initial state of the molecule can be recovered by white light shining or heating. In fact, PMC absorbs light with the wavelength around 600 nm. The absorption is originated by the electron promotion from the bonding level (π) to anti-bonding level ($\pi*$). Figure 9.2a shows the absorption spectra of a 40 nm film of composite consisted of SPO molecules embedded in a PS matrix and deposited on a glass substrate. One can clearly see the appearance of a new resonance peak at around 600 nm upon UV irradiation. Despite of the weak resonance peak of the composite on the glass substrate, once such composite is deposited on a gold film (metal), the absorption intensity is considerably enhanced. Figure 9.2b displays the absorption spectra of a gold film coated with PS-SPO composite before (solid line) and after (dashed line) illumination by UV light. The present metamaterial derives its unique properties from the molecular-plasmonic coupling which can diminish the reflection of the metal layer [320] down to 2% under UV illumination, and turn surprisingly the gold mirror into a broadband photo-switchable super absorber. In Figure 9.2c, the photograph of the composite deposited on a gold film is shown. It is apparent that the shiny color of bare gold (Figure 9.2c (left)) is dimmed (Figure 9.2c (right)) upon ultraviolet irradiation. In this metamaterial absorber, the absorption band can be widened in range by more than 150 nm in visible under UV illumination. Hence, the first demonstration of a photodriven super absorber wherein the reflectivity can be recovered by white light irradiation is reported. In spite of slight absorption increment in the case of composite on a glass substrate (around 20%), the enhancement of up to 4 times of initial magnitude (up to 90%) was recorded, when the hybrid film is deposited on a thick metallic film instead. In fact, the absorption enhancement is significant mainly at the frequency of molecular absorption (600 nm) and the change at higher frequencies (wavelength shorter than 500 nm) are still small. As discussed before, the absorption at higher frequencies (around 400 nm wavelength) is attributed to the $n \rightarrow \pi*$ molecule transition [321] while the considerably intensified absorption maximum at around 600 nm is originated from the electron promotion from the highest occupied molecular orbital (HOMO) to the lowest unoccupied molecular orbital (LUMO). However, the intrinsic absorption of the PS-SPO composite is considerably enhanced upon illumination. We attributed the enhancement to the presence of the metal mirror in proximity of

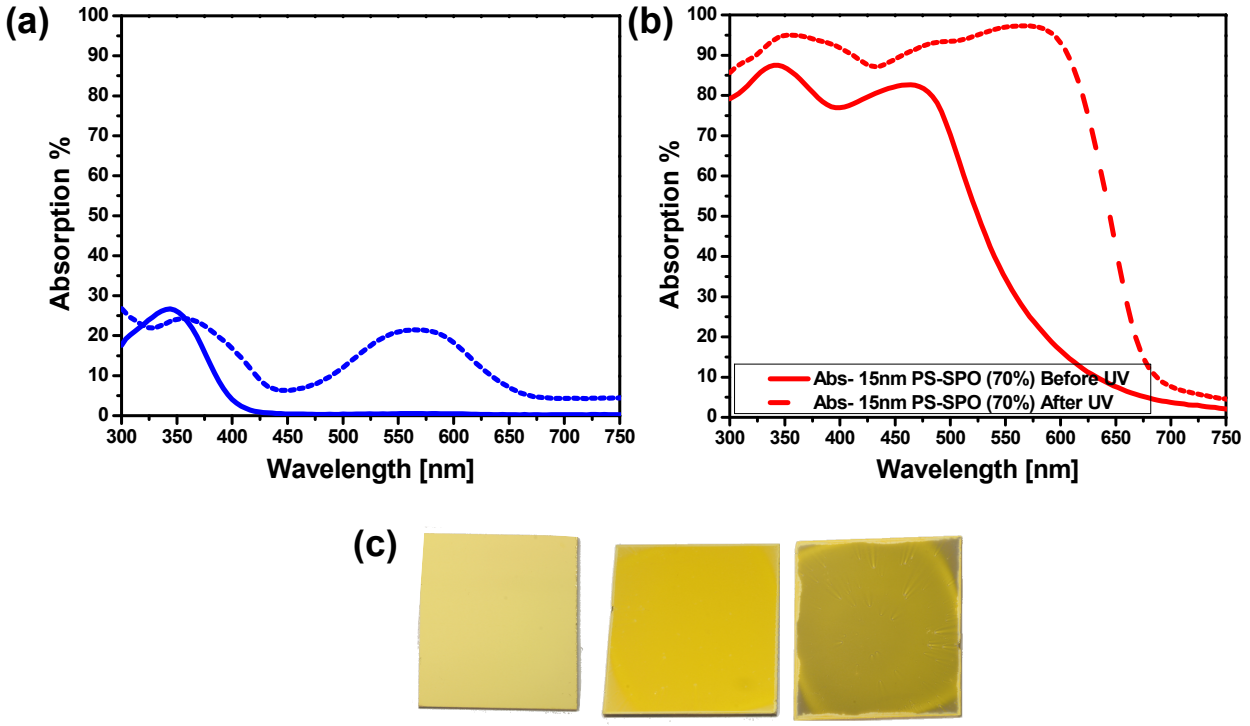

Figure 9.2: *Absorption spectra of PS-SPO composite (solid line) as deposited and upon UV irradiation (dashed line) deposited on (a) glass and (b) 100nm gold, respectively. (c) Photograph of bare gold film (left) and PS-SPO coated gold film before (middle) and after (right) UV irradiation.*

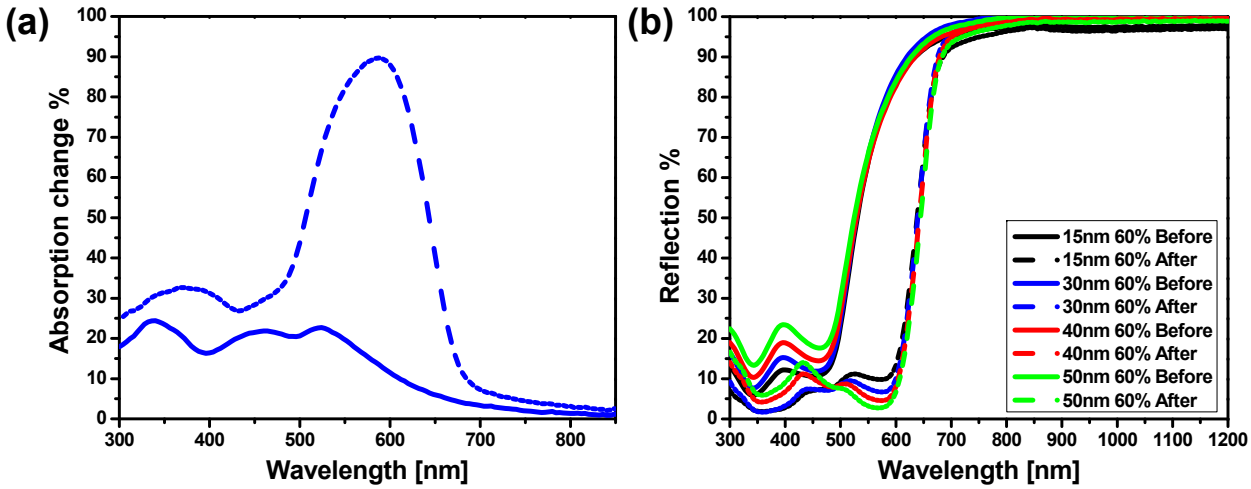

Figure 9.3: *(a) Absorption difference between the on (dashed line) and off (solid line) state of composite on gold film relative to the absorption of bare gold. (b) Reflection spectra of PS − SPO coated gold film with different thickness as follow: 15 nm (black), 30 nm (blue), 40 nm (red) and 50 nm (green). Solid lines are the data of as deposited samples while the dotted-lines represents the illuminated samples.*

the molecules. On the other hand, multiple reflection of incident light from the metal mirror could potentially multi-excite the molecules and hence enhancing the absorption. Likewise, plasmonic coupling on the surface of the metal mirror and light interference between the layer further intensify the absorption as explained latter. Note that, the symmetric molecular absorption band of the composite deposited on glass (which appeared at 568 nm) shifts to 584 nm once the molecules get close to the gold film. Apparently, the absorption band shape becomes asymmetric. These observations can be explained by interaction of polarized molecules (PMC) and electric charges induced in the metallic film thus giving rise to a weak molecular-plasmon coupling. While a surface plasmon-polariton (SPP) can not be activated (excited) on a planar metal surface without a coupler, the polarized molecules could induce charges on the surface [322] and facilitate a dipole induced plasmonic coupling on the metal surface [132]. Indeed, the SPO not only absorbs but also emits light in the visible spectrum [321].

When any dipole locates in proximity of a metallic film, a number of energytransport processes could happen, in particular, when surface plasmon polariton (SPP) quanta for dipoles overlapping spectrally with SPP electric fields [233]. For instance, the excited dipoles could create spontaneously electronhole pairs in the metal via dipole dipole coupling (for molecules in proximity of the metal surface) and emit spontaneously radiative modes [233]. In our previous work, we showed the possibility of using photoswitchable molecules as a couplers (charge inducers) on a thin metal film [132]. Indeed, the coupling occurred in off state where the molecules are supposed to be un-polarized. But it seems that they are anyway partially polarized due to the local thermal equilibrium with their open form (on state) and therefore they can perform as charge inducer (coupler) [132]. In the present work, a similar phenomenon is expected, however, due to the higher reflectivity of the thick gold film the quantity of the induced charges might be different.

Figure 9.3a exhibits the absorption variation of a gold film coated with PS-SPO composite in off and on states. In Figure 9.3a, the absorption of the bare gold film (the substrate) is subtracted from the absorption of the PS-SPO coated film on the substrate to remove absorption caused by the intrinsic properties of the base layer from the absorption spectra of the stacks. Based on the absorption change calculation, the appearance of the gold plasmonic resonance peak at 530 nm is obvious (in off state) which in principle cannot be realized unless the SPO molecules excite the SPP (c.f. Figure 9.3a (solid line)). It seems that upon UV illumination, a weak plasmon-molecular coupling is established and a broad asymmetric shape resonance appears (c.f. Figure 9.3a (dashed line)). It should be noted that the intense absorption band of the illuminated sample originates not only from the coupling. Also the multiple reflections between the layers and interference [48, 323] contribute to the reflection drop (absorption growth) in the stack. Thickness variation of the coating on the same substrate (gold mirror) showed (Figure 9.3b) that the coupling does not rely on the thickness of the PS-SPO (coupler) layer. The reflection drop irrespective of the thickness of the coating shows the same trends and the drop appears at the same frequency. Since the thickness of the coating is sub-wavelength and the considerable reflection drop happens dynamically (upon illumination), one could consider the current approach as a novel absorbing anti-reflector [146, 275] wherein no bothering by thickness restrictions of common antireflective films exist.

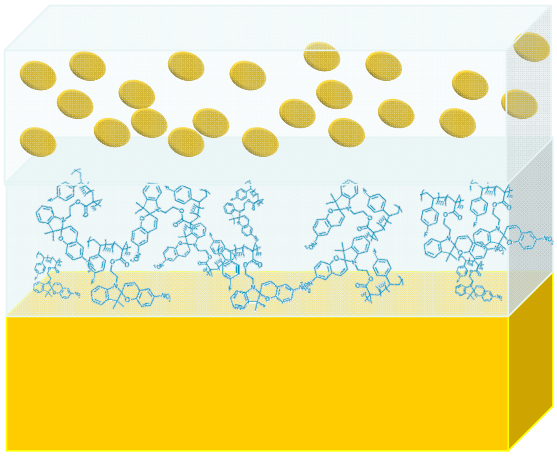

Figure 9.4: *Schematic of the geometry used in the metamaterial stack.*

Besides the coupling between surface plasmons and dyes molecules discussed above, the strong coupling of localized plasmons and excited molecules can happen. In the last case, the coupling strength strongly depends on the spectral overlap of the molecular and plasmonic resonances [324]. An exciton-plasmon coupling regime has been demonstrated either in a weak or strong regime [325–327], whereas in the strong coupling case an exciton-plasmon (hybridization) coupling leads mainly to splitting of a single band into two or more bands [325–327]. We introduce a metamaterial, which modulates the molecular-plasmonic interaction from weak to strong coupling by type of illumination. In that design, the PS-SPO composite is integrated as a spacer layer in a nanocomposite perfect absorber [146–148,277]. The nanocomposite absorber used for proof-of-principle is composed of gold nanoparticles and Polytetrafluorethylen ($PTFE$), which is deposited atop of the PS-SPO coated gold film. The schematic of the geometry used in this design is depicted in Figure 9.4.

Figure 9.5a shows the reflection spectra of a multi-stack made of a 20 nm $Au-PTFE$ composite (40%) separated from a 100 nm gold film by a 40 nm PS-SPO composite as well as the same composition but with an un-doped polymer as a reference. It is obvious that the reflection drop of the absorber using the un-doped polymer is broadened a bit and significantly red-shifted by adding of the Spirooxazine molecules in the metamaterial. In other words, the absorption maximum of the stack when the spacer is un-doped (Figure 9.5a (black curve)) is at 450 nm but once the spacer is replaced with SPO doped polymer (Figure 9.5a (blue solid curve)), the peak shifts to the lager wavelengths (red-shift), which we attribute to the weak plasmon-molecule coupling. On the other hand, when such a stack is UV irradiated, the molecular-plasmon interaction turns to the strong coupling regime, and consequently, the peak splitting occurs revealing two separate peaks. These peaks correspond to two hybrid modes, and such splitting with the energy difference between the modes of 780 meV (wavelength shift of 270 nm) is the indicator of a coherent strong coupling of molecules and plasmons. Conversely, white light illumination leads to a relatively weak coupling (Figure 9.5b). To the best of our knowledge, this energy value is the highest reported splitting in plasmon-molecular coupling systems. Although the induced alteration of the refractive

index of the composite (PS-SPO) upon illumination could be one of the contributor to the observed switching, we believe that plasmonic coupling plays a more significant role. To confirm experimentally the plasmon origin of the mentioned shift and coupling, the similar experiment on a non-plasmon bottom layer was carried out. Deposition of the same stack on top of a silicon wafer (Figure 9.5b) reveals that no splitting occurs, which guides us to the fact that the presence of an optical cavity together with a surface plasmon resonance of the metal film is essential for realization of the strong coupling regime. Considering the metal-dielectric nanocomposite [328] based absorber [147] as a plasmonic cavity alomg the layers, one could conclude that the PS-SPO composite film in the "*on*" exhibits a strong molecular plasmon hybridized behavior that is switched to the weak coupling regime in the off state. This is indeed a demonstration of a fast photodriven plasmonic modulator.

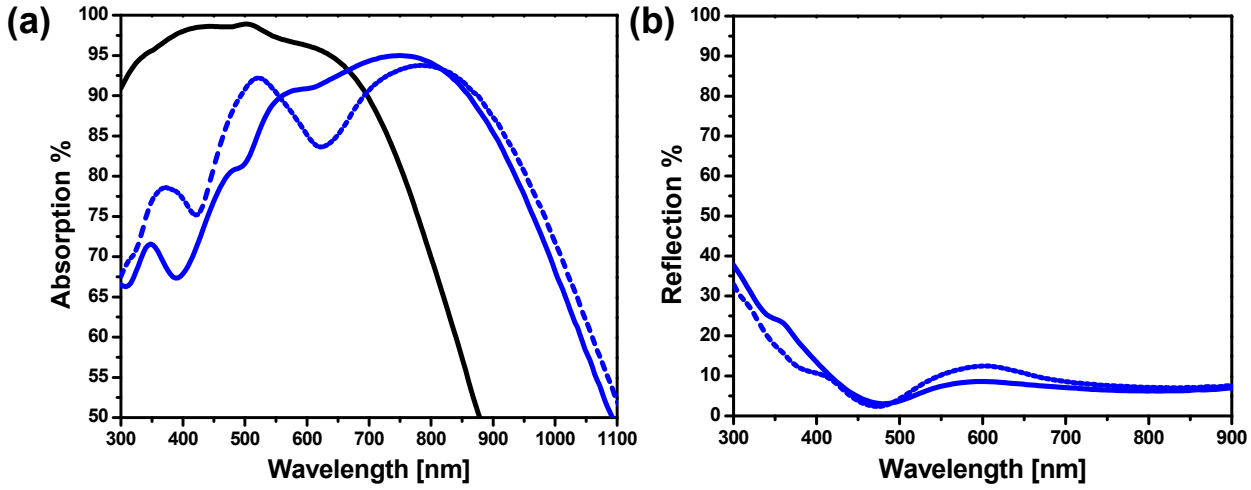

Figure 9.5: *(a) Absorption spectra of a multi-stack out of 20 nm Au-PTFE composite(40%) separated from 100 nm gold film with 40 nm highly concentrated PS-SPO composite deposited on glass substrate before (solid blue) and after (dashed line blue) UV-illumination, respectively. Black curve show the same stack but the spacer layer is pure PS film as reference.(b) Reflection spectra of multi-stack out of 20 nm Au-PTFE composite(40%) separated from silicon wafer with 40 nm PS-SPO composite with 50% concentration of SPO before (solid) and after (dashed line)UV illumination, respectively.*

9.3 Summary

In short, we have designed, fabricated and characterized a multi-stack system consisting of a polymer-SPO composite layer either on the top of a thick metallic film or as a spacer layer between a metal-dielectric nanocomposite and thick metallic film. We observed that the structure in the former case can function as a photoswitchable super absorber . It is due to the induction of electric charges on the surface of the mirror followed by facilitated excitation of the weak molecular-plasmon coupling regime, which results in a significant reflection reduction and increment upon UV or visible irradiation, respectively. Furthermore,

by sandwiching the PS-SPO composite between the metal film and polymer highly doped with gold nanoparticles, we could demonstrate a tunable weak to strong coupling switching with a pronounced 780 meV energy difference between the two peaks in absorption after UV illumination. The presented experimental data could pave the way for utilization of perfect absorbers as remote optical sensors and plasmonic switches as modulators. Nevertheless, exploring the real mechanism behind the observation needs further theoretical analysis, which is beyond the scope of this manuscript.

9.4 Acknowledgements

We gratefully acknowledge the financial support by the German Research Foundation (DFG) through the projects SFB 677 (C1, C9) and EL 554/1-1. M.E. would like to thank the Initiative and Networking Fund of the Helmholtz Association's (grant No. VH-NG-523) for providing the financial base for the start-up of his research group.

Chapter 10

Summary and Outlook

Two classes of perfect absorbers namely passive and active metamaterials and a new type of plasmonic anti-reflective coating are demonstrated. Hence the summary is divided into three different subchapters to cover each one of the structures individually.

10.1 (Passive) Metamaterials Perfect Absorber

The passive absorber demonstrated in this work consisted of three main layers. The top, middle and base layer are a metal-dielectric nanocomposite film, a dielectric film and an optically thick metal film, respectively. The metals used for fabrication and characterization were gold, silver and copper. Silicon dioxide, titanium dioxide and PTFE were the dielectric materials implemented for the composite and spacer layers. It is shown that with all possible combinations of metals and dielectric, complete absorption of light in a range of frequency can be realized however the filling factor and thickness of the films are not equal in all the configurations. In order to reduce the number of variable parameters for optimization, a 20 nm thickness was selected for all types of the composites. Therefore, filling factor of the nanocomposite, thickness of the spacer layer and matrix/spacer materials were the variables in this study. It turns out that the interband absorption frequency of the metal and its plasmon resonance enforce position of the absorption maximum. Accordingly, the gold and copper based nanocomposite give rise to a broad absorption peak with resonance at yellow part of visible but the silver absorber maximum appears at the blue part of the spectrum. The optimum filling factor of the composite (irrespective of the type of metal) was the near percolation value. On the other hand, upon exceeding the percolation threshold, the composite becomes a semi-continuous film which increases the reflection of the top layer and results in an absorption drop. Since one of the reasons of high absorption in such a stack is the plasmon coupling, variation of the the spacer layer thickness alters the absorption intensity and shape. In other words, there is an optimum thickness of the interlayer which provides the maximum absorption intensity while the deviation from the optimum value reduces the light extinction. The matrix of the composite also influences the performance of the metamaterial absorber due to the plasmonic nature of absorption. So, incorporation of metal particles in

a dielectric with high or low refractive index shifts the absorption maximum to longer and shorter wavelengths, respectively. The mentioned shift is not surprising since based on the Mie theory, there is a linear relationship between the refractive index of the environment and the plasmon frequency [329]. Changing the thickness of the composite or dielectric layers shifts the absorption band which is an evidence that interference also contributes to the high absorption of the present metamaterials. However, we believe that the role of interference is less than that of plasmon absorption because the latter is signified by the reflecting nature of the substrate. In other words, the multiple reflection of the transmitted light through the nanocomposite, could potentially re-excite the localized plasmon of the particles and further enhance the absorption. Moreover, the small gap between the particles acts as a hot-spot and considerable confinement of the electromagnetic wave occurs in this small area (less than 5 nm). In short, the huge absorption of this metamaterial can be attributed to many phenomena, however it seems that the dominant contributors are localized plasmon resonance and coupling.

10.2 Photoresponsive (Active) Perfect Absorber

The interaction of molecule-plasmon and its influence on the plasmon resonance peak in different ways such as shifting and splitting are demonstrated. Here, we show that an optically driven perfect absorbing system (active or smart metamaterials absorber) in which molecule and plasmon interacts, can be realized. It is composed of a thin polymer-photoswitchable film (PS-SPO) and a metal mirror. Although the presented data in the frame of this dissertation are limited to gold as the base layer, a silver film was also used and analyzed (data not shown here). A flat gold film absorbs light in visible due to the interband transition and its intensity can reach up to 60% from the blue to green part of spectrum. By coating the gold film with a PS-SPO film the absorption increases considerably and reaches to around 90% in the mentioned range of frequency. This happens due to the interaction of partially polarized molecules and the base mirror. Indeed, fractions of the molecules are in equilibrium with their excited states even without activation by UV irradiation. Therefore, these active molecules raise the absorption of the stack before irradiation. Upon UV illumination, the absorption band considerably broadens up to 650 nm while its intensity reaches to 98%. The switching between the two absorption states enables us to show the first optically driven perfect absorber in visible frequency. It seems that in the present stack, a weak plasmonic-molecular coupling would set-in upon UV irradiation. In other words, the molecules in open form induce charges on the surface of the base metals and hence couple the incidence photon to the surface plasmon. Since the metal film is thicker than the skin depth, the reflection is considerably high (no transmission). Consequently the reflected wave from the mirror can enhance the interaction of molecule-metal and results in a higher absorption of the stack. To further confirm the occurrence of coupling in such a system, the PS-SPO film is incorporated to the passive metamaterial absorber as a spacer layer. It is found that presence of the excited molecules in the interlayer of the metamaterial absorber could provide a strong plasmon-molecule coupling which splits the absorption band with an energy difference of more than 700 meV. Note that the strong coupling was only observed in the open state of

the molecules while the weak coupling happens in the close form (non irradiated). In short, the hybrid system out of plasmonic materials and photoswitchable molecules enables the realization of a photodriven perfect absorber. Additionally, the potential of such a system for switching between the strong and weak coupling is demonstrated when the molecule containing film is stacked between a metal film and a metal-polymer nanocomposite.

10.3 Plasmonic antireflection coating

A broadband antireflection coating (ARC) based on a metal-dielectric nanocomposite is presented in which the thickness of the layers is far below the quarter-wavelength which is generally a required condition for reflection reduction. The ARC demonstrated in this work was designed for silicon wafer and made of two layers; silver-silicon dioxide nanocomposite and silicon dioxide film. The key feature of this hybrid ARC is using two quasi arrangements for the dielectric layers in one design where the refractive indices ascend or descend in consecutive layers with a descending order, albeit at a different wavelength. The high performance of the coating as a new broadband ARC originates from the strong dispersion in the permittivity of plasmonic nanocomposites around their resonance. Therefore, by using a plasmonic nanocomposite as a strongly dispersive material, we could have a system of layers where both the Rayleigh and reverse-Rayleigh conditions are fulfilled which we named it "Hybrid". In other words, below the resonance wavelength the composite/dielectric layers act as a graded-index coating while they perform as a Bragg-mirror at longer wavelengths. This provides the opportunity to considerably lower the reflection across a broad range of wavelengths with only a minor angular sensitivity. Moreover, as a proof-of-principle, we showed that the silicon reflectivity can be reduced upon coating with two dielectric layers of TiO_2 and SiO_2 where the former is deposited atop of the later (reverse-Rayleigh). However the reflection drop is rather narrow and practically limited. We further made use of potential of the nanocomposite as a reflection tuning medium. Accordingly, we coated the composite with a variety of filling factors on a gold mirror to tune the color of the stack and demonstrate the creation of different colors by using a very thin film. The colors originated from different reflection drops associated with each filling factor which show the other potential of our hybrid concept for realization of plasmonic rainbow colors.

10.4 Outlook

The field of metamaterials perfect absorbers is still immature. Bridging the gap between the lab-scale fabrication to industrial application still remains a challenge. Nevertheless, current achievements both in theory and experiment show the immense potential of this new type of metamaterials for a variety of applications. One of the prime potential applications of perfect absorbers is solar industry where energy harnessing is desired. For instance, thermophotovoltaic systems might be the host of a plasmonic perfect absorber as their collector, in which the light is concentrated and absorbed. Another application of metamaterial perfect absorbers is in the area of research where the huge light confinement is desired such as

surface enhanced molecular spectroscopy (SEMS). Indeed, the metamaterials absorber like other plasmonic materials can be implemented as a sensor where the absorption peak can be tuned by environmental changes. In particular, the latter application is more relevant for photoswitchable absorbers where it can potentially be a robust UV sensor. The usefulness of the reverse-Rayleigh antireflector is very broad and can be principally applied onto any reflective substrates. However the application of a hybrid antireflector (nanocomposite based ARC) for photovoltaics needs special cares. In other words, the substrate surface has to be passivated properly prior to deposition of the nanocomposite to avoid electron-hole recombination at the interface.

Bibliography

[1] M. Z. Jacobson, "Review of solutions to global warming, air pollution, and energy security," *Energy & Environmental Science*, vol. 2, pp. 148–173, 2009.

[2] I. Dincer, "Renewable energy and sustainable development: a crucial review," *Renewable and Sustainable Energy Reviews*, vol. 4, no. 2, pp. 157 – 175, 2000.

[3] S. A. Kalogirou, "Solar thermal collectors and applications," *Progress in Energy and Combustion Science*, vol. 30, no. 3, pp. 231 – 295, 2004.

[4] OECD/IEA, *Solar energy perspectives.*
International Energy Agency, November 2011.

[5] H. A. Atwater and A. Polman, "Plasmonics for improved photovoltaic devices," *Nature Materials*, vol. 9, no. 3, pp. 205–213, 2010.

[6] W. Murray and W. Barnes, "Plasmonic materials," *Advanced Materials*, vol. 19, no. 22, pp. 3771–3782, 2007.

[7] W. L. Barnes, A. Dereux, and T. W. Ebbesen, "Surface plasmon subwavelength optics," *Nature*, vol. 424, no. 6950, pp. 824–830, 2003.

[8] S. A. Maier, *Plasmonics: fundamentals and applications.*
Springer, 2007.

[9] G. V. Naik, V. M. Shalaev, and A. Boltasseva, "Alternative plasmonic materials: beyond gold and silver," *Advanced Materials*, vol. 25, p. 32643294, 2013.

[10] A. Meldrum, J. Haglund, R. F., L. A. Boatner, and C. W. White, "Nanocomposite materials formed by ion implantation," *Advanced Materials*, vol. 13, no. 19, pp. 1431–1444, 2001.

[11] L. Osete-Cortina, M. T. Doménech-Carbó, A. Doménech, D. J. Yusá-Marco, and H. Ahmadi, "Multimethod analysis of iranian ilkhanate ceramics from the takht-e soleyman palace," *Analytical and Bioanalytical Chemistry*, vol. 397, no. 1, pp. 319–329, 2010.

[12] P. Holakooei, F. Tisato, C. Vaccaro, and F. C. Petrucci, "Haft rang or cuerda seca? spectroscopic approaches to the study of overglaze polychrome tiles from seventeenth century persia," *Journal of Archaeological Science*, vol. 41, pp. 447–460, 2014.

[13] A. Y. Al-Hassan, "An eightth century arabic treatise on the colouring of glass: Kitab al-durra al-maknuna (the book of hidden pearl) of jabir ibn hayyan (c. 721c. 815)," *Arabic Sciences and Philosophy*, vol. 19, p. 121156, 2009.

[14] T. Pradell, J. Molera, A. Smith, and M. Tite, "Early islamic lustre from egypt, syria and iran (10th to 13th century ad)," *Journal of Archaeological Science*, vol. 35, no. 9, pp. 2649–2662, 2008.

[15] J. Pérez-Arantegui, J. Molera, A. Larrea, T. Pradell, M. Vendrell-Saz, I. Borgia, B. G. Brunetti, F. Cariati, P. Fermo, M. Mellini, *et al.*, "Luster pottery from the thirteenth century to the sixteenth century: a nanostructured thin metallic film," *Journal of the American Ceramic Society*, vol. 84, no. 2, pp. 442–46, 2001.

[16] S. Padovani, D. Puzzovio, C. Sada, P. Mazzoldi, I. Borgia, A. Sgamellotti, B. Brunetti, L. Cartechini, F. Dacapito, C. Maurizio, *et al.*, "Xafs study of copper and silver nanoparticles in glazes of medieval middle-east lustreware (10th–13th century)," *Applied Physics A*, vol. 83, no. 4, pp. 521–528, 2006.

[17] J. M. Garnett, "Colours in metal glasses and in metallic films," *Proceedings of the Royal Society of London*, vol. 73, no. 488-496, pp. 443–445, 1904.

[18] G. Mie, "Beiträge zur optik trüber medien, speziell kolloidaler metallösungen," *Annalen der Physik*, vol. 330, no. 3, pp. 377–445, 1908.

[19] J. Homola, S. S. Yee, and G. Gauglitz, "Surface plasmon resonance sensors: review," *Sensors and Actuators B: Chemical*, vol. 54, no. 1, pp. 3–15, 1999.

[20] Y. Mizukoshi, T. Fujimoto, Y. Nagata, R. Oshima, and Y. Maeda, "Characterization and catalytic activity of core-shell structured gold/palladium bimetallic nanoparticles synthesized by the sonochemical method," *The Journal of Physical Chemistry B*, vol. 104, no. 25, pp. 6028–6032, 2000.

[21] L. Hirsch, R. Stafford, J. Bankson, S. Sershen, B. Rivera, R. Price, J. Hazle, N. Halas, and J. West, "Nanoshell-mediated near-infrared thermal therapy of tumors under magnetic resonance guidance," *Proceedings of the National Academy of Sciences*, vol. 100, no. 23, pp. 13549–13554, 2003.

[22] L. He, M. D. Musick, S. R. Nicewarner, F. G. Salinas, S. J. Benkovic, M. J. Natan, and C. D. Keating, "Colloidal au-enhanced surface plasmon resonance for ultrasensitive detection of dna hybridization," *Journal of the American Chemical Society*, vol. 122, no. 38, pp. 9071–9077, 2000.

[23] O. Stenzel, A. Stendal, K. Voigtsberger, and C. von Borczyskowski, "Enhancement of the photovoltaic conversion efficiency of copper phthalocyanine thin film devices by incorporation of metal clusters," *Solar Energy Materials and Solar Cells*, vol. 37, no. 3, pp. 337 – 348, 1995.

[24] W. J. Padilla, D. N. Basov, and D. R. Smith, "Negative refractive index metamaterials," *Materials Today*, vol. 9, no. 7, pp. 28–35, 2006.

[25] D. R. Smith, W. J. Padilla, D. C. Vier, S. C. Nemat-Nasser, and S. Schultz, "Composite medium with simultaneously negative permeability and permittivity," *Physicaly Review Letters*, vol. 84, pp. 4184–4187, May 2000.

[26] J. Pendry, A. J. Holden, D. J. Robbins, and W. J. Stewart, "Magnetism from conductors and enhanced nonlinear phenomena," *Microwave Theory and Techniques, IEEE Transactions on*, vol. 47, no. 11, pp. 2075–2084, 1999.

[27] J. B. Pendry, "Negative refraction makes a perfect lens," *Physicaly Review Letters*, vol. 85, pp. 3966–3969, Oct 2000.

[28] J. B. Pendry, D. Schurig, and D. R. Smith, "Controlling electromagnetic fields," *Science*, vol. 312, no. 5781, pp. 1780–1782, 2006.

[29] N. I. Zheludev, S. Prosvirnin, N. Papasimakis, and V. Fedotov, "Lasing spaser," *Nature Photonics*, vol. 2, no. 6, pp. 351–354, 2008.

[30] A. Boltasseva and H. A. Atwater, "Low-loss plasmonic metamaterials," *Science*, vol. 331, no. 6015, pp. 290–291, 2011.

[31] N. Landy, S. Sajuyigbe, J. Mock, D. Smith, and W. Padilla, "Perfect metamaterial absorber," *Physical Review Letters*, vol. 100, no. 20, p. 207402, 2008.

[32] C. M. Watts, X. Liu, and W. J. Padilla, "Metamaterial electromagnetic wave absorbers," *Advanced Materials*, vol. 24, no. 23, pp. OP98–OP120, 2012.

[33] S. Kachan, O. Stenzel, and A. Ponyavina, "High-absorbing gradient multilayer coatings with silver nanoparticles," *Applied Physics B*, vol. 84, no. 1-2, pp. 281–287, 2006.

[34] A. Pfund, "Bismuth black and its applications," *Review of Scientific Instruments*, vol. 1, no. 7, pp. 397–399, 1930.

[35] N. Nelms and J. Dowson, "Goldblack coating for thermal infrared detectors," *Sensors and Actuators A: Physical*, vol. 120, no. 2, pp. 403–407, 2005.

[36] J. Hao, J. Wang, X. Liu, W. J. Padilla, L. Zhou, and M. Qiu, "High performance optical absorber based on a plasmonic metamaterial," *Applied Physics Letters*, vol. 96, no. 25, pp. 251104–251104, 2010.

[37] H. Tao, C. M. Bingham, A. C. Strikwerda, D. Pilon, D. Shrekenhamer, N. I. Landy, K. Fan, X. Zhang, W. J. Padilla, and R. D. Averitt, "Highly flexible wide angle of incidence terahertz metamaterial absorber: Design, fabrication, and characterization," *Physical Review B*, vol. 78, p. 241103, Dec 2008.

[38] N. I. Landy, C. M. Bingham, T. Tyler, N. Jokerst, D. R. Smith, and W. J. Padilla, "Design, theory, and measurement of a polarization-insensitive absorber for terahertz imaging," *Physicaly Review B*, vol. 79, p. 125104, Mar 2009.

[39] A. K. Azad, D. Y. Shchegolkov, H.-T. Chen, A. J. Taylor, E. Smirnova, and J. F. O'Hara, "Perfect terahertz absorber using fishnet based metafilm," in *Lasers and Electro-Optics (CLEO) and Quantum Electronics and Laser Science Conference (QELS), 2010 Conference on*, pp. 1–2, IEEE, 2010.

[40] X. Liu, T. Starr, A. F. Starr, and W. J. Padilla, "Infrared spatial and frequency selective metamaterial with near-unity absorbance," *Physicaly Review Letters*, vol. 104, p. 207403, May 2010.

[41] M. Diem, T. Koschny, and C. M. Soukoulis, "Wide-angle perfect absorber/thermal emitter in the terahertz regime," *Physical Review B*, vol. 79, p. 033101, Jan 2009.

[42] Z. Sun and X. Zuo, "Tunable absorption of light via localized plasmon resonances on a metal surface with interspaced ultra-thin metal gratings," *Plasmonics*, vol. 6, no. 1, pp. 83–89, 2011.

[43] N. Liu, M. Mesch, T. Weiss, M. Hentschel, and H. Giessen, "Infrared perfect absorber and its application as plasmonic sensor," *Nano Letters*, vol. 10, no. 7, pp. 2342–2348, 2010.

[44] T. V. Teperik, F. G. De Abajo, A. Borisov, M. Abdelsalam, P. Bartlett, Y. Sugawara, and J. Baumberg, "Omnidirectional absorption in nanostructured metal surfaces," *Nature Photonics*, vol. 2, no. 5, pp. 299–301, 2008.

[45] C. Hu, Z. Zhao, X. Chen, and X. Luo, "Realizing near-perfect absorption at visible frequencies," *Optics Express*, vol. 17, pp. 11039–11044, Jun 2009.

[46] J. Hao, L. Zhou, and M. Qiu, "Nearly total absorption of light and heat generation by plasmonic metamaterials," *Physical Review B*, vol. 83, no. 16, p. 165107, 2011.

[47] J. Wang, Y. Chen, X. Chen, J. Hao, M. Yan, and M. Qiu, "Photothermal reshaping of gold nanoparticles in a plasmonic absorber," *Optics Express*, vol. 19, no. 15, pp. 14726–14734, 2011.

[48] H.-T. Chen, "Interference theory of metamaterial perfect absorbers," *Optics Express*, vol. 20, no. 7, pp. 7165–7172, 2012.

[49] S. Shu, Z. Li, and Y. Y. Li, "Triple-layer fabry-perot absorber with near-perfect absorption in visible and near-infrared regime," *Optics Express*, vol. 21, no. 21, pp. 25307–25315, 2013.

[50] V. G. Kravets, F. Schedin, and A. N. Grigorenko, "Plasmonic blackbody: Almost complete absorption of light in nanostructured metallic coatings," *Physicaly Review B*, vol. 78, p. 205405, Nov 2008.

[51] C. Hu, L. Liu, Z. Zhao, X. Chen, and X. Luo, "Mixed plasmons coupling for expanding the bandwidth of near-perfect absorption at visible frequencies," *Optics Express*, vol. 17, pp. 16745–16749, Sep 2009.

[52] Z. Fan, R. Kapadia, P. W. Leu, X. Zhang, Y.-L. Chueh, K. Takei, K. Yu, A. Jamshidi, A. A. Rathore, D. J. Ruebusch, *et al.*, "Ordered arrays of dual-diameter nanopillars for maximized optical absorption," *Nano Letters*, vol. 10, no. 10, pp. 3823–3827, 2010.

[53] J. Lehman, A. Sanders, L. Hanssen, B. Wilthan, J. Zeng, and C. Jensen, "Very black infrared detector from vertically aligned carbon nanotubes and electric-field poling of lithium tantalate," *Nano Letters*, vol. 10, no. 9, pp. 3261–3266, 2010.

[54] C.-H. Lin, R.-L. Chern, and H.-Y. Lin, "Polarization-independent broad-band nearly perfect absorbers in the visible regime," *Optics Express*, vol. 19, no. 2, pp. 415–424, 2011.

[55] V. Kravets, S. Neubeck, A. Grigorenko, and A. Kravets, "Plasmonic blackbody: Strong absorption of light by metal nanoparticles embedded in a dielectric matrix," *Physical Review B*, vol. 81, no. 16, p. 165401, 2010.

[56] L. Mo, L. Yang, and S. He, "Broadband and polarization-independent solar absorber based on plasmonic coaxial tapered holes," in *Asia Communications and Photonics Conference*, Optical Society of America, 2012.

[57] T. Søndergaard, S. M. Novikov, T. Holmgaard, R. L. Eriksen, J. Beermann, Z. Han, K. Pedersen, and S. I. Bozhevolnyi, "Plasmonic black gold by adiabatic nanofocusing and absorption of light in ultra-sharp convex grooves," *Nature Communications*, vol. 3, p. 969, 2012.

[58] Y. Cui, K. H. Fung, J. Xu, H. Ma, Y. Jin, S. He, and N. X. Fang, "Ultrabroadband light absorption by a sawtooth anisotropic metamaterial slab," *Nano Letters*, vol. 12, no. 3, pp. 1443–1447, 2012.

[59] F. Ding, Y. Cui, X. Ge, Y. Jin, and S. He, "Ultra-broadband microwave metamaterial absorber," *Applied Physics Letters*, vol. 100, no. 10, pp. 103506–103506, 2012.

[60] M. G. Nielsen, A. Pors, O. Albrektsen, and S. I. Bozhevolnyi, "Efficient absorption of visible radiation by gap plasmon resonators," *Optics Express*, vol. 20, no. 12, pp. 13311–13319, 2012.

[61] K. Aydin, V. E. Ferry, R. M. Briggs, and H. A. Atwater, "Broadband polarization-independent resonant light absorption using ultrathin plasmonic super absorbers," *Nature Communications*, vol. 2, p. 517, 2011.

[62] J. Wang, C. Fan, P. Ding, J. He, Y. Cheng, W. Hu, G. Cai, E. Liang, and Q. Xue, "Tunable broad-band perfect absorber by exciting of multiple plasmon resonances at optical frequency," *Optics Express*, vol. 20, no. 14, pp. 14871–14878, 2012.

[63] X. Chen, H. Gong, S. Dai, D. Zhao, Y. Yang, Q. Li, and M. Qiu, "Near-infrared broadband absorber with film-coupled multilayer nanorods," *Optics Letters*, vol. 38, no. 13, pp. 2247–2249, 2013.

[64] R. Abdelaziz, D. Disci-Zayed, M. K. Hedayati, J.-H. Pöhls, A. U. Zillohu, B. Erkartal, V. S. K. Chakravadhanula, V. Duppel, L. Kienle, and M. Elbahri, "Green chemistry and nanofabrication in a levitated leidenfrost drop," *Nature Communications*, vol. 4, 2013.

[65] M. Elbahri, S. Homaeigohar, R. Abdelaziz, T. Dai, R. Khalil, and A. U. Zillohu, "Smart metal–polymer bionanocomposites as omnidirectional plasmonic black absorber formed by nanofluid filtration," *Advanced Functional Materials*, vol. 22, no. 22, pp. 4771–4777, 2012.

[66] J.-Y. Ou, E. Plum, J. Zhang, and N. I. Zheludev, "An electromechanically reconfigurable plasmonic metamaterial operating in the near-infrared," *Nature Nanotechnology*, vol. 8, p. 252255, 2013.

[67] B. Zhu, C. Huang, Y. Feng, J. Zhao, and T. Jiang, "Dual band switchable metamaterial electromagnetic absorber," *Progress In Electromagnetics Research B*, vol. 24, pp. 121–129, 2010.

[68] B. Zhu, Y. Feng, J. Zhao, C. Huang, and T. Jiang, "Switchable metamaterial reflector/absorber for different polarized electromagnetic waves," *Applied Physics Letters*, vol. 97, no. 5, pp. 051906–051906, 2010.

[69] Y. Zhao, Q. Hao, Y. Ma, M. Lu, B. Zhang, M. Lapsley, I.-C. Khoo, and T. Jun Huang, "Light-driven tunable dual-band plasmonic absorber using liquid-crystal-coated asymmetric nanodisk array," *Applied Physics Letters*, vol. 100, no. 5, pp. 053119–053119, 2012.

[70] D. Shrekenhamer, W.-C. Chen, and W. J. Padilla, "Liquid crystal tunable metamaterial absorber," *Physical Review Letters*, vol. 110, no. 17, p. 177403, 2013.

[71] L. Rayleigh, "On reflection of vibrations at the confines of two media between which the transition is gradual," *Proceedings of the London Mathematical Society*, vol. 1, no. 1, pp. 51–56, 1879.

[72] H. K. Raut, V. A. Ganesh, A. S. Nair, and S. Ramakrishna, "Anti-reflective coatings: A critical, in-depth review," *Energy & Environmental Science*, vol. 4, no. 10, pp. 3779–3804, 2011.

[73] H. Moulton, "Optical characteristics," *Industrial & Engineering Chemistry*, vol. 32, no. 11, pp. 1428–1432, 1940.

[74] J. Strong, "On a method of decreasing the reflection from nonmetallic substances," *Journal of the Optical Society of America A*, vol. 26, no. 1, pp. 73–74, 1936.

[75] A. J. Fresnel, *Mémoire sur la loi des modifications que la réflexion imprime a la lumiere polarisée*.
De l'Imprimerie de Firmin Didot Fréres, 1832.

[76] R. Azzam, "Phase shifts that accompany total internal reflection at a dielectric–dielectric interface," *Journal of the Optical Society of America A*, vol. 21, no. 8, pp. 1559–1563, 2004.

[77] H. Craighead, R. Howard, J. Sweeney, and D. Tennant, "Textured surfaces: Optical storage and other applications," *Journal of Vacuum Science and Technology*, vol. 20, no. 3, pp. 316–319, 1982.

[78] C. Bernhard, "Structural and functional adaptation in a visual system," *Endeavour*, vol. 26, no. 98, pp. 79–84, 1967.

[79] P. Clapham and M. Hutley, "Reduction of lens reflexion by the moth eye principle," *Nature*, vol. 244, pp. 281–282, 1973.

[80] P. Campbell and M. A. Green, "Light trapping properties of pyramidally textured surfaces," *Journal of Applied Physics*, vol. 62, no. 1, pp. 243–249, 1987.

[81] Y.-F. Huang, S. Chattopadhyay, Y.-J. Jen, C.-Y. Peng, T.-A. Liu, Y.-K. Hsu, C.-L. Pan, H.-C. Lo, C.-H. Hsu, Y.-H. Chang, *et al.*, "Improved broadband and quasi-omnidirectional anti-reflection properties with biomimetic silicon nanostructures," *Nature Nanotechnology*, vol. 2, no. 12, pp. 770–774, 2007.

[82] S. Chhajed, M. F. Schubert, J. K. Kim, and E. F. Schubert, "Nanostructured multilayer graded-index antireflection coating for si solar cells with broadband and omnidirectional characteristics," *Applied Physics Letters*, vol. 93, no. 25, pp. 251108–251108, 2008.

[83] D. Derkacs, S. Lim, P. Matheu, W. Mar, and E. Yu, "Improved performance of amorphous silicon solar cells via scattering from surface plasmon polaritons in nearby metallic nanoparticles," *Applied Physics Letters*, vol. 89, p. 093103, 2006.

[84] K. Nakayama, K. Tanabe, and H. A. Atwater, "Plasmonic nanoparticle enhanced light absorption in gaas solar cells," *Applied Physics Letters*, vol. 93, no. 12, pp. 121904–121904, 2008.

[85] K. Nishioka, T. Sueto, and N. Saito, "Formation of antireflection nanostructure for silicon solar cells using catalysis of single nano-sized silver particle," *Applied Surface Science*, vol. 255, no. 23, pp. 9504–9507, 2009.

[86] J. N. Munday and H. A. Atwater, "Large integrated absorption enhancement in plasmonic solar cells by combining metallic gratings and antireflection coatings," *Nano Letters*, vol. 11, no. 6, pp. 2195–2201, 2010.

[87] P. Spinelli, B. Macco, M. Verschuuren, W. Kessels, and A. Polman, "al_2o_3 / tio_2 nano-pattern antireflection coating with ultralow surface recombination," *Applied Physics Letters*, vol. 102, p. 233902, 2013.

[88] W. Ding, R. Jia, H. Li, C. Chen, Y. Sun, Z. Jin, and X. Liu, "Design of two dimensional silicon nanowire arrays for antireflection and light trapping in silicon solar cells," *Journal of Applied Physics*, vol. 115, no. 1, p. 014307, 2014.

[89] S. Pillai, K. Catchpole, T. Trupke, and M. Green, "Surface plasmon enhanced silicon solar cells," *Journal of Applied Physics*, vol. 101, p. 093105, 2007.

[90] S.-S. Kim, S.-I. Na, J. Jo, D.-Y. Kim, and Y.-C. Nah, "Plasmon enhanced performance of organic solar cells using electrodeposited ag nanoparticles," *Applied Physics Letters*, vol. 93, p. 073307, 2008.

[91] R. A. Pala, J. White, E. Barnard, J. Liu, and M. L. Brongersma, "Design of plasmonic thin-film solar cells with broadband absorption enhancements," *Advanced Materials*, vol. 21, no. 34, pp. 3504–3509, 2009.

[92] P. R. Pudasaini and A. A. Ayon, "Design guidelines for high efficiency plasmonics silicon solar cells," in *High-Efficiency Solar Cells*, pp. 497–514, Springer, 2014.

[93] P. Spinelli, M. Hebbink, R. De Waele, L. Black, F. Lenzmann, and A. Polman, "Optical impedance matching using coupled plasmonic nanoparticle arrays," *Nano Letters*, vol. 11, no. 4, pp. 1760–1765, 2011.

[94] P. Spinelli, M. Verschuuren, and A. Polman, "Broadband omnidirectional antireflection coating based on subwavelength surface mie resonators," *Nature Communications*, vol. 3, p. 692, 2012.

[95] M. J. Minot, "Single-layer, gradient refractive index antireflection films effective from 0.35 to 2.5 μ," *Journal of the Optical Society of America A*, vol. 66, no. 6, pp. 515–519, 1976.

[96] H. Taylor, F. Kollmorgen, T. S. I. Eng, and J. Strong, "Chemical methods for increasing the transparency of glass surfaces," *Journal of the Optical Society of America A*, vol. 31, pp. 34–37, 1941.

[97] F. Nicoll and F. Williams, "Properties of low reflection films produced by the action of hydrofluoric acid vapor," *Journal of the Optical Society of America A*, vol. 33, no. 8, pp. 434–435, 1943.

[98] J. Hiller, J. D. Mendelsohn, and M. F. Rubner, "Reversibly erasable nanoporous antireflection coatings from polyelectrolyte multilayers," *Nature Materials*, vol. 1, no. 1, pp. 59–63, 2002.

[99] X. Li, J. Gao, L. Xue, and Y. Han, "Porous polymer films with gradient-refractive-index structure for broadband and omnidirectional antireflection coatings," *Advanced Functional Materials*, vol. 20, no. 2, pp. 259–265, 2010.

[100] X. Li, L. Xue, and Y. Han, "Broadband antireflection of block copolymer/homopolymer blend films with gradient refractive index structures," *Journal of Materials Chemistry*, vol. 21, no. 15, pp. 5817–5826, 2011.

[101] X. Li, X. Yu, and Y. Han, "Polymer thin films for antireflection coatings," *Journal of Materials Chemistry C*, vol. 1, pp. 2266–2285, 2013.

[102] C. Martinet, V. Paillard, A. Gagnaire, and J. Joseph, "Deposition of sio2 and tio2 thin films by plasma enhanced chemical vapor deposition for antireflection coating," *Journal of Non-Crystalline Solids*, vol. 216, pp. 77–82, 1997.

[103] D. N. Wright, E. S. Marstein, and A. Holt, "Double layer anti-reflective coatings for silicon solar cells," in *Photovoltaic Specialists Conference, 2005. Conference Record of the Thirty-first IEEE*, pp. 1237–1240, IEEE, 2005.

[104] J. Zhao, A. Wang, P. Altermatt, and M. Green, "Twenty-four percent efficient silicon solar cells with double layer antireflection coatings and reduced resistance loss," *Applied Physics Letters*, vol. 66, no. 26, pp. 3636–3638, 1995.

[105] J.-Q. Xi, M. F. Schubert, J. K. Kim, E. F. Schubert, M. Chen, S.-Y. Lin, W. Liu, and J. A. Smart, "Optical thin-film materials with low refractive index for broadband elimination of fresnel reflection," *Nature Photonics*, vol. 1, no. 3, pp. 176–179, 2007.

[106] S. Chhajed, D. J. Poxson, X. Yan, J. Cho, E. F. Schubert, R. E. Welser, A. K. Sood, and J. K. Kim, "Nanostructured multilayer tailored-refractive-index antireflection coating for glass with broadband and omnidirectional characteristics," *Applied Physics Express*, vol. 4, no. 052503, 2011.

[107] J. M. Ha, S. H. Yoo, J. H. Cho, Y. H. Cho, and S. O. Cho, "Enhancement of antireflection property of silicon using nanostructured surface combined with a polymer deposition," *Nanoscale Research Letters*, vol. 9, no. 1, p. 9, 2014.

[108] H. Dürr and H. Bouas-Laurent, *Photochromism: Molecules and Systems: Molecules and Systems*.
Access Online via Elsevier, 2003.

[109] P. Kelly and R. Arnell, "Magnetron sputtering: a review of recent developments and applications," *Vacuum*, vol. 56, no. 3, pp. 159–172, 2000.

[110] U. Schürmann, W. Hartung, H. Takele, V. Zaporojtchenko, and F. Faupel, "Controlled syntheses of ag–polytetrafluoroethylene nanocomposite thin films by co-sputtering from two magnetron sources," *Nanotechnology*, vol. 16, no. 8, p. 1078, 2005.

[111] G. Anderson, W. N. Mayer, and G. Wehner, "Sputtering of dielectrics by high-frequency fields," *Journal of Applied Physics*, vol. 33, p. 2991, 1962.

[112] D. A. Glocker, "Influence of the plasma on substrate heating during low-frequency reactive sputtering of ain," *Journal of Vacuum Science & Technology A: Vacuum, Surfaces, and Films*, vol. 11, no. 6, pp. 2989–2993, 1993.

[113] O. G. E. LOT, *M-2000 specification sheet*, 2012.

[114] P. Sciau, *The Delivery of Nanoparticles.*
InTech, 2012.

[115] I. Reiche, S. Röhrs, J. Salomon, B. Kanngießer, Y. Höhn, W. Malzer, and F. Voigt, "Development of a nondestructive method for underglaze painted tilesdemonstrated by the analysis of persian objects from the nineteenth century," *Analytical and Bioanalytical Chemistry*, vol. 393, no. 3, pp. 1025–1041, 2009.

[116] I. Freestone, N. Meeks, M. Sax, and C. Higgitt, "The lycurgus cupa roman nanotechnology," *Gold Bulletin*, vol. 40, no. 4, pp. 270–277, 2007.

[117] H. A. Atwater, "The promise of plasmonics," *Scientific American*, vol. 296, no. 4, pp. 56–62, 2007.

[118] K. A. Willets and R. P. Van Duyne, "Localized surface plasmon resonance spectroscopy and sensing," *The Annual Review of Physical Chemistry*, vol. 58, pp. 267–297, 2007.

[119] S. A. Maier and H. A. Atwater, "Plasmonics: Localization and guiding of electromagnetic energy in metal/dielectric structures," *Journal of Applied Physics*, vol. 98, no. 1, pp. 011101–011101, 2005.

[120] G. Niklasson and C. Granqvist, "Surfaces for selective absorption of solar energy: an annotated bibliography 1955–1981," *Journal of Materials Science*, vol. 18, no. 12, pp. 3475–3534, 1983.

[121] D. McKenzie, "Gold, silver, chromium, and copper cermet selective surfaces for evacuated solar collectors," *Applied Physics Letters*, vol. 34, no. 1, pp. 25–28, 1979.

[122] Q.-C. Zhang, "Recent progress in high-temperature solar selective coatings," *Solar Energy Materials and Solar Cells*, vol. 62, no. 1, pp. 63–74, 2000.

[123] P. K. Jain, X. Huang, I. H. El-Sayed, and M. A. El-Sayed, "Review of some interesting surface plasmon resonance-enhanced properties of noble metal nanoparticles and their applications to biosystems," *Plasmonics*, vol. 2, no. 3, pp. 107–118, 2007.

[124] C. J. Murphy, T. K. Sau, A. M. Gole, C. J. Orendorff, J. Gao, L. Gou, S. E. Hunyadi, and T. Li, "Anisotropic metal nanoparticles: synthesis, assembly, and optical applications," *The Journal of Physical Chemistry B*, vol. 109, no. 29, pp. 13857–13870, 2005.

[125] A. De Luca, N. Depalo, E. Fanizza, M. Striccoli, M. L. Curri, M. Infusino, A. R. Rashed, M. LaDeda, and G. Strangi, "Plasmon mediated super-absorber flexible nanocomposite for metamaterials," *Nanoscale*, vol. 5, pp. 6097–6105, 2013.

[126] A. U. Zillohu, R. Abdelaziz, M. K. Hedayati, T. Emmler, S. Homaeigohar, and M. Elbahri, "Plasmon-mediated embedding of nanoparticles in a polymer matrix:

nanocomposites patterning, writing, and defect healing," *The Journal of Physical Chemistry C*, vol. 116, no. 32, pp. 17204–17209, 2012.

[127] A. V. Zayats and I. I. Smolyaninov, "Near-field photonics: surface plasmon polaritons and localized surface plasmons," *Journal of Optics A: Pure and Applied Optics*, vol. 5, no. 4, p. S16, 2003.

[128] G. Lévêque, O. J. Martin, *et al.*, "Optical interactions in a plasmonic particle coupled to a metallic film," *Optics Express*, vol. 14, no. 21, pp. 9971–9981, 2006.

[129] M. R. Singh, "Enhancement of the second-harmonic generation in a quantum dot–metallic nanoparticle hybrid system," *Nanotechnology*, vol. 24, no. 12, p. 125701, 2013.

[130] S. M. R. v. B. C. Cox, J. D. and A. V. Bragas, "A nonlinear switching mechanism in quantum dot and metallic nanoparticle hybrid systems," *Advanced Optical Materials*, vol. 1, p. 460467, 2013.

[131] M. R. Singh, D. G. Schindel, and A. Hatef, "Dipole-dipole interaction in a quantum dot and metallic nanorod hybrid system," *Applied Physics Letters*, vol. 99, no. 18, pp. 181106–181106, 2011.

[132] M. Jamali, M. K. Hedayati, B. Mozooni, M. Javaherirahim, R. Abdelaziz, A. U. Zillohu, and M. Elbahri, "Photoresponsive transparent conductive metal with a photobleaching nose," *Advanced Materials*, vol. 23, no. 37, pp. 4243–4247, 2011.

[133] A. Christ, T. Zentgraf, S. Tikhodeev, N. Gippius, J. Kuhl, and H. Giessen, "Controlling the interaction between localized and delocalized surface plasmon modes: Experiment and numerical calculations," *Physical Review B*, vol. 74, no. 15, p. 155435, 2006.

[134] M. Elbahri, M. K. Hedayati, V. S. Kiran Chakravadhanula, M. Jamali, T. Strunkus, V. Zaporojtchenko, and F. Faupel, "An omnidirectional transparent conducting-metal-based plasmonic nanocomposite," *Advanced Materials*, vol. 23, no. 17, pp. 1993–1997, 2011.

[135] W. Holland and D. Hall, "Frequency shifts of an electric-dipole resonance near a conducting surface," *Physical Review Letters*, vol. 52, no. 12, p. 1041, 1984.

[136] Y. Borensztein, F. Abeles, and T. Lopez-Rios, "Frequency shifts of an ensemble of electric dipole resonances near a conducting surface," *Physical Review Letters*, vol. 53, p. 854, 1984.

[137] J. Cesario, R. Quidant, G. Badenes, and S. Enoch, "Electromagnetic coupling between a metal nanoparticle grating and a metallic surface," *Optics Letters*, vol. 30, no. 24, pp. 3404–3406, 2005.

[138] G. Lévêque and O. J. Martin, "Tunable composite nanoparticle for plasmonics," *Optics letters*, vol. 31, no. 18, pp. 2750–2752, 2006.

[139] J. J. Mock, R. T. Hill, A. Degiron, S. Zauscher, A. Chilkoti, and D. R. Smith, "Distance-dependent plasmon resonant coupling between a gold nanoparticle and gold film," *Nano Letters*, vol. 8, no. 8, pp. 2245–2252, 2008.

[140] Y. Chu and K. B. Crozier, "Experimental study of the interaction between localized and propagating surface plasmons," *Optics Letters*, vol. 34, no. 3, pp. 244–246, 2009.

[141] N. Papanikolaou, "Optical properties of metallic nanoparticle arrays on a thin metallic film," *Physical Review B*, vol. 75, no. 23, p. 235426, 2007.

[142] V. G. Veselago, "The electrodynamics of substances with simultaneously negative values of ϵ and μ.," *Soviet Physics Uspekhi*, vol. 10, no. 4, pp. 509–514, 1968.

[143] J. Lee, M. Seo, J. Sohn, Y. Ahn, D. Kim, S. Jeoung, C. Lienau, and Q.-H. Park, "Invisible plasmonic meta-materials through impedance matching to vacuum," *Optics Express*, vol. 13, no. 26, pp. 10681–10687, 2005.

[144] P. B. Johnson and R.-W. Christy, "Optical constants of the noble metals," *Physical Review B*, vol. 6, no. 12, p. 4370, 1972.

[145] C. Etrich, S. Fahr, M. K. Hedayati, F. Faupel, M. Elbahri, and C. Rockstuhl, "Effective optical properties of plasmonic nanocomposites," *Materials*, vol. 7, no. 2, pp. 727–741, 2014.

[146] M. Hedayati, A. Zillohu, T. Strunskus, F. Faupel, and M. Elbahri, "Plasmonic tunable metamaterial absorber as ultraviolet protection film," *Applied Physics Letters*, vol. 104, no. 4, p. 041103, 2014.

[147] M. K. Hedayati, M. Javaherirahim, B. Mozooni, R. Abdelaziz, A. Tavassolizadeh, V. S. K. Chakravadhanula, V. Zaporojtchenko, T. Strunkus, F. Faupel, and M. Elbahri, "Design of a perfect black absorber at visible frequencies using plasmonic metamaterials," *Advanced Materials*, vol. 23, no. 45, pp. 5410–5414, 2011.

[148] M. K. Hedayati, F. Faupel, and M. Elbahri, "Tunable broadband plasmonic perfect absorber at visible frequency," *Applied Physics A*, vol. 109, no. 4, pp. 769–773, 2012.

[149] F. Faupel, V. Zaporojtchenko, T. Strunskus, and M. Elbahri, "Metal-polymer nanocomposites for functional applications," *Advanced Engineering Materials*, vol. 12, no. 12, pp. 1177–1190, 2010.

[150] T. Hanemann and D. V. Szabó, "Polymer-nanoparticle composites: from synthesis to modern applications," *Materials*, vol. 3, no. 6, pp. 3468–3517, 2010.

[151] H. Beyene, V. Chakravadhanula, C. Hanisch, T. Strunskus, V. Zaporojtchenko, M. Elbahri, and F. Faupel, "Vapor phase deposition, structure, and plasmonic properties of polymer-based composites containing ag–cu bimetallic nanoparticles," *Plasmonics*, vol. 7, no. 1, pp. 107–114, 2012.

[152] V. Zaporojtchenko, J. Zekonyte, A. Biswas, and F. Faupel, "Controlled growth of nanosize metal clusters on polymers by using vpd method," *Surface Science*, vol. 532, pp. 300–305, 2003.

[153] V. Chakravadhanula, T. Hrkac, V. Zaporojtchenko, R. Podschun, V. Kotnur, A. Kulkarni, T. Strunskus, L. Kienle, and F. Faupel, "Nanostructural and functional properties of ag-tio2 coatings prepared by co-sputtering deposition technique," *Journal of Nanoscience and Nanotechnology*, vol. 11, no. 6, pp. 4893–4899, 2011.

[154] A. Biswas, Z. Márton, J. Kanzow, J. Kruse, V. Zaporojtchenko, F. Faupel, and T. Strunskus, "Controlled generation of ni nanoparticles in the capping layers of teflon af by vapor-phase tandem evaporation," *Nano Letters*, vol. 3, no. 1, pp. 69–73, 2003.

[155] E. Kay and A. Dilks, "Metal-containing plasma polymerized fluorocarbon filmstheir synthesis, structure, and polymerization mechanism," *Journal of Vacuum Science and Technology*, vol. 16, no. 2, pp. 428–430, 1979.

[156] B. Gojdka, V. Hrkac, T. Strunskus, V. Zaporojtchenko, L. Kienle, and F. Faupel, "Study of cobalt clusters with very narrow size distribution deposited by high-rate cluster source," *Nanotechnology*, vol. 22, no. 46, p. 465704, 2011.

[157] H. Takele, U. Schurmann, H. Greve, D. Paretkar, V. Zaporojtchenko, and F. Faupel, "Controlled growth of au nanoparticles in co-evaporated metal/polymer composite films and their optical and electrical properties," *European Physical Journal-Applied Physics*, vol. 33, no. 2, pp. 83–90, 2006.

[158] M.-C. Daniel and D. Astruc, "Gold nanoparticles: assembly, supramolecular chemistry, quantum-size-related properties, and applications toward biology, catalysis, and nanotechnology," *Chemical Reviews*, vol. 104, no. 1, pp. 293–346, 2004.

[159] S. Eustis and M. A. El-Sayed, "Why gold nanoparticles are more precious than pretty gold: noble metal surface plasmon resonance and its enhancement of the radiative and nonradiative properties of nanocrystals of different shapes," *Chemical Society Reviews*, vol. 35, no. 3, pp. 209–217, 2006.

[160] M. E. Stewart, C. R. Anderton, L. B. Thompson, J. Maria, S. K. Gray, J. A. Rogers, and R. G. Nuzzo, "Nanostructured plasmonic sensors," *Chemical Reviews*, vol. 108, no. 2, pp. 494–521, 2008.

[161] W. Caseri, "Nanocomposites of polymers and metals or semiconductors: historical background and optical properties," *Macromolecular rapid communications*, vol. 21, no. 11, pp. 705–722, 2000.

[162] R. Maddin, T. S. Wheeler, and J. Muhly, "Distinguishing artifacts made of native copper," *Journal of Archaeological Science*, vol. 7, no. 3, pp. 211–225, 1980.

[163] S. Stookey, "Coloration of glass by gold, silver, and copper," *Journal of the American Ceramic Society*, vol. 32, no. 8, pp. 246–249, 1949.

[164] I. Nakai, C. Numako, H. Hosono, and K. Yamasaki, "Origin of the red color of aatsuma copper-ruby glass as determined by exafs and optical absorption spectroscopy," *Journal of the American Ceramic Society*, vol. 82, no. 3, pp. 689–695, 1999.

[165] B. Wang, T. Koschny, and C. M. Soukoulis, "Wide-angle and polarization-independent chiral metamaterial absorber," *Physical Review B*, vol. 80, no. 3, p. 033108, 2009.

[166] N. I. Zheludev, A. Papakostas, A. Potts, H. J. Coles, and D. M. Bagnall, "Layered chiral metallic meta-materials," in *Proc. SPIE*, vol. 4806, p. 113, 2002.

[167] Y. Cheng, H. Yang, Z. Cheng, and N. Wu, "Perfect metamaterial absorber based on a split-ring-cross resonator," *Applied Physics A*, vol. 102, no. 1, pp. 99–103, 2011.

[168] Y. Yong-Jun, H. Yong-Jun, W. Guang-Jun, Z. Jing-Ping, S. Hai-Bin, and O. Gordon, "Tunable broadband metamaterial absorber consisting of ferrite slabs and a copper wire," *Chinese Physics B*, vol. 21, no. 3, p. 038501, 2012.

[169] Y. Qiu Xu, P. Heng Zhou, H. Bin Zhang, L. Chen, and L. Jiang Deng, "A wide-angle planar metamaterial absorber based on split ring resonator coupling," *Journal of Applied Physics*, vol. 110, no. 4, pp. 044102–044102, 2011.

[170] H. Li, L. H. Yuan, B. Zhou, X. P. Shen, Q. Cheng, and T. J. Cui, "Ultrathin multiband gigahertz metamaterial absorbers," *Journal of Applied Physics*, vol. 110, no. 1, pp. 014909–014909, 2011.

[171] P. Tuong, J. Park, V. Lam, K. Kim, H. Cheong, W. Jang, and Y. Lee, "Simplified perfect absorber structure," *Computational Materials Science*, vol. 61, pp. 243–247, 2012.

[172] B. Zhu, Z. Wang, C. Huang, Y. Feng, J. Zhao, and T. Jiang, "Polarization insensitive metamaterial absorber with wide incident angle," *Progress In Electromagnetics Research*, vol. 101, pp. 231–239, 2010.

[173] L. Huang and H. Chen, "Multi-band and polarization insensitive metamaterial absorber," *Progress In Electromagnetics Research*, vol. 113, pp. 103–110, 2011.

[174] C. Hu, X. Li, Q. Feng, X. Chen, and X. Luo, "Investigation on the role of the dielectric loss in metamaterial absorber," *Optics Express*, vol. 18, pp. 6598–6603, Mar 2010.

[175] L. Li, Y. Yang, and C. Liang, "A wide-angle polarization-insensitive ultra-thin metamaterial absorber with three resonant modes," *Journal of Applied Physics*, vol. 110, no. 6, pp. 063702–063702, 2011.

[176] J. Sun, L. Liu, G. Dong, and J. Zhou, "An extremely broad band metamaterial absorber based on destructive interference," *Optics Express*, vol. 19, no. 22, pp. 21155–21162, 2011.

[177] S. Gu, J. Barrett, T. Hand, B.-I. Popa, and S. Cummer, "A broadband low-reflection metamaterial absorber," *Journal of Applied Physics*, vol. 108, no. 6, pp. 064913–064913, 2010.

[178] Y. Zhi Cheng, Y. Wang, Y. Nie, R. Zhou Gong, X. Xiong, and X. Wang, "Design, fabrication and measurement of a broadband polarization-insensitive metamaterial absorber based on lumped elements," *Journal of Applied Physics*, vol. 111, no. 4, pp. 044902–044902, 2012.

[179] Q.-Y. Wen, H.-W. Zhang, Q.-H. Yang, Z. Chen, Y. Long, Y.-L. Jing, Y. Lin, and P.-X. Zhang, "A tunable hybrid metamaterial absorber based on vanadium oxide films," *Journal of Physics D: Applied Physics*, vol. 45, no. 23, p. 235106, 2012.

[180] V. S. K. Chakravadhanula, C. Kübel, T. Hrkac, V. Zaporojtchenko, T. Strunskus, F. Faupel, and L. Kienle, "Surface segregation in tio2-based nanocomposite thin films," *Nanotechnology*, vol. 23, no. 49, p. 495701, 2012.

[181] H.-T. Chen, "Interference theory of metamaterial perfect absorbers," *arXiv preprint arXiv:1112.5168*, 2011.

[182] S. Magdassi, M. Grouchko, and A. Kamyshny, "Copper nanoparticles for printed electronics: routes towards achieving oxidation stability," *Materials*, vol. 3, no. 9, pp. 4626–4638, 2010.

[183] M. Rai, A. Yadav, and A. Gade, "Silver nanoparticles as a new generation of antimicrobials," *Biotechnology advances*, vol. 27, no. 1, pp. 76–83, 2009.

[184] M. Noginov, H. Li, Y. A. Barnakov, D. Dryden, G. Nataraj, G. Zhu, C. Bonner, M. Mayy, Z. Jacob, and E. Narimanov, "Controlling spontaneous emission with metamaterials," *Optics Letters*, vol. 35, no. 11, pp. 1863–1865, 2010.

[185] P. Nagpal, N. C. Lindquist, S.-H. Oh, and D. J. Norris, "Ultrasmooth patterned metals for plasmonics and metamaterials," *Science*, vol. 325, no. 5940, pp. 594–597, 2009.

[186] B. T. Schwartz and R. Piestun, "Total external reflection from metamaterials with ultralow refractive index," *Journal of the Optical Socity of America B*, vol. 20, no. 12, pp. 2448–2453, 2003.

[187] M. Noginov, Y. A. Barnakov, G. Zhu, T. Tumkur, H. Li, and E. Narimanov, "Bulk photonic metamaterial with hyperbolic dispersion," *Applied Physics Letters*, vol. 94, no. 15, pp. 151105–151105, 2009.

[188] V. A. Tamma, J.-H. Lee, Q. Wu, and W. Park, "Visible frequency magnetic activity in silver nanocluster metamaterial," *Applied Optics*, vol. 49, no. 7, pp. A11–A17, 2010.

[189] J. Valentine, S. Zhang, T. Zentgraf, E. Ulin-Avila, D. A. Genov, G. Bartal, and X. Zhang, "Three-dimensional optical metamaterial with a negative refractive index," *nature*, vol. 455, no. 7211, pp. 376–379, 2008.

[190] M. S. Rill, C. Plet, M. Thiel, I. Staude, G. Von Freymann, S. Linden, and M. Wegener, "Photonic metamaterials by direct laser writing and silver chemical vapour deposition," *Nature Materials*, vol. 7, no. 7, pp. 543–546, 2008.

[191] G. Dolling, C. Enkrich, M. Wegener, C. M. Soukoulis, and S. Linden, "Low-loss negative-index metamaterial at telecommunication wavelengths," *Optics Letters*, vol. 31, no. 12, pp. 1800–1802, 2006.

[192] G. Dolling, M. Wegener, C. M. Soukoulis, and S. Linden, "Negative-index metamaterial at 780 nm wavelength," *Optics Letters*, vol. 32, no. 1, pp. 53–55, 2007.

[193] J. Yao, Z. Liu, Y. Liu, Y. Wang, C. Sun, G. Bartal, A. M. Stacy, and X. Zhang, "Optical negative refraction in bulk metamaterials of nanowires," *Science*, vol. 321, no. 5891, pp. 930–930, 2008.

[194] N. Fang, H. Lee, C. Sun, and X. Zhang, "Sub–diffraction-limited optical imaging with a silver superlens," *Science*, vol. 308, no. 5721, pp. 534–537, 2005.

[195] X. Wang, D.-H. Kwon, D. H. Werner, I.-C. Khoo, A. V. Kildishev, and V. M. Shalaev, "Tunable optical negative-index metamaterials employing anisotropic liquid crystals," *Applied Physics Letters*, vol. 91, no. 14, pp. 143122–143122, 2007.

[196] W. Cai, U. K. Chettiar, A. V. Kildishev, and V. M. Shalaev, "Optical cloaking with metamaterials," *Nature Photonics*, vol. 1, no. 4, pp. 224–227, 2007.

[197] B.-h. Choi, H.-H. Lee, S. Jin, S. Chun, and S.-H. Kim, "Characterization of the optical properties of silver nanoparticle films," *Nanotechnology*, vol. 18, no. 7, p. 075706, 2007.

[198] A. Leitner, Z. Zhao, H. Brunner, F. R. Aussenegg, and A. Wokaun, "Optical properties of a metal island film close to a smooth metal surface," *Applied optics*, vol. 32, no. 1, pp. 102–110, 1993.

[199] M. B. Schubert and J. H. Werner, "Flexible solar cells for clothing," *Materials Today*, vol. 9, no. 6, pp. 42–50, 2006.

[200] J. Biener, G. W. Nyce, A. M. Hodge, M. M. Biener, A. V. Hamza, and S. A. Maier, "Nanoporous plasmonic metamaterials," *Advanced Materials*, vol. 20, no. 6, pp. 1211–1217, 2008.

[201] F. Yu, S. Ahl, A.-M. Caminade, J.-P. Majoral, W. Knoll, and J. Erlebacher, "Simultaneous excitation of propagating and localized surface plasmon resonance in nanoporous gold membranes," *Analytical Chemistry*, vol. 78, no. 20, pp. 7346–7350, 2006.

[202] M. Kaltenbrunner, M. S. White, E. D. Głowacki, T. Sekitani, T. Someya, N. S. Sariciftci, and S. Bauer, "Ultrathin and lightweight organic solar cells with high flexibility," *Nature Communications*, vol. 3, p. 770, 2012.

[203] C. E. Kennedy, *Review of mid-to high-temperature solar selective absorber materials*, vol. 1617.
National Renewable Energy Laboratory Golden Colorado, 2002.

[204] D. Zawischa, "Scattering: The colours of the sky."

[205] N. F. Hadley, "Wax secretion and color phases of the desert tenebrionid beetle cryptoglossa verrucosa (leconte)," *Science*, vol. 203, no. 4378, pp. 367–369, 1979.

[206] K. Liu, H. Hu, H. Song, X. Zeng, D. Ji, S. Jiang, and Q. Gan, "Wide-angle and polarization-insensitive perfect absorber for organic photovoltaic layers," *IEEE Photonics Technology Letters*, vol. 25, no. 13, pp. 1266–1269, 2013.

[207] K. Liu, B. Zeng, H. Song, Q. Gan, F. J. Bartoli, and Z. H. Kafafi, "Super absorption of ultra-thin organic photovoltaic films," *Optics Communications*, vol. 314, pp. 48–56, 2014.

[208] Y. Li, L. Su, C. Shou, C. Yu, J. Deng, and Y. Fang, "Surface-enhanced molecular spectroscopy (sems) based on perfect-absorber metamaterials in the mid-infrared," *Scientific Reports*, vol. 3, 2013.

[209] B. Kearney, F. Alves, D. Grbovic, and G. Karunasiri, "Al/siox/al single and multiband metamaterial absorbers for terahertz sensor applications," *Optical Engineering*, vol. 52, no. 1, pp. 013801–013801, 2013.

[210] D. Wang, W. Zhu, M. D. Best, J. P. Camden, and K. B. Crozier, "Wafer-scale metasurface for total power absorption, local field enhancement and single molecule raman spectroscopy," *Scientific Reports*, vol. 3, 2013.

[211] R. Alaee, C. Menzel, C. Rockstuhl, and F. Lederer, "Perfect absorbers on curved surfaces and their potential applications," *Optics Express*, vol. 20, no. 16, pp. 18370–18376, 2012.

[212] J. Mei, G. Ma, M. Yang, Z. Yang, W. Wen, and P. Sheng, "Dark acoustic metamaterials as super absorbers for low-frequency sound," *Nature Communications*, vol. 3, p. 756, 2012.

[213] F. Alves, D. Grbovic, B. Kearney, and G. Karunasiri, "Microelectromechanical systems bimaterial terahertz sensor with integrated metamaterial absorber," *Optics Letters*, vol. 37, no. 11, pp. 1886–1888, 2012.

[214] G. Li, X. Chen, O. Li, C. Shao, Y. Jiang, L. Huang, B. Ni, W. Hu, and W. Lu, "A novel plasmonic resonance sensor based on an infrared perfect absorber," *Journal of Physics D: Applied Physics*, vol. 45, no. 20, p. 205102, 2012.

[215] A. Tittl, P. Mai, R. Taubert, D. Dregely, N. Liu, and H. Giessen, "Palladium-based plasmonic perfect absorber in the visible wavelength range and its application to hydrogen sensing," *Nano Letters*, vol. 11, no. 10, pp. 4366–4369, 2011.

[216] L. Dai and C. Jiang, "Anomalous near-perfect extraordinary optical absorption on subwavelength thin metal film grating," *Optics Express*, vol. 17, pp. 20502–20514, Oct 2009.

[217] Y. Avitzour, Y. A. Urzhumov, and G. Shvets, "Wide-angle infrared absorber based on a negative-index plasmonic metamaterial," *Physicaly Review B*, vol. 79, p. 045131, Jan 2009.

[218] H. Takele, A. Kulkarni, S. Jebril, V. S. K. Chakravadhanula, C. Hanisch, T. Strunskus, V. Zaporojtchenko, and F. Faupel, "Plasmonic properties of vapour-deposited polymer composites containing ag nanoparticles and their changes upon annealing," *Journal of Physics D: Applied Physics*, vol. 41, no. 12, p. 125409, 2008.

[219] C. F. Bohren and D. R. Huffman, *Absorption and scattering by an arbitrary particle*, pp. 57–81.
Wiley-VCH Verlag GmbH, 2007.

[220] N. Liu, H. Guo, L. Fu, S. Kaiser, H. Schweizer, and H. Giessen, "Plasmon hybridization in stacked cut-wire metamaterials," *Advanced Materials*, vol. 19, no. 21, pp. 3628–3632, 2007.

[221] H. Takele, H. Greve, C. Pochstein, V. Zaporojtchenko, and F. Faupel, "Plasmonic properties of ag nanoclusters in various polymer matrices," *Nanotechnology*, vol. 17, no. 14, p. 3499, 2006.

[222] A. Christ, O. J. F. Martin, Y. Ekinci, N. A. Gippius, and S. G. Tikhodeev, "Symmetry breaking in a plasmonic metamaterial at optical wavelength," *Nano Letters*, vol. 8, no. 8, pp. 2171–2175, 2008.
PMID: 18578551.

[223] J. N. Munday and H. A. Atwater, "Large integrated absorption enhancement in plasmonic solar cells by combining metallic gratings and antireflection coatings," *Nano Letters*, vol. 11, no. 6, pp. 2195–2201, 2011.

[224] J. A. Hutchison, D. M. O'Carroll, T. Schwartz, C. Genet, and T. W. Ebbesen, "Absorption-induced transparency," *Angewandte Chemie International Edition*, vol. 50, no. 9, pp. 2085–2089, 2011.

[225] F. Yu, H. Wang, and S. Zou, "Efficient and tunable light trapping thin films," *The Journal of Physical Chemistry C*, vol. 114, no. 5, pp. 2066–2069, 2010.

[226] H. Liao, R. Xiao, J. Fu, P. Yu, G. Wong, and P. Sheng, "Large third-order optical nonlinearity in au: Sio2 composite films near the percolation threshold," *Applied Physics Letters*, vol. 70, no. 1, pp. 1–3, 1997.

[227] M. Elbahri, M. K. Hedayati, F. Faupel, T. Strunskus, and V. Zaporojtchenko, "Absorberschicht für den vis-und/oder nir-spektralbereich," Aug. 1 2013.
DE Patent 102, 011,113,571.

[228] U. Schürmann, H. Takele, V. Zaporojtchenko, and F. Faupel, "Optical and electrical properties of polymer metal nanocomposites prepared by magnetron co-sputtering," *Thin Solid Films*, vol. 515, no. 2, pp. 801–804, 2006.

[229] J.-Y. Bigot, J.-Y. Merle, O. Cregut, and A. Daunois, "Electron dynamics in copper metallic nanoparticles probed with femtosecond optical pulses," *Physical Review Letters*, vol. 75, no. 25, p. 4702, 1995.

[230] A. Boltasseva and V. M. Shalaev, "Fabrication of optical negative-index metamaterials: Recent advances and outlook," *Metamaterials*, vol. 2, no. 1, pp. 1 – 17, 2008.

[231] A. K. Sarychev and G. Tartakovsky, "Magnetic plasmonic metamaterials in actively pumped host medium and plasmonic nanolaser," *Physical Review B*, vol. 75, p. 085436, FEB 2007.

[232] R. F. Oulton, "Surface plasmon lasers: sources of nanoscopic light," *Materials Today*, vol. 15, no. 1, pp. 26–34, 2012.

[233] P. Berini and I. De Leon, "Surface plasmon-polariton amplifiers and lasers," *Nature Photonics*, vol. 6, no. 1, pp. 16–24, 2011.

[234] J. C. Fan and P. M. Zavracky, "Selective black absorbers using mgo/au cermet films," *Applied Physics Letters*, vol. 29, no. 8, pp. 478–480, 1976.

[235] H. Craighead and R. Buhrman, "Optical properties of selectively absorbing Ni/Al_2O_3 composite films," *Applied Physics Letters*, vol. 31, no. 7, pp. 423–425, 1977.

[236] H. Craighead and R. Buhrman, "Optical properties of selectively absorbing metal insulator composite films," *Journal of Vacuum Science and Technology*, vol. 15, no. 2, pp. 269–271, 1978.

[237] J. Gittleman, "Application of granular semiconductors to photothermal conversion of solar energy," *Applied Physics Letters*, vol. 28, p. 370, 1976.

[238] J. Dai, F. Ye, Y. Chen, M. Muhammed, M. Qiu, and M. Yan, "Light absorber based on nano-spheres on a substrate reflector," *Optics Express*, vol. 21, no. 6, pp. 6697–6706, 2013.

[239] P. Ding, E. Liang, G. Cai, W. Hu, C. Fan, and Q. Xue, "Dual-band perfect absorption and field enhancement by interaction between localized and propagating surface

plasmons in optical metamaterials," *Journal of Optics*, vol. 13, no. 7, p. 075005, 2011.

[240] B. Lamprecht, J. Krenn, G. Schider, H. Ditlbacher, M. Salerno, N. Felidj, A. Leitner, F. Aussenegg, and J. Weeber, "Surface plasmon propagation in microscale metal stripes," *Applied Physics Letters*, vol. 79, no. 1, pp. 51–53, 2001.

[241] M. Zayat, P. Garcia-Parejo, and D. Levy, "Preventing uv-light damage of light sensitive materials using a highly protective uv-absorbing coating," *Chemical Society Reviews*, vol. 36, no. 8, pp. 1270–1281, 2007.

[242] A. Moreau, C. Ciracì, J. J. Mock, R. T. Hill, Q. Wang, B. J. Wiley, A. Chilkoti, and D. R. Smith, "Controlled-reflectance surfaces with film-coupled colloidal nanoantennas," *Nature*, vol. 492, no. 7427, pp. 86–89, 2012.

[243] T. R. Jensen, M. D. Malinsky, C. L. Haynes, and R. P. Van Duyne, "Nanosphere lithography: tunable localized surface plasmon resonance spectra of silver nanoparticles," *The Journal of Physical Chemistry B*, vol. 104, no. 45, pp. 10549–10556, 2000.

[244] B. Mahltig, H. Böttcher, K. Rauch, U. Dieckmann, R. Nitsche, and T. Fritz, "Optimized uv protecting coatings by combination of organic and inorganic uv absorbers," *Thin Solid Films*, vol. 485, no. 1, pp. 108–114, 2005.

[245] N. L. Thomas and J. D. Wolfe, "Uv-shifted durable silver coating for astronomical mirrors," in *Astronomical Telescopes and Instrumentation*, pp. 312–323, International Society for Optics and Photonics, 2000.

[246] Y. Saito, J. Wang, D. Batchelder, and D. Smith, "Simple chemical method for forming silver surfaces with controlled grain sizes for surface plasmon experiments," *Langmuir*, vol. 19, no. 17, pp. 6857–6861, 2003.

[247] S. Mandal, R. Roy, and A. Pal, "Surface plasmon resonance in nanocrystalline silver particles embedded in sio2 matrix," *Journal of Physics D: Applied Physics*, vol. 35, no. 17, p. 2198, 2002.

[248] T. Huen, G. Irani, and F. Wooten, "Scanning ultrahigh vacuum reflectometer," *Applied Optics*, vol. 10, no. 3, pp. 552–556, 1971.

[249] P. Taneja, P. Ayyub, and R. Chandra, "Size dependence of the optical spectrum in nanocrystalline silver," *Physical Review B*, vol. 65, no. 24, p. 245412, 2002.

[250] R. Watanabe, M. Iwanaga, and T. Ishihara, "s-polarization brewster's angle of stratified metal–dielectric metamaterial in optical regime," *Physica Status Solidi (b)*, vol. 245, no. 12, pp. 2696–2701, 2008.

[251] T. Oates and A. Mücklich, "Evolution of plasmon resonances during plasma deposition of silver nanoparticles," *Nanotechnology*, vol. 16, no. 11, p. 2606, 2005.

[252] J.-B. Brückner, J. Le Rouzo, L. Escoubas, G. Berginc, O. Calvo-Perez, N. Vukadinovic, and F. Flory, "Metamaterial filters at optical-infrared frequencies," *Optics Express*, vol. 21, no. 14, pp. 16992–17006, 2013.

[253] N. Engheta, "Thin absorbing screens using metamaterial surfaces," in *Antennas and Propagation Society International Symposium, 2002. IEEE*, vol. 2, pp. 392–395, IEEE, 2002.

[254] B. Gupta and R. Verma, "Surface plasmon resonance-based fiber optic sensors: principle, probe designs, and some applications," *Journal of Sensors*, vol. 2009, 2009.

[255] M. Hillenkamp, G. Di Domenicantonio, O. Eugster, and C. Félix, "Instability of ag nanoparticles in sio2 at ambient conditions," *Nanotechnology*, vol. 18, no. 1, p. 015702, 2007.

[256] D. Bouhafs, A. Moussi, A. Chikouche, and J. Ruiz, "Design and simulation of antireflection coating systems for optoelectronic devices: Application to silicon solar cells," *Solar Energy Materials and Solar Cells*, vol. 52, no. 1, pp. 79–93, 1998.

[257] J. Cox, G. Hass, and A. Thelen, "Triple-layer antireflection coatings on glass for the visible and near infrared," *Journal of the Optical Society of America A*, vol. 52, no. 9, pp. 965–968, 1962.

[258] A. Turner, "Some current developments in multilayer optical films," *Le Journal de Physique et le Radium*, vol. 11, pp. 444–460, 1950.

[259] W. Lowdermilk and D. Milam, "Graded-index antireflection surfaces for high-power laser applications," *Applied Physics Letters*, vol. 36, no. 11, pp. 891–893, 1980.

[260] S. Mukherjee and W. Lowdermilk, "Gel-derived single layer antireflection films," *Journal of Non-Crystalline Solids*, vol. 48, no. 1, pp. 177–184, 1982.

[261] M. Minot, "The angluar reflectance of single-layer gradient refractive-index films," *Journal of the Optical Society of America A*, vol. 67, no. 8, pp. 1046–1050, 1977.

[262] R. Peterson and J. Ramsey, "Thin film coatings in solar-thermal power systems," *Journal of Vacuum Science and Technology*, vol. 12, no. 1, pp. 174–181, 1975.

[263] J. Zhao and M. A. Green, "Optimized antireflection coatings for high-efficiency silicon solar cells," *Electron Devices, IEEE Transactions on*, vol. 38, no. 8, pp. 1925–1934, 1991.

[264] J. K. Kim, S. Chhajed, M. F. Schubert, E. F. Schubert, A. J. Fischer, M. H. Crawford, J. Cho, H. Kim, and C. Sone, "Light-extraction enhancement of gainn light-emitting diodes by graded-refractive-index indium tin oxide anti-reflection contact," *Advanced Materials*, vol. 20, no. 4, pp. 801–804, 2008.

[265] Y. Wang, Y. Liu, H. Liang, Z. Mei, and X. Du, "Broadband antireflection on the silicon surface realized by ag nanoparticle-patterned black silicon," *Physical Chemistry Chemical Physics*, vol. 15, no. 7, pp. 2345–2350, 2013.

[266] A. Kabiri, E. Girgis, and F. Capasso, "Buried nanoantenna arrays: versatile antireflection coating," *Nano Letters*, vol. 13, no. 12, pp. 6040–6047, 2013.

[267] X.-R. Huang, R.-W. Peng, and R.-H. Fan, "Making metals transparent for white light by spoof surface plasmons," *Physical Review Letters*, vol. 105, no. 24, p. 243901, 2010.

[268] R.-H. Fan, L.-H. Zhu, R.-W. Peng, X.-R. Huang, D.-X. Qi, X.-P. Ren, Q. Hu, and M. Wang, "Broadband antireflection and light-trapping enhancement of plasmonic solar cells," *Physical Review B*, vol. 87, no. 19, p. 195444, 2013.

[269] D. M. Braun and R. L. Jungerman, "Broadband multilayer antireflection coating for semiconductor laser facets," *Optics Letters*, vol. 20, no. 10, pp. 1154–1156, 1995.

[270] B. Moys, "The theory of double-layer antireflection coatings," *Thin Solid Films*, vol. 21, no. 1, pp. 145–157, 1974.

[271] Y. Fink, J. N. Winn, S. Fan, C. Chen, J. Michel, J. D. Joannopoulos, and E. L. Thomas, "A dielectric omnidirectional reflector," *Science*, vol. 282, no. 5394, pp. 1679–1682, 1998.

[272] M. F. Schubert, J.-Q. Xi, J. K. Kim, and E. F. Schubert, "Distributed bragg reflector consisting of high-and low-refractive-index thin film layers made of the same material," *Applied Physics Letters*, vol. 90, no. 14, pp. 141115–141115, 2007.

[273] M. Ettenberg, "A new dielectric facet reflector for semiconductor lasers," *Applied Physics Letters*, vol. 32, p. 724, 1978.

[274] M. A. Kats, D. Sharma, J. Lin, P. Genevet, R. Blanchard, Z. Yang, M. M. Qazilbash, D. Basov, S. Ramanathan, and F. Capasso, "Ultra-thin perfect absorber employing a tunable phase change material," *Applied Physics Letters*, vol. 101, no. 22, pp. 221101–221101, 2012.

[275] M. A. Kats, R. Blanchard, P. Genevet, and F. Capasso, "Nanometre optical coatings based on strong interference effects in highly absorbing media," *Nature Materials*, vol. 12, pp. 20–24, 2012.

[276] X. Xiong, S.-C. Jiang, Y.-H. Hu, R.-W. Peng, and M. Wang, "Structured metal film as a perfect absorber," *Advanced Materials*, vol. 25, no. 29, pp. 3994–4000, 2013.

[277] M. K. Hedayati, F. Faupel, and M. Elbahri, "Review of plasmonic nanocomposite etamaterial absorber," *Materials*, vol. 7, pp. 1221–1248, 2014.

[278] E. T. Hamden, F. Greer, M. E. Hoenk, J. Blacksberg, M. R. Dickie, S. Nikzad, D. C. Martin, and D. Schiminovich, "Ultraviolet antireflection coatings for use in silicon detector design," *Applied Optics*, vol. 50, no. 21, pp. 4180–4188, 2011.

[279] M. Radecka, K. Zakrzewska, H. Czternastek, T. Stapiński, and S. Debrus, "The influence of thermal annealing on the structural, electrical and optical properties of TiO_2 thin films," *Applied surface science*, vol. 65, pp. 227–234, 1993.

[280] H.-T. Chen, J. Zhou, J. F. OHara, F. Chen, A. K. Azad, and A. J. Taylor, "Antireflection coating using metamaterials and identification of its mechanism," *Physical Review Letters*, vol. 105, no. 7, p. 073901, 2010.

[281] D. L. Caballero, "A theoretical development of exact solution of reflectance of multiple layer optical coatings," *Journal of the Optical Society of America A*, vol. 37, no. 3, pp. 176–178, 1947.

[282] K. Renk and L. Genzel, "Interference filters and fabry-perot interferometers for the far infrared," *Applied Optics*, vol. 1, no. 5, pp. 643–648, 1962.

[283] T. C. Choy, *Effective medium theory: principles and applications*, vol. 102. Oxford University Press, 1999.

[284] A. Tavlove and S. C. Hagness, "Computational electrodynamics: the finite-difference time-domain method," *Artech House, Norwood, MA*, vol. 2062, p. 1006, 2005.

[285] U. Schürmann, "Eigenschaften von polymer-silber-nanokompositen hergestellt durch co-sputtern," *Dissertationsschrift, Technische Fakultät der Christian-Albrechts-Universität zu Kiel*, 2006.

[286] J. De Sande, R. Serna, J. Gonzalo, C. N. Afonso, D. Hole, and A. Naudon, "Refractive index of ag nanocrystals composite films in the neighborhood of the surface plasmon resonance," *Journal of applied physics*, vol. 91, no. 3, pp. 1536–1541, 2002.

[287] S. G. Moiseev, "Composite medium with silver nanoparticles as an anti-reflection optical coating," *Applied Physics A*, vol. 103, no. 3, pp. 619–622, 2011.

[288] S. Dutta Gupta, "Strong-interactionmediated critical coupling at two distinct frequencies," *Optics letters*, vol. 32, no. 11, pp. 1483–1485, 2007.

[289] T. Huang and X.-H. N. Xu, "Synthesis and characterization of tunable rainbow colored colloidal silver nanoparticles using single-nanoparticle plasmonic microscopy and spectroscopy," *Journal of materials chemistry*, vol. 20, no. 44, pp. 9867–9876, 2010.

[290] S. Kawata, *Near-field optics and surface plasmon polaritons*, vol. 81. Springer, 2001.

[291] C. Menzel, C. Rockstuhl, T. Paul, F. Lederer, and T. Pertsch, "Retrieving effective parameters for metamaterials at oblique incidence," *Physical Review B*, vol. 77, no. 19, p. 195328, 2008.

[292] R. Potember, T. Poehler, and D. Cowan, "Electrical switching and memory phenomena in cu-tcnq thin films," *Applied Physics Letters*, vol. 34, no. 6, pp. 405–407, 1979.

[293] A. Sawa, "Resistive switching in transition metal oxides," *Materials Today*, vol. 11, no. 6, pp. 28–36, 2008.

[294] M. Irie, "Photochromism: Memories and switches introduction," *Chemical Reviews*, vol. 100, no. 5, pp. 1683–1684, 2000.

[295] J. Ouyang, C.-W. Chu, C. R. Szmanda, L. Ma, and Y. Yang, "Programmable polymer thin film and non-volatile memory device," *Nature Materials*, vol. 3, no. 12, pp. 918–922, 2004.

[296] X. Ma and G.-S. Kuo, "Optical switching technology comparison: optical mems vs. other technologies," *Communications Magazine, IEEE*, vol. 41, no. 11, pp. S16–S23, 2003.

[297] J. Svensson and C. Granqvist, "Electrochromic coatings for smart windows," in *28th Annual Technical Symposium*, pp. 30–37, International Society for Optics and Photonics, 1984.

[298] R. Goldner, T. Haas, G. Seward, K. Wong, P. Norton, G. Foley, G. Berera, G. Wei, S. Schulz, and R. Chapman, "Thin film solid state ionic materials for electrochromic smart $window^{TM}$ glass," *Solid State Ionics*, vol. 28, pp. 1715–1721, 1988.

[299] K. Bange and T. Gambke, "Electrochromic materials for optical switching devices," *Advanced Materials*, vol. 2, no. 1, pp. 10–16, 1990.

[300] G. Ibarz, L. Dähne, E. Donath, and H. Moehwald, "Smart micro-and nanocontainers for storage, transport, and release," *Advanced Materials*, vol. 13, no. 17, pp. 1324–1327, 2001.

[301] N. Nath and A. Chilkoti, "Creating smart surfaces using stimuli responsive polymers," *Advanced Materials*, vol. 14, no. 17, pp. 1243–1247, 2002.

[302] T. Duerig, A. Pelton, and D. Stöckel, "An overview of nitinol medical applications," *Materials Science and Engineering: A*, vol. 273, pp. 149–160, 1999.

[303] Y. Liu, L. Mu, B. Liu, and J. Kong, "Controlled switchable surface," *Chemistry-A European Journal*, vol. 11, no. 9, pp. 2622–2631, 2005.

[304] B. L. Feringa and W. R. Browne, *Molecular switches*, vol. 42. Wiley Online Library, 2001.

[305] D. Dulić, S. J. van der Molen, T. Kudernac, H. Jonkman, J. De Jong, T. Bowden, J. Van Esch, B. Feringa, and B. Van Wees, "One-way optoelectronic switching of photochromic molecules on gold," *Physical Review Letters*, vol. 91, no. 20, p. 207402, 2003.

[306] J. Dintinger, I. Robel, P. V. Kamat, C. Genet, and T. W. Ebbesen, "Terahertz all-optical molecule-plasmon modulation," *Advanced Materials*, vol. 18, no. 13, pp. 1645–1648, 2006.

[307] S. J. van der Molen, J. Liao, T. Kudernac, J. S. Agustsson, L. Bernard, M. Calame, B. J. van Wees, B. L. Feringa, and C. Scho?nenberger, "Light-controlled conductance switching of ordered metal- molecule- metal devices," *Nano Letters*, vol. 9, no. 1, pp. 76–80, 2008.

[308] J. Dintinger, S. Klein, and T. W. Ebbesen, "Molecule–surface plasmon interactions in hole arrays: enhanced absorption, refractive index changes, and all-optical switching," *Advanced materials*, vol. 18, no. 10, pp. 1267–1270, 2006.

[309] V. M. Shalaev, "Optical negative-index metamaterials," *Nature Photonics*, vol. 1, no. 1, pp. 41–48, 2007.

[310] H.-T. Chen, W. J. Padilla, J. M. Zide, A. C. Gossard, A. J. Taylor, and R. D. Averitt, "Active terahertz metamaterial devices," *Nature*, vol. 444, no. 7119, pp. 597–600, 2006.

[311] M.-Y. Yoo and S. Lim, "Switchable electromagnetic metamaterial reflector/absorber," in *Microwave Conference Proceedings (APMC), 2012 Asia-Pacific*, pp. 445–447, IEEE, 2012.

[312] X. Wu, C. Hu, Y. Wang, M. Pu, C. Huang, C. Wang, and X. Luo, "Active microwave absorber with the dual-ability of dividable modulation in absorbing intensity and frequency," *AIP Advances*, vol. 3, no. 2, pp. 022114–022114, 2013.

[313] J. Zhao, Q. Cheng, J. Chen, M. Q. Qi, W. X. Jiang, and T. J. Cui, "A tunable metamaterial absorber using varactor diodes," *New Journal of Physics*, vol. 15, no. 4, p. 043049, 2013.

[314] A. Tennant, "Reflection properties of a phase modulating planar screen," *Electronics Letters*, vol. 33, no. 21, pp. 1768–1769, 1997.

[315] W. W. Lam, C. F. Jou, H. Z. Chen, K. S. Stolt, N. C. Luhmann Jr, and D. B. Rutledge, "Millimeter-wave diode-grid phase shifters," *Microwave Theory and Techniques, IEEE Transactions on*, vol. 36, no. 5, pp. 902–907, 1988.

[316] M. D. Bushbeck and C. H. Chan, "A tuneable, switchable dielectric grating," *Microwave and Guided Wave Letters, IEEE*, vol. 3, no. 9, pp. 296–298, 1993.

[317] V. A. Lokshin, A. Samat, and A. V. Metelitsa, "Spirooxazines: synthesis, structure, spectral and photochromic properties," *Russian Chemical Reviews*, vol. 71, no. 11, pp. 893–916, 2002.

[318] B. Schaudel, C. Guermeur, C. Sanchez, K. Nakatani, and J. A. Delaire, "Spirooxazine- and spiropyran-doped hybrid organic–inorganic matrices with very fast photochromic responses," *Journal of Materials Chemistry*, vol. 7, no. 1, pp. 61–65, 1997.

[319] C. Salemi-Delvaux, B. Luccioni-Houze, G. Baillet, G. Giusti, and R. Guglielmetti, "Effect of photodegradation on the thermal bleaching rate constant of photochromic compounds in spiro [indoline-pyran] and spiro [indoline-oxazine] series," *Journal of Photochemistry and Photobiology A: Chemistry*, vol. 91, no. 3, pp. 223–232, 1995.

[320] P. Vasa, R. Pomraenke, G. Cirmi, E. De Re, W. Wang, S. Schwieger, D. Leipold, E. Runge, G. Cerullo, and C. Lienau, "Ultrafast manipulation of strong coupling in metal-molecular aggregate hybrid nanostructures," *Acs Nano*, vol. 4, no. 12, pp. 7559–7565, 2010.

[321] M. R. d. Nunzio, A. Romani, and G. Favaro, "Excited-state properties of a photochromic spirooxazine: Double pathways for both fluorescence emission and camphorquinone-sensitized reaction," *The Journal of Physical Chemistry A*, vol. 113, no. 34, pp. 9424–9433, 2009.

[322] J. R. Lakowicz, "Radiative decay engineering 5: metal-enhanced fluorescence and plasmon emission," *Analytical Biochemistry*, vol. 337, no. 2, pp. 171–194, 2005.

[323] M. K. Hedayati, S. Fahr, C. Etrich, F. Faupel, C. Rockstuhl, and M. Elbahri, "The hybrid concept for realization of an ultra-thin plasmonic metamaterial antireflection coating and plasmonic rainbow," *Nanoscale*, vol. 6, no. 11, pp. 6037–6045, 2014.

[324] W. Ni, Z. Yang, H. Chen, L. Li, and J. Wang, "Coupling between molecular and plasmonic resonances in freestanding dye- gold nanorod hybrid nanostructures," *Journal of the American Chemical Society*, vol. 130, no. 21, pp. 6692–6693, 2008.

[325] J. Bellessa, C. Bonnand, J. Plenet, and J. Mugnier, "Strong coupling between surface plasmons and excitons in an organic semiconductor," *Physical Review Letters*, vol. 93, no. 3, p. 036404, 2004.

[326] N. T. Fofang, T.-H. Park, O. Neumann, N. A. Mirin, P. Nordlander, and N. J. Halas, "Plexcitonic nanoparticles: plasmon- exciton coupling in nanoshell- j-aggregate complexes," *Nano Letters*, vol. 8, no. 10, pp. 3481–3487, 2008.

[327] J. Dintinger, S. Klein, F. Bustos, W. L. Barnes, and T. Ebbesen, "Strong coupling between surface plasmon-polaritons and organic molecules in subwavelength hole arrays," *Physical Review B*, vol. 71, no. 3, p. 035424, 2005.

[328] H. Eilers, A. Biswas, T. Pounds, M. G. Norton, and M. Elbahri, "Teflon AF/Ag nanocomposites with tailored optical properties," *Journal of materials research*, vol. 21, no. 09, pp. 2168–2171, 2006.

[329] J. J. Mock, D. R. Smith, and S. Schultz, "Local refractive index dependence of plasmon resonance spectra from individual nanoparticles," *Nano Letters*, vol. 3, no. 4, pp. 485–491, 2003.